Pressure induced deformation measurements on atherosclerotic porcine iliac arteries: An MRI study

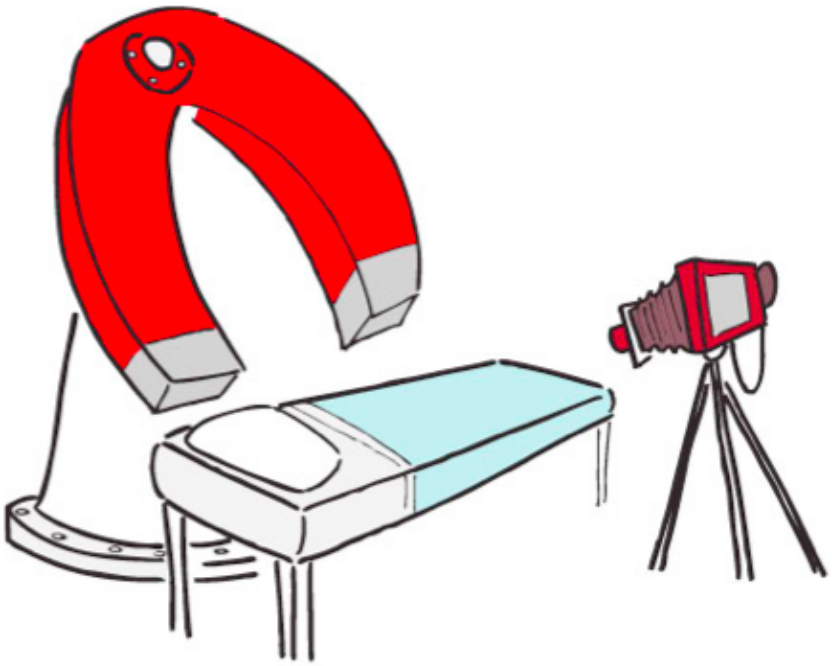

Student: Marco Goffi
1220187

TU Delft
Faculteit 3ME
MSc Biomedical engineering

Supervisors: Dr. Ir. F.J.H. Gijsen (EMC)
Ir. A.C. Akyildiz (EMC)

Professor: Prof. Dr. J. Dankelman (TUD)

Erasmus MC Rotterdam
Biomechanical engineering department (Ee2322)

11-10-2011

Contents

1. Introduction

Cardiovascular disease (CVD) such as heart attack and stroke remains the leading cause of death in developing and developed countries [3]. Heart attacks and strokes occur when the blood supply to the heart muscle and brain are severely reduced. A reason for the reduced blood supply is an occlusion. The occlusion can either be caused by a stenosis or a blood clot, which is the result of a rupture of an atherosclerotic plaque.
A healthy artery consists out of three main layers; the intima, the media and the adventitia (Figure 1a). The lumen is the inside of the artery where red blood cells, white blood cells, blood platelets and many other molecules flow through. One of the molecules that flow through the artery is low density lipoproteins (LDL). Atherosclerosis is an arterial disease associated with LDL (Figure 1b). When there is an excess of LDL, these particles accumulate in the intima and undergo chemical changes, which cause endothelial cells to attract monocytes and T-cells. Monocytes and T-cells play a central role in the inflammation process. The monocytes turn into macrophages, which will start to remove the LDL by absorption. These fat laden macrophages form the fatty streak, which is the early phase of an atherosclerotic plaque. Inflammatory molecules promote the growth of the plaque followed by the formation of a cap over the fat laden core (lipid core, Figure 1c) [4]. As long as the atherosclerotic plaque does not obstruct the blood flow a person will not notice that he has a plaque. However, this does not mean that there is no risk. If the cap of the plaque ruptures and the content of the lipid core gets into the bloodstream, a thrombus will form, which creates the occlusion spoken of earlier (Figure 1d).

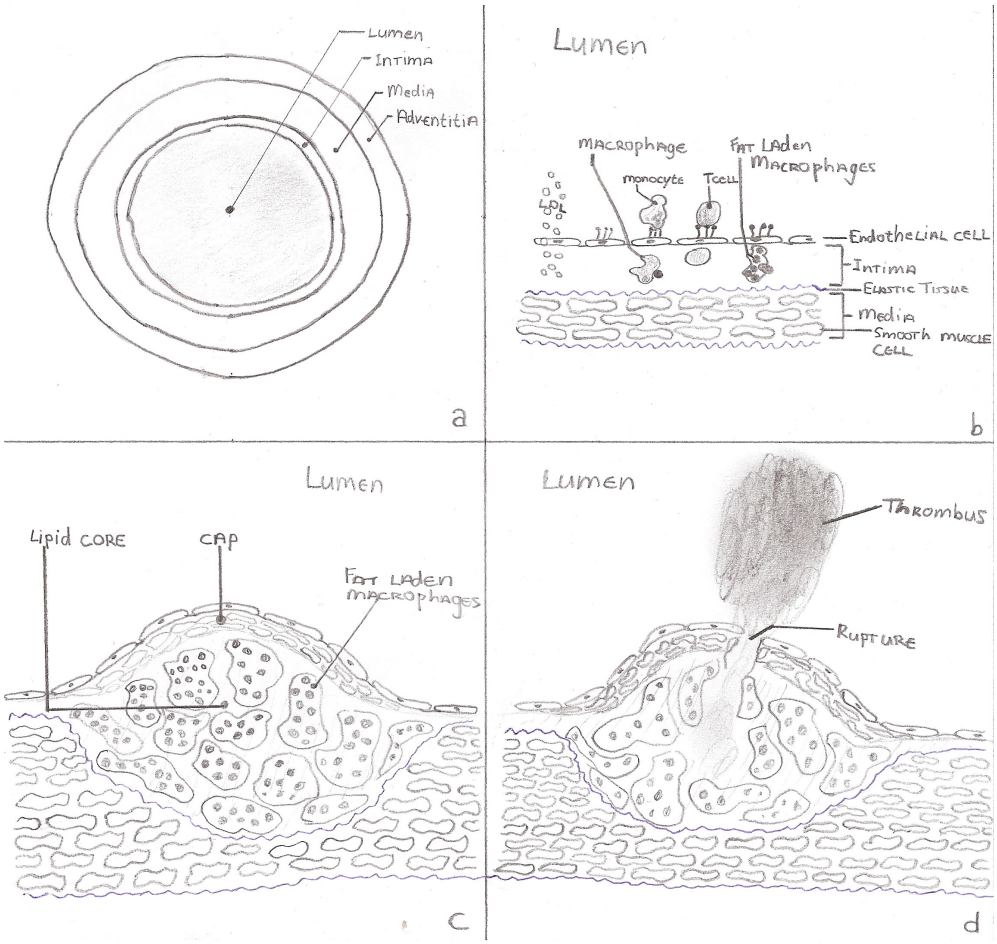

Figure 1 a. Representation of a healthy artery. b, The initiation of an atherosclerotic plaque. c, A vulnerable plaque with a big lipid core and thin cap. d, A rupture of the cap, which causes a thrombus.

The rupture of a cap can only happen if the mechanical stress in the cap exceeds the cap strength. There are two main stresses present in the artery. These are shear stress and tensile stress. The velocity of the blood in the lumen is greater in the middle than near the wall (Figure 2a). The velocity at the wall is zero, which is due to friction of the blood with the wall. This friction creates stress in the longitudinal direction of the artery, which is called the shear stress. Research has shown that areas with low shear stress are more prone to form atherosclerotic plaques [5-7]. In time the shear stress also seems to weaken the cap of the plaque. However, shear stress can only be sensed by the endothelial cells and is not high enough to exceed the cap strength. Tensile stress is created by the blood pressure. The tensile stress is about a factor 10.000 greater then the shear stress [7]. The heart pumps the blood around the body and at each beat the pressure increases and decreases in the artery. This pressure creates an outward force on the artery wall and thus on the plaque (Figure 2b). When the blood pressure becomes to too high, stresses in the cap might exceed the cap strength and then the cap ruptures.

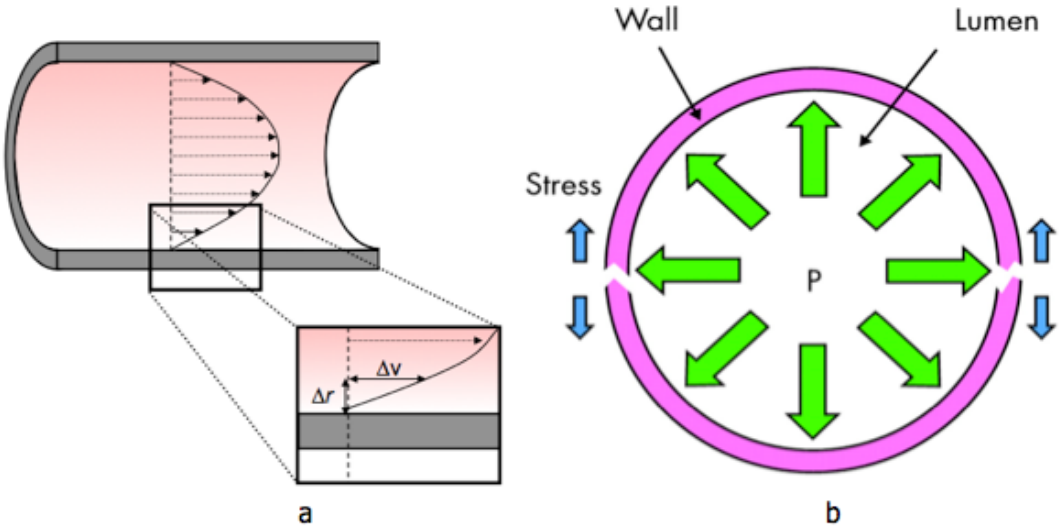

Figure 2 a, Representation of a laminar flow in an artery. The velocity field indicates a low velocity close to the wall [8]. b, The reactive force created by the blood pressure is indicated with the green arrows [9].

The arteries in a human body may contain many plaques, but not all of these plaques can be treated. A model that can predict which plaques are at risk would help to treat the right plaques. With a biomechanical model of an atherosclerotic plaque it is possible to simulate the effect of different blood pressures on the stresses in the plaque. This makes it possible to identify vulnerable plaques. To create a biomechanical model we need the 3D geometry of the plaque components, the material properties and the boundary conditions. The components that are important for a biomechanical model of an atherosclerotic plaque can be seen in Figure 3. The second thing that is needed is the material properties. In literature some material properties can be found, but the material properties for the intima vary a lot between papers. The intima shows Young's modulus of 500-1000kPa, even up to 2300kPa [10-16]. However, a recent study showed that the intima had a much lower Young's modulus 33kPa [17]. Biomechanical models are currently used to predict pressure induced deformations and stresses in atherosclerotic models, but no experimental validation of these models is

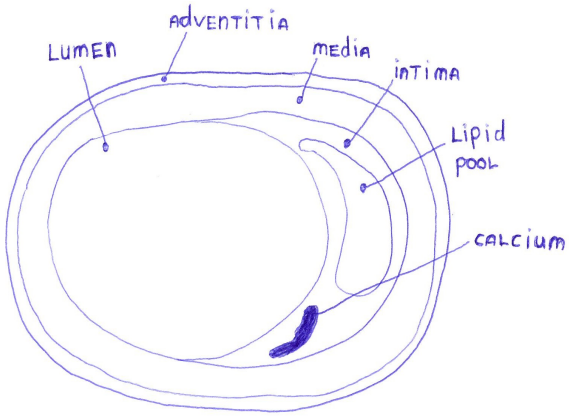

Figure 3 The components of a diseased atherosclerotic plaque.

available. Especially the effect of the intima properties needs to be studied. If pressure induced deformations can be measured and a model can be build, it is possible to validate this model and retrieve the material properties for the intima. The aim of this research is to find an image sequence that can image all the components and investigate if pressure induced deformation measurements can be done on these images.
To achieve this aim an imaging protocol is needed. The only modality that can be applied in vivo and gives good contrast for these components is magnetic resonance imaging (MRI). To find an imaging sequence, basic knowledge of MRI is needed (Chapter 2). With the theoretical knowledge it is still not possible to create an imaging sequence, because the sequence depends on the scanner that is used and the software the scanner has. To find a good imaging sequence the obtained knowledge will be applied in pilot experiments to the MRI scanner that is going to be used (Chapter 3). If a good imaging sequence for the MRI is created the experiments can be done for pressure induced deformations. The methods results and conclusion of these experiments will be discussed in Chapter 4. In chapter 5 a final discussion and conclusion of the whole project will be discussed.

2. Magnetic resonance imaging

For this project MRI will be used to obtain the data for making a biomechanical model. However, before pressure induced deformations are performed it is important to develop an imaging protocol. To create this, the basic concept of MRI needs to be known (Section 2.1). When the basic concept of MRI is explained, the process behind contrast is discussed (Section 2.2). Each contrast is a different signal that is observed by the MRI scanner. These signals need to be encoded to obtain an image, which is a complicated process that is explained in Section 2.3. After the general theory of MRI is discussed, the focus will be placed on MRI of atherosclerotic plaques (Section 2.4). At the end of this chapter there will be concluding remarks based on the theory obtained about MRI and papers found in literature (Section 2.5). All the theory about MRI is collected from the books MRI the basics [2] and MRI in practice [18].

2.1 The basic concept of MRI

MRI was first named Nuclear Magnetic Resonance Imaging (NMRI). However, the word nuclear was associated with radioactivity so they changed the name to MRI. The word nuclear was used, because the imaging process is made possible by the angular momentum of the nucleus. Atoms consist of a nucleus and an electron cloud. The nucleus consists of protons, which have a positive charge, and neutrons. These protons and neutrons present the mass of an atom. If the atom has an odd atomic number, than the nucleus has an angular momentum. This means that the positive charged nuclei will rotate around their axis (spin). This spin creates a magnetic field and so the atom will act like a small bar magnet (Figure 4a). The hydrogen atom (H_1) is one of these atoms. The magnetic field created by each H_1 atom is in a random direction (Figure 4b), leading to a net magnetic field that is zero. However, it is possible to manipulate all these magnetic H_1 atoms.

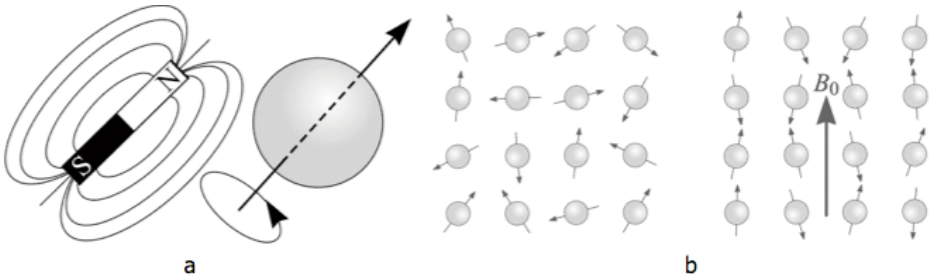

Figure 4 a, An atom with an angular momentum has a magnetic field, like a bar magnet. b, The magnetic fields of these atoms point in a random direction. When an external magnetic field is applied the magnetic fields will mainly align with the external field. [1]

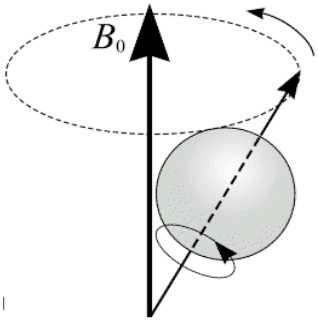

Figure 5 Representation of the precession of an atom around the direction of B_0. [1]

When there is an external magnetic field (B_0) the orientation of the small magnetic fields will either align or oppose this external magnetic field (Figure 4b). The opposing fields have a nucleus with a down spin (high energy state of the atom) and the aligning fields have a nucleus with an up spin (low energy state of the atom). However, after some time there will be more atoms aligned with the external magnetic field. This will give a net magnetization (M_0) in the direction of B_0. Due to B_0 the nucleus does not only spin, but it will also start to precess around the direction of B_0, which is the longitudinal plane (B_0 points in the z-direction) (Figure 5). The rotation around the z-axis has a frequency, which is called the Larmor frequency. In MRI scanners the field B_0 is created with a large super-

conducting magnet. The MRI scanners used in hospitals usually have fields ranging from 0.5 to 3 Tesla (T). However the experimental MRI scanners have fields that go up to 21.1 T [19]. When the external field B_0 is changed then the Larmor frequency (ω) changes as well:

$$\omega = \gamma \cdot B_0 \qquad \text{(Equation 1)}$$

The symbol γ is the gyromagnetic ratio, which expresses the relationship between the angular momentum and the magnetic momentum of each nucleus. Because every nucleus is different, it also means that the gyromagnetic ratio for each atom is different.
The Larmor frequencies of atoms are in the radiofrequency (RF) range (10^5-10^9Hz). When an RF-pulse with the Larmor frequency is send towards these atoms, they will start to resonate. Resonance can be seen as pushing a person on a swing. If you push the person at the right moment he will go higher. If you repeat this at the right frequency you keep adding energy to this person, which is called resonance. So when resonation occurs the energy of the atoms increases and they start to flip into a different plane. Since B_0 points into the longitudinal plane, the net magnetization (M_0) of the H_1 atoms will flip into the transversal plane (x,y-plane) (Figure 6a, 90° flip). The amount of degrees that the magnetization is flipped into the transversal plain is called the flip angle (FA).

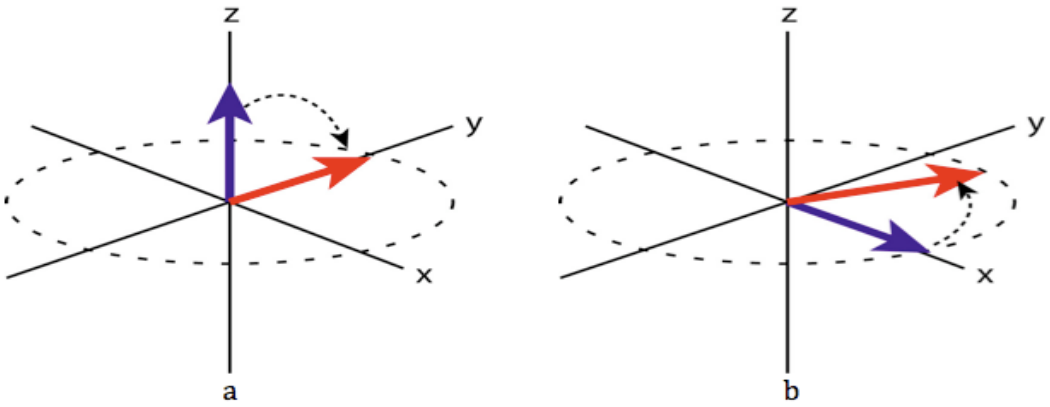

Figure 6 a, The magnetization (M_0) of the atoms is flipped into the transverse-plane (90°). b, After the magnetization of the atoms has flipped into the transversal plane, this magnetization will start to precess around the z-axes. [20]

When the M_0 goes from the z-direction into the x,y-plane it will continue its precession around the z-axis (Figure 6b). When M_0 makes a 90° flip then the magnetization in the longitudinal plane will be equal to zero and in the transversal plane it will be M_0.
Because M_0 is now rotating in the transversal plane, it means that the magnetization in the x- and y-direction increase and decrease with a certain frequency. If a coil is placed in the x direction, then it will first experience a rising magnetization, until there is a maximum and after a decreasing magnetization (Figure 7).

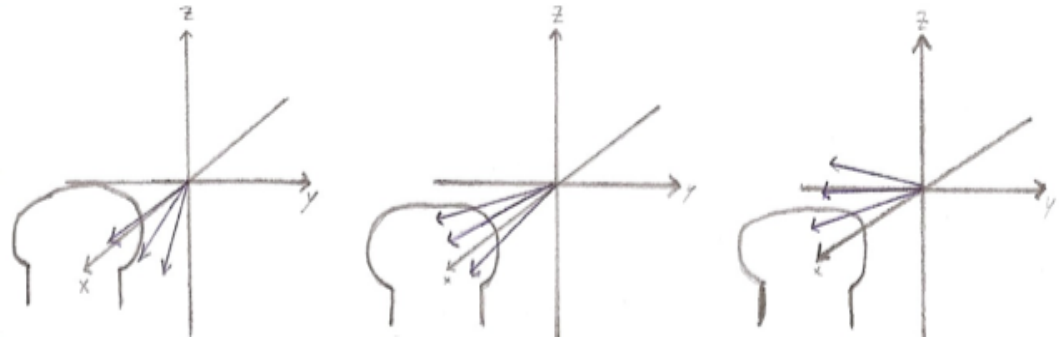

Figure 7 The coil experiences an increase in magnetic field, then the coil experiences a maximum magnetic field strength when the whole field points through the coil. Finally, the magnetic field strength is decreasing again.

This change in field strength that the coil experiences, induces an alternating current in the coil. The frequency of this alternating current is the same as the Larmor frequency of the atoms from which the signal came. The induced current is the signal from which MR images are created. The signal can only be measured in the transverse plane, because this is where a changing magnetic field is experienced.
After the RF pulse is over the magnetization of the atoms will start to align with B_0 again. The signal that is received will also decay in time. This is called Free Induction Decay (FID). The recovery of the magnetization in the longitudinal direction is a slower process than the decay of the magnetization in the transverse plane. The time it takes for the magnetization to recover in the longitudinal direction (T1) is five to ten times longer than the time it takes for the magnetization to decay in the transverse plane (T2). T1 is a time constant, which describes the time needed for the magnetization to recover 63% of the original magnetization in the longitudinal direction (Figure 8a). T1 recovery is caused by nuclei that give their energy to the surrounding lattice (spin-lattice interaction). T2 is the time constant that describes the time needed to decay 63% of the magnetization in the transversal plane (Figure 9b). The magnetic fields of neighboring nuclei interact with each other and this causes energy exchange between these nuclei (spin-spin relaxation).

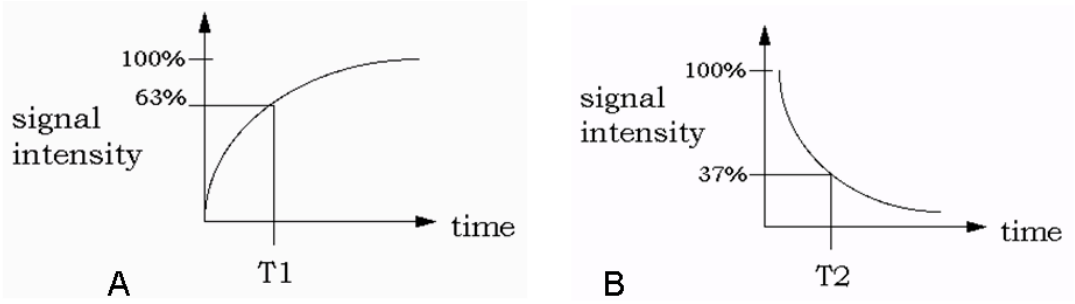

Figure 8 a, A recovery graph of the magnetization into the longitudinal plane. b, A decay graph of the magnetization in the transversal plane. [1]

A third time constant is T2*, which describes the loss of signal due to de-phasing of the magnetization in the transverse plane. When one atom is flipped into the transverse plane the precession around the z-axis will continue and this is what creates the signal. However, when several atoms flip into the transverse plane they will all have a precession around the z-axis, but not necessarily with the same frequency. When they first flip into the transverse plane all atoms are in phase (Figure 9a), but because the precession of one atom is faster then the other they go out of phase after some time (Figure 9b). This means that after some time each magnetization is pointing in a different direction and thus the signal will be cancelled (Figure 9c). This effect is called the T2* decay which is faster then T2 decay.

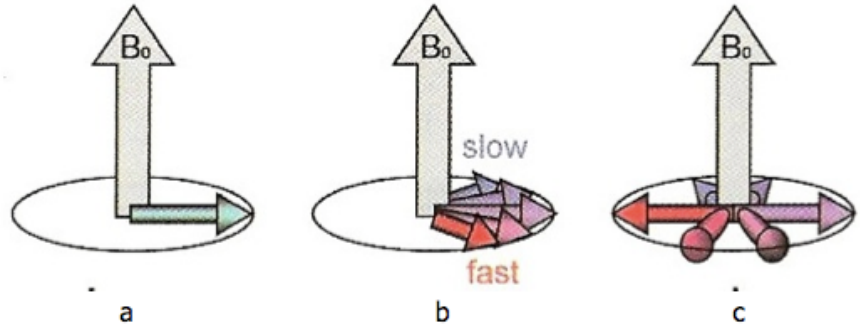

Figure 9 a, All nuclei point in the same direction and are in phase after the flip. b, Due to frequency differences the nuclei will go out of phase. c, The nuclei are so much out of phase that they cancel each other's magnetic field. [18]

2.2 Contrast in MRI

In MRI, contrast is the difference in signal intensity between two different structures. The signal comes from the atoms with an angular momentum. The body of a human contains a lot of water and fat. Each of these substances contains H_1 atoms and can thus be used for MRI. Even though both water and fat contain H_1 atoms it does not mean they give the same signal. In water the H_1 atom is connected to an oxygen (O_8) atom and in fat the H_1 atom is connected to a carbon (C_6) atom. Due to this fact each molecule has a different T1 and T2 time. By making use of these differences contrast between tissues can be achieved. There are three types of contrast namely:

- T1-contrast
- T2/T2*-contrast
- Proton Density (PD) contrast

To create each of these contrasts the timing between the RF-pulses, the measuring of the signal and the FA must be tuned correctly. The time between each RF-pulse is called the repetition time (TR), the time when the signal is measured is called echo time (TE). In MRI there are two main sequences to acquire images, which are spin echo (SE) sequences and gradient echo (GE) sequences. Both sequences have their own combination of parameters to create contrast. The SE contrast is discussed in section 2.2.1 and the GE contrast is discussed in section 2.2.2.

2.2.1 Contrast in spin echo sequences

First it is important to realize that the signal is measured in the transverse plane as explained in section 1.1.3. In a SE sequence the FA is always 90°. T1 contrast is accomplished by acquiring the signal from the recovery of the magnetization (Figure 8a). When the atoms in tissue A and B are both flipped into the transverse plane their recovery will be different from each other (Figure 10a). Both tissues A and B will start with zero magnetization in the longitudinal direction when a FA of 90° is used. To get the effects of T1 contrast you want the signal difference to be maximal from each other. To measure the difference in magnetization an RF-pulse can be used to flip them in the transversal plane where the difference can be measured as explained in Section 2.1. To have a maximal signal difference the TR must be short (Figure 10a, TR1), because else both tissues are recovered and their signal strength will almost be equal (Figure 10a, TR2).

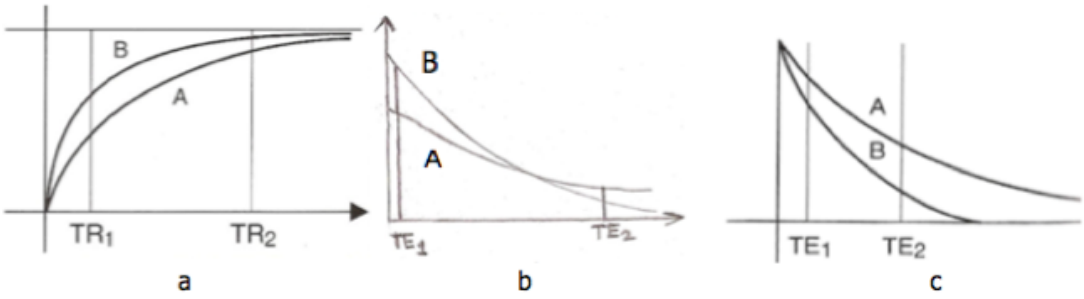

Figure 10 a, The T1 recovery curve of two different tissues [2]. b, A T2 decay curve of two different tissues after a short TR. c, A T2 decay curve of two different tissues after a long TR [2].

When the contrast is at a maximum the magnitudes of the magnetization will be flipped into the transverse plane due to the RF-pulse. As soon as the magnetization is flipped the signal must be measured (Figure 10b, TE1), because else the T1 contrast will start to decay due to spin-spin interaction (Figure 10b, TE2). This means that the TE must be very short. After the signal is measured this process is repeated by applying another RF pulse when the magnetization has recovered to the value before the previous RF-pulse. The time between these pulses is the TR.

To create T2 contrast the effects of T1 contrast must be minimal and of T2 contrast maximal. As can be seen in Figure 10a the contrast of T1 is minimal for large TR. When the transverse

magnetization of tissue A and B are flipped into the transverse plane they will both start with equal magnitude (Figure 10c). The decay pattern looks different from Figure 9b due to the longer TR. At TE1 the contrast between tissue A and B is still low. At TE2 the contrast between tissue A and B has already increased. This means that to obtain T2-contrast a long TE is needed in contrary to T1-contrast. However, due to de-phasing of the magnetization in the transverse plane, the signal will decrease over the time constant T2* as explained in Section 2.1. This effect can be compensated by applying a 180° RF-pulse after the 90° RF-pulse. Figure 11 explains this principle by using running athletes. Three athletes start at the same time (Figure 11a), but not every athlete runs with the same speed. So after some time every athlete is at a different position. Now the 180° RF-pulse comes after 0.5TE (Figure 11b), which turns the athletes around. At TE the athletes will be back at the finish simultaneously (Figure 11c). When we look to the arrows in Figure 9c, then the 180° RF-pulse will bring the magnetization back in phase again as in Figure 9a. When the arrows are in phase the signal will be at its peak. This is the time when you want to measure your signal (TE). After this peak they will go out of phase again.

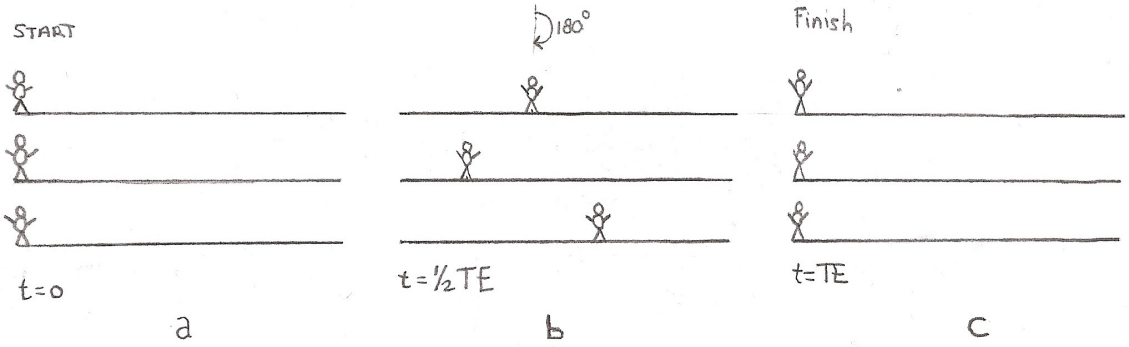

Figure 11 Representation the 180° RF-pulse, which aligns all magnetic moments again. a, All athletes start at the same time at the same position. b, A 180° RF-pulse turns the athletes around. c, The athletes will all reach the finish again at the same time.

These 180° RF-pulses can be applied multiple times and every time the signal will reach a peak again, but the signal strength will be lower each time due to the normal T2 decay (Figure 12).

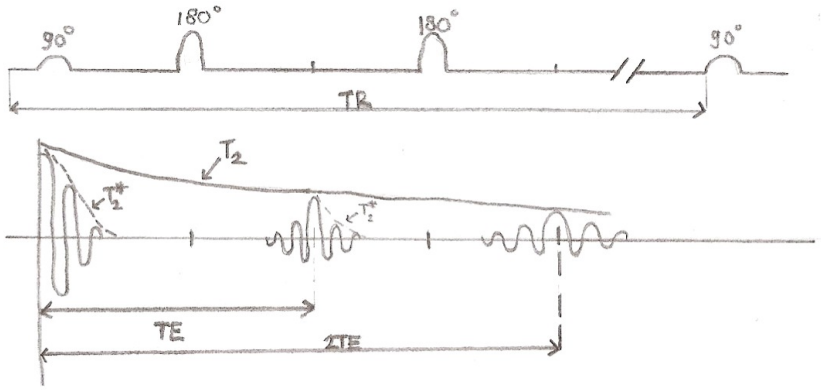

Figure 12 The intensity of the echo decreases due to T2* decay, but after each 180° RF-pulse the peak of the signal will return. This peak is lower than the first peak due to T2 decay.

PD contrast is achieved by canceling both the T1- and T2-contrast. To cancel the T1-contrast a large TR is needed and to cancel the T2-contrast a short TE is needed. In this case the contrast due to magnetization is equal. The only difference now is the difference in nuclei concentration of both tissues. If tissue A has a higher concentration of contributing nuclei, in comparison to tissue B, then the signal of tissue A will be higher than that of B. This is how PD-contrast is created.
In short, T1-, T2-, and PD-contrast for SE can be achieved by applying the settings in Table 1

Table 1 Timing of TR, TE and FA to obtain T1-, T2- or PD-contrast with SE. TR_{short}=~300-700ms, TR_{long}=~2000ms, TE_{short}=~10-25ms, TE_{long}=~60ms+[18] . These values are not a rule, but an indication. The range of values reflects the wide variation of parameters that can be found in literature.

	TR	TE	FA
T1	Short	Short	90°
T2	Long	Long	90°
PD	Long	Short	90°

2.2.2 Contrast in gradient echo sequences

The important thing to realize when contrast has to be created in GE imaging, is that the FA can vary (Figure 13a). The shorter the flip angle, the shorter T1 will be. This means that the TR must be short for every contrast in comparison with SE (Figure 13b). To obtain T1 contrast it is still necessary to capture the effects of the T1 recovery. In Figure 13b it can be seen that the difference in magnetization for tissue A and B at a 10° angle is small. When the flip angle is 40° the difference between A en B is increased and thus T1-contrast improves. The TR must be short again to capture T1 contrast at a 40° angle. The TE should still be as short as possible. However, with gradient echo there is no 180° FA, so the T2* effect will reduce the signal rapidly. GE sequences are used to decrease the time because TR is much shorter when there is only a partial flip angle. If a 180° FA was used it would take a long time for the magnetization to recover and thus the time advantage is gone. Instead of the 180° FA, with gradient echo a gradient is used to get the magnetization vectors back in phase.
A gradient is an additional linearly changing magnetic field that is added to the homogenous field of the bore in the MRI scanner. Due to this additional field the Larmor frequency of the nuclei increases or decreases depending on the magnitude of the gradient at a certain point in the scanner. When using the athlete example from Figure 11 the athletes do not turn around, but the slow athletes increase their speed and the fast athletes reduce their speed if the gradient is applied in the right way. This means that all athletes will reach the finish at the same time and are back in phase again.

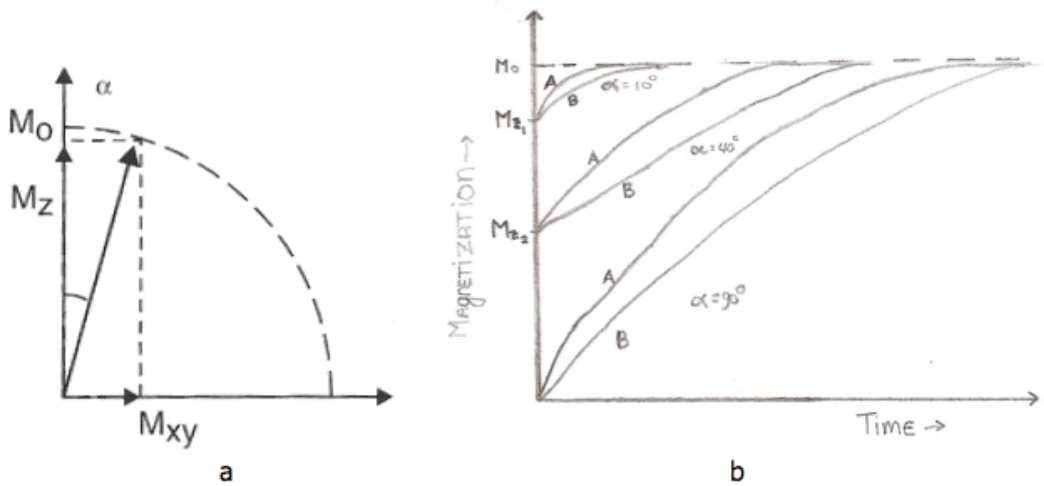

a b

Figure 13 a, The partial flip of the magnetization into the transversal plane [2]. b, When the flip angle changes the recovery time also changes. It will take less time for all the magnetization to return to the longitudinal direction.

Because there is no 180° flip angle T2*-contrast is measured with gradient echo. We want to minimize T1-contrast when we measure T2*-contrast so the FA must be small. This also means that the TR becomes small (Figure 13b), because the magnetization is now fully recovered in a much shorter time due to the small FA. The echo time for T2*-contrast is large in comparison to T1-contrast.
For PD-contrast the T1- and T2*-contrast must be suppressed. This can be achieved by taking a small flip angle and a short TE. Due to the small FA the TR will also be small. In short, T1-, T2-, and PD-contrast for GE can be achieved by applying the settings in Table 2.

Table 2 Timing of TR, TE and FA to obtain T1-, T2- or PD-contrast. $TR_{short} \leq 50ms$, $TR_{long} \geq 100ms$, TE_{short}=5-10ms, TE_{long}=15-25ms, FA_{small}=5°-20°, FA_{large}=30°-70° [18]. These values are not a rule, but an indication. The range of values reflects the wide variation of parameters that can be found in literature.

	TR	TE	FA
T1	Short	Short	Large
T2	Long	Long	Small
PD	Long	Short	Small

2.3 Spatial encoding

How the signals can be obtained and the contrast between tissues can be made visible were discussed in the previous sections, but how the location of each signal is retrieved is not yet explained. To explain this we first need to define an axial system (Figure 14). The slice selection will be done in the z-direction, the phase encoding will be done in the y-direction and the frequency encoding will be done in the x-direction (Section 2.3.1). The encoded signals are stored in 'k-space' (Section 2.3.2).

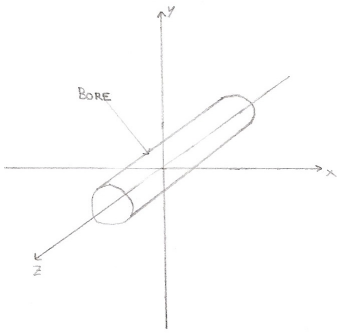

Figure 14 The axial system used in MRI. The bore is where the object is placed in.

2.3.1 Spatial encoding of the x-, y-, and z-coordinates

A patient lies with his head into the negative z-direction when he is in the MRI scanner. There is a main magnetic field of 1.5T, which is supposed to be homogenous. However, if an RF-pulse is created with the Larmor frequency of H_1 atoms, then every H_1 nuclei in the body will tip over and the location of each signal will remain unknown. To determine which part sends a signal a gradient is applied in the z-direction. This gradient makes sure that each part of the body is exposed to a different magnetic field strength (Figure 15).
The fact that the magnetic field is varying over the length of the body means that the Larmor frequency of the H_1 atoms will also differ, according to equation 1. By applying an RF pulse with a certain bandwidth, lets say 66-67MHz, it is possible the image a slice of the neck and shoulders (Figure 15). By decreasing the bandwidth of the RF pulse, the slice thickness will also decrease. This is how the slices are selected and the slice thickness is determined.

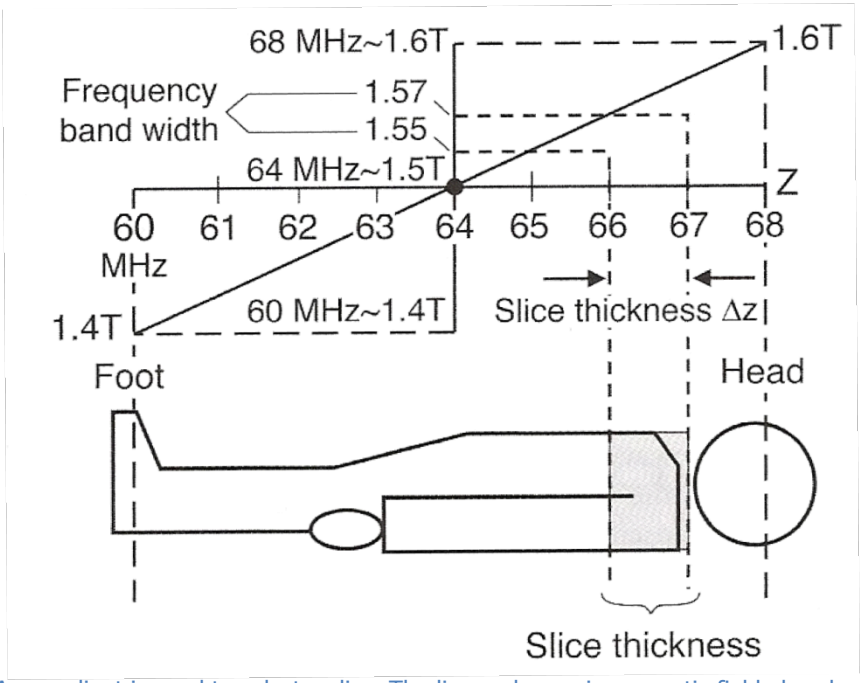

Figure 15 A z-gradient is used to select a slice. The linear change in magnetic field also changes the Larmor frequency of the hydrogen molecules in a linear fashion. [2]

To find out from which part in the y-direction the signal comes, another linear gradient is applied, but now in the y-direction. Due to this gradient the speed, and thus the frequency, of the nuclei will vary due to the linear increase of the gradient. Because the frequency for nuclei is different they will start to go out of phase. When the gradient is then switched of the frequency will go back to normal, but the magnetization of the nuclei in the y-direction will stay out of phase (Figure 16). Because the nuclei are out of phase the signal will decrease. As can be seen the top row has a positive phase change and the bottom row has a negative phase change. The amount of phase change is known, because the gradient that is used is also known. So the position in the y-direction can be encoded, because signals with a different phase are measured and the phase is linked to the known applied gradient.

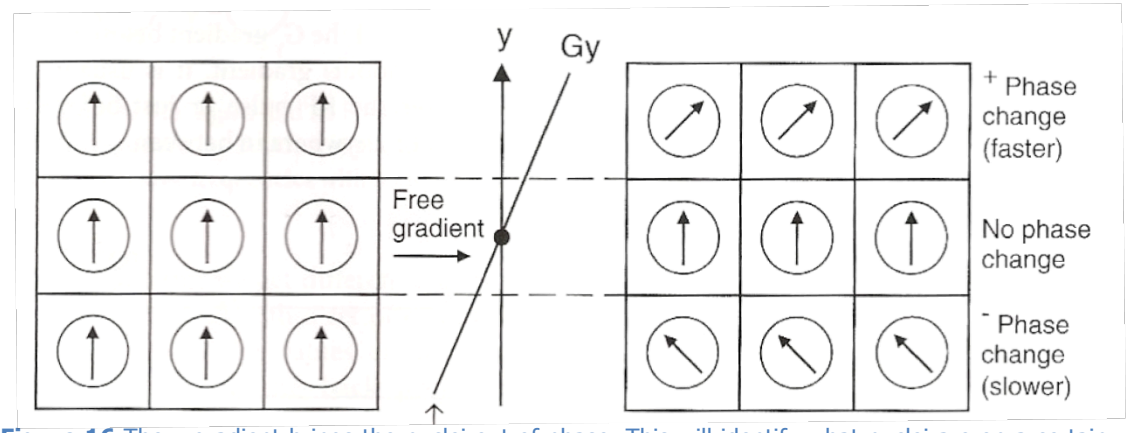

Figure 16 The y-gradient brings the nuclei out of phase. This will identify what nuclei are on a certain line in the transversal plane. [2]

Frequency encoding is done in the x-direction and is applied to determine the locations of the pixels in the x-direction. To achieve this, a linear gradient will be applied in the x-direction. This will increase the frequency of the nuclei in the x-direction in a linear fashion. Contrary to phase encoding, with frequency encoding the gradient is changing during one TR. This is done so that all frequency-encoding steps are done in one TR, which saves time. This is possible, because the signal is measured while the gradient in the x-direction is on. Together with the phase change in the y-direction it now also marks the x-direction (Figure 17).

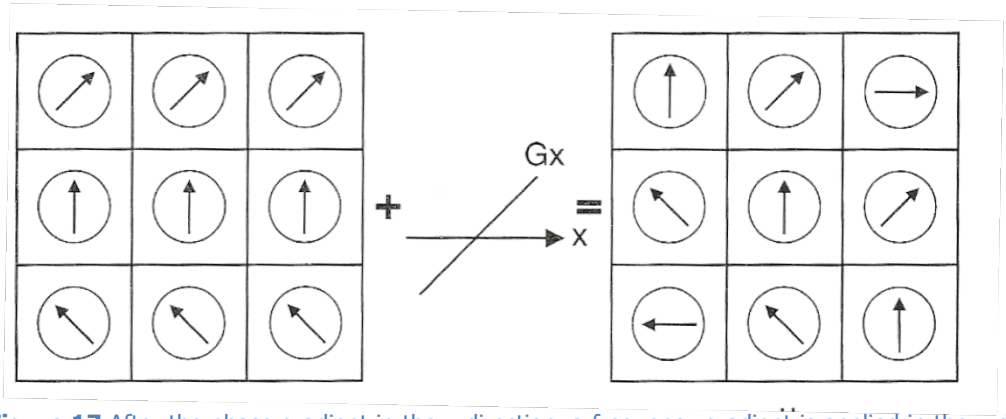

Figure 17 After the phase gradient in the y-direction, a frequency gradient is applied in the x-direction. By applying the x-gradient the voxels can be allocated. [2]

The previous discussed encoding steps were for 2D MRI scans. With both 2D and 3D MRI scans slice selection is applied in the z-direction. However, with 3D MRI scans there is also a phase difference applied in the slice that is selected. This phase difference is encoded in the same way as is done in the y-direction. This means that with 3D MRI scans thinner slice can be obtained, but the time it takes to obtain this image also increases.

2.3.2 K-space

The received signals have a certain magnitude, frequency and phase. It can be described as a wave. An appropriate way to store and process wave like signals, is in the Fourier domain. The Fourier domain is an analytical transformation from the time domain to the frequency domain. Since the signal that is obtained is frequency depended it will be stored in the k-space, which is the Fourier domain. When all signals are obtained it can be transformed to the time domain by applying an inverse Fourier transformation.

In k-space the frequency encoding steps are stored in the x-direction (horizontal axis) and the phase encoding steps in the y-direction (vertical axis) (Figure 18). As can be seen, for every TR one line in the phase encoding direction is filled, but all lines in the frequency encoding direction are filled during one TR. The time in which all the frequencies are read is called the sampling time. After this sampling time the TR has not yet passed (for SE sequences) so to fill this time a second slice can be excited and a phase step plus frequency readout can be made in this new slice. This will be done till the TR time has passed and then the next phase step will be made for every slice that fits into one TR. Each slice has its own k-space. The number of lines in the phase and frequency encoding direction depends on the size of the matrix that is used. The bigger the matrix the higher the resolution will be. K-space can be compared with a guitar. The snares can be seen as the phase encoding direction and all the frets represent the frequency encoding direction. First, you hit the first string (first phase step), and then you slide your finger across all the frets (all frequency steps). Then you grab the next guitar (next slice) and hit the same string and go over all frets. When TR is over you go back to the first guitar and repeat the process for the next string. This is basically how k-space is being filled.

At the zero line there is no gradient and thus the signal is the strongest (Figure 18). This is because at this point the nuclei are in phase. When moving from the center of k-space the gradients will become steeper and thus the signal decays, because the nuclei are going more out of phase. However, though the signal decreases the resolution increases, because of the steep gradient the difference in phase between adjacent pixels becomes greater and thus their location can be better calculated.

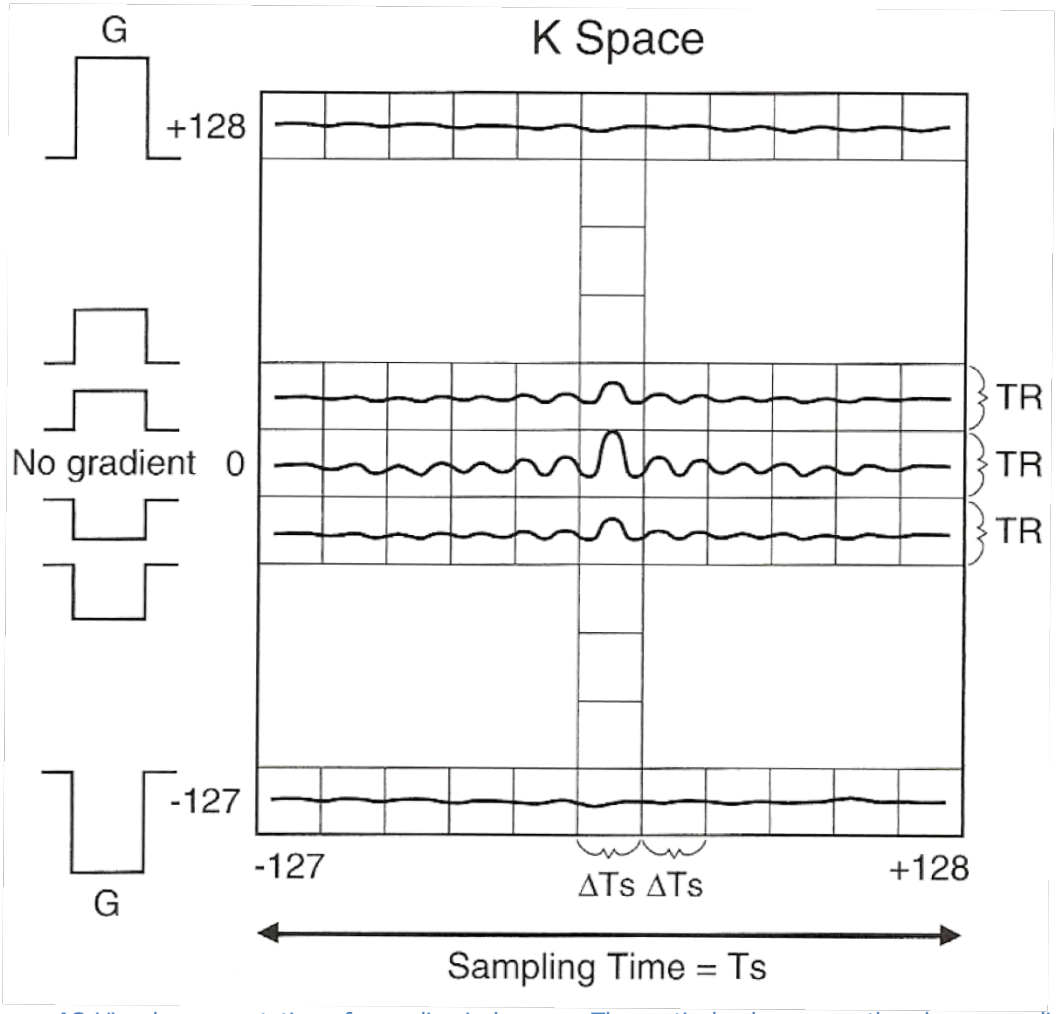

Figure 18 Visual representation of one slice in k-space. The vertical columns are the phase-encoding direction and the horizontal rows are the frequency encoding direction. As can be seen at each phase a different gradient is applied. [2]

In Figure 19 the picture of a lady can be seen. When the middle of k-space is left out, the bulk of the signal disappears and only the resolution data remains, but when only the middle of k-space is present the signal is present but the resolution is poor.

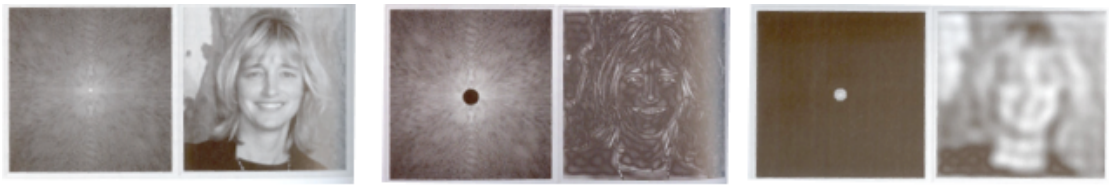

Figure 19 a, In the left picture you can see the magnitude-phase image in k-space. The information in this k-space is a photo of a lady in the time domain. b, When the middle of k-space is removed, all the contrast is gone but the details remain (resolution). c, When the outskirts of k-space are removed the contrast remains, but the details are gone. [2]

As explained, with 3D imaging the slices in z-direction will be additionally encoded by using phase encoding. This means that k-space needs to be 3D as well. With 2D imaging each slice has its own k-space, but with 3D imaging all the data is stored in one k-space.

2.4 MRI of atherosclerotic plaques

The general concepts of MRI are discussed, but this research focuses on imaging atherosclerotic plaques. In this section the focus will move to MRI on atherosclerotic plaques. With MRI there is always a trade-off between resolution, SNR and acquisition time (AT) (Section 2.4.1). As explained there are SE and GE sequences. Both SE and GE have several sub sequences, which might improve the images (Section 2.4.2 for SE and 2.4.3 for GE). When imaging atherosclerotic plaques there are some artefacts that might occur and influence the image quality. These artefacts will be discussed in Section 2.4.4.

2.4.1 Balance between resolution, signal to noise ratio and acquisition time

Resolution, signal to noise ratio/contrast to noise ratio (SNR/CNR) and AT are three factors that are intertwined with each other and when one is increased the other is decreased. The image quality depends on various factors including; hardware, software, setup and imaging parameters. This section will discuss the influence of different imaging parameters on the resolution, SNR/CNR and AT.

Resolution

The resolution is the size of the pixels/voxels. The smaller the pixels/voxels the higher the resolution. The resolution can be described by equation 2.

$$\Delta x,y,z = \frac{FOV_{x,y,z}}{N_{x,y,z}} \qquad \text{(Equation 2)}$$

The FOV is the field of view of the imaging volume. N shows the number of encoding steps that are taken in this image. By dividing these two parameters the size of a voxel in a certain direction is calculated, which represents the resolution. To increase the resolution Δx, Δy and Δz need to be decreased. This can be done by increasing the number of encoding steps or by decreasing the imaging volume. However, decreasing the volume will also decrease the SNR.

SNR/CNR

The SNR tells what the ratio between the received signal and the received noise signal is. The CNR is the ratio between the difference of two signals (from different tissues) and the noise. As explained in the last section the resolution influences the SNR. This can be seen in equation 3.

$$SNR \propto \Delta x \cdot \Delta y \cdot \Delta z \sqrt{\frac{N_x N_y \cdot NEX}{BW}} \qquad \text{(Equation 3)}$$

Equation 3 is a rough calculation for the SNR of a 2D image. In equation 3 there are two new parameters that are not present in equation 2. The NEX is the number of acquisitions that are taken. By taken several acquisitions the noise can be reduced by averaging. The BW is the bandwidth of the signal that is received. By decreasing this bandwidth the high frequency noise is filtered. If the resolution is increased by halving the voxel size in al direction this means that the SNR will be eight times lower. Now the only way to compensate for this without changing the resolution again is by increasing the NEX 64 times or decreasing the BW 64 times. However, the NEX will influence the acquisition time. Decreasing the receive BW increases the sampling time, which means that the minimum TE becomes bigger. This is a problem if T1- or PD-weighted images are required, because these need a small TE.
The SNR can also be influenced with the contrast parameters TR, TE and FA. However, this needs to be prevented, because once a good contrast is obtained you don not want to change it again just to increase SNR. A more robust way to increase the SNR is by using a stronger external magnetic field. The stronger the magnetic field is, more atoms will align with it and thus a stronger signal can be achieved.

Acquisition time

The acquisition time is the time needed to complete the whole scanning process. The time for a normal 2D SE sequence can be calculated with equation 4.

$$AT = TR \cdot N_y \cdot NEX \qquad \text{(Equation 4)}$$

N_y is the number of phase encoding steps. Each phase encoding step takes one TR. The acquisition can be done multiple times, which is indicated by the NEX. If a 3D scan is done then equation 3 needs to be multiplied with N_z phase encoding steps. Both N_y and N_z influence the resolution and thus also the SNR. When the voxel size is halved the losses in SNR can be compensated by increasing the NEX sixteen times. By increasing the NEX sixteen times the AT will also increase sixteen times according to equation 4.

2.4.2 Spin echo sequences

In section 2.2.1 is explained how contrast is obtained for spin echo (SE) and gradient echo (GE) sequences. Basically these are the only two sequences and from these sequences variations are created. These variations are created to make the imaging process faster and to improve the image quality for different imaging volumes. Certain organs contain a lot of fatty tissue and others a lot of water. Both give different signals and a different sequence might improve the image quality. The SE sequences with its variations will first be summarized and after the GE sequences with its variations are summarized. To give a better visual feedback on how SE and GE work, a pulse sequence diagram (PSD) will be used. The PSD shows in which order the RF-pulses, the gradients and the signal are processed. For this research only 2D SE sequences and 2D fast SE (FSE) sequences can be used and also inversion recovery techniques can be used to suppress fat.

To explain the variations in SE sequences it is first important to see how a standard SE sequence is described in a PSD (Figure 20).

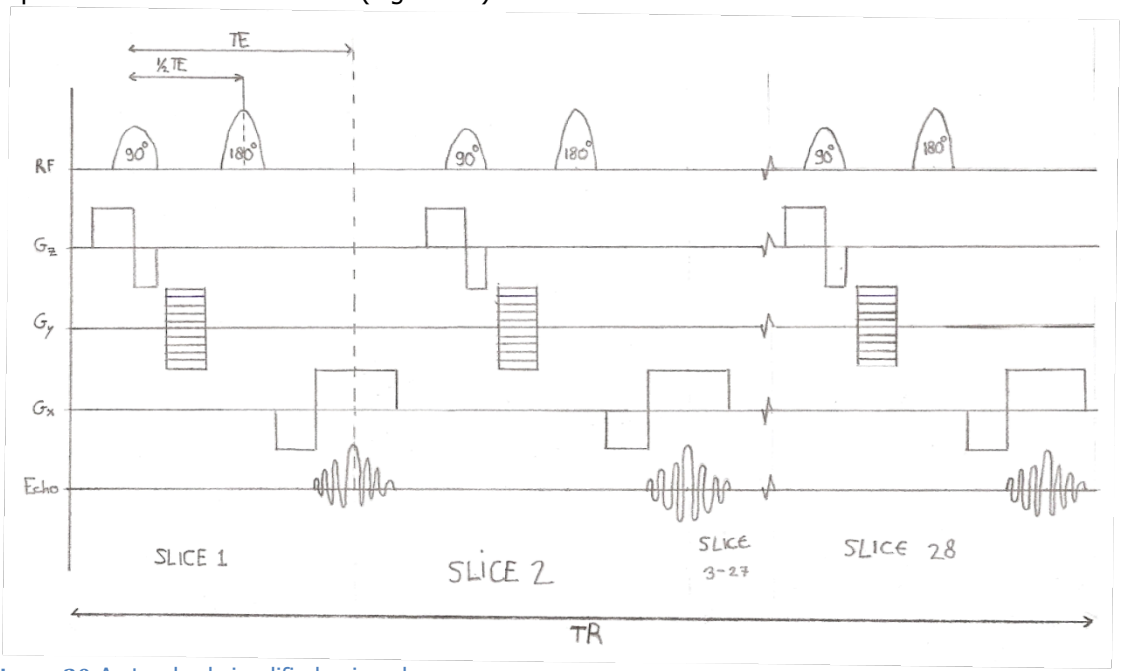

Figure 20 A standard simplified spin echo sequence.

The RF excitation pulses that are applied in a SE sequence are always 90°. The z-gradient is turned on before the 90° RF-pulse is applied so that the right nuclei are excited by this pulse. When a gradient is applied for a short time the nuclei get out of phase. During the slice selection the nuclei of the selected slice get out of phase, which is why a negative z-gradient is applied after the positive to refocus the phase of these nuclei again. The y-gradient is applied after the z-gradient to get the nuclei out of phase for the phase encoding. Each line in the y-gradient is applied at a different TR, because only one phase encoding step is done

each TR. The 180° RF-pulse is now used to reverse the direction of the precession again so that the nuclei get back in phase (Figure 11). The phase difference created by the y-gradient is not overcome by this 180° RF-pulse just the dephasing due to the T2* effect (Section 2.2). When the nuclei get back into phase the signal will start to increase and after that decrease again. During the refocusing of the nuclei an x-gradient is applied and at the same time the signal is read and processed. However, if only a positive x-gradient is applied during the signal the nuclei will de-phase much faster and thus a lower signal will be received (figure 21b). This is why first a negative x-gradient is applied. Due to the negative gradient the nuclei will go a bit more out of phase, but by applying the same gradient in the positive direction the signal will be back in phase at the peak of the signal (Figure 21a).

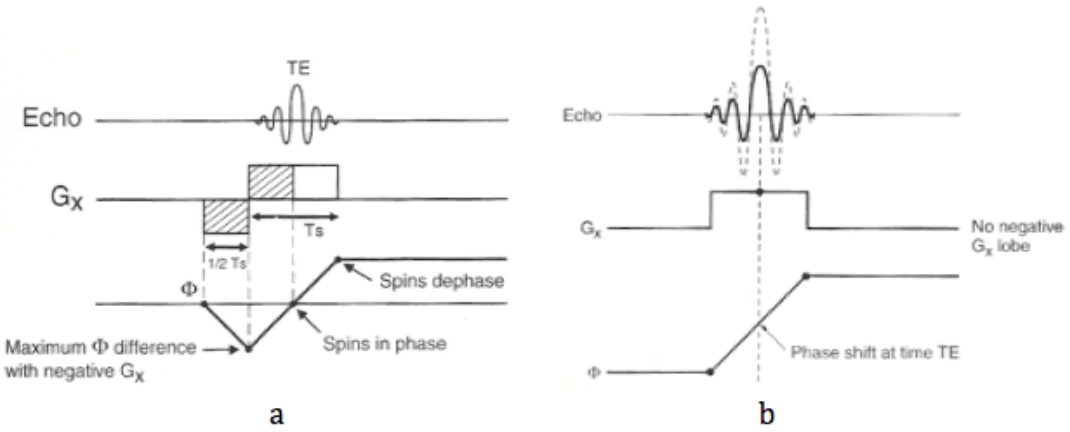

Figure 21 a, A negative x-gradient ensures that at the peak of the signal the net-gradient is zero. This gives a maximal signal. b, If the negative gradient is not applied the peak of the signal will be at the moment when the nuclei are already getting out of phase again. [2]

After the signal is obtained the same phase encoding step is done for a different slice. After all 28 slices are obtained the TR is over and a different phase gradient will be applied for all slices during one TR.

Fast/Turbo spin echo (FSE/TSE)

FSE is mainly used to increase the scanning speed. In normal SE only one phase encoding step is done for several slices during one TR. With FSE however, several phase encoding steps are done by applying more 180° pulses within one TR. The last 180° pulse will generate the lowest signal according to T2-decay. However, the strength of the signal is also influenced by the strength of the y-gradient. The stronger the gradient the more the nuclei get out of phase and thus the signal gets lower (Figure 22).

Depending on the kind of weighting you need, T1- , T2-, or PD-weighting, you choose your lowest gradient to be on a certain moment so you get the strongest signal from that echo. If you want a T2-weighted image you need a long TE, so the strongest signal has to come at a later time as can be seen in Figure 22. The number of 180° pulses used is called the echo train length (ETL). The longer the ETL the smaller the AT will be, because in FSE the AT is divided by the ETL. Since the highest signal is obtained from the lowest gradient this signal will be put in the center of k-space, which is where all the contrast is. The lower signals are placed in the outskirts of k-space, which provide the resolution and thus do not need a high signal (Figure 22). For T1- and PD-weighting a small ETL is used, because you want your maximal signal to be as soon as possible. This does mean that your scan time is a bit longer then for T2-weighted. However, because the ETL is smaller more time is left to scan other slices and thus more slices can be obtained with a shorter ETL.

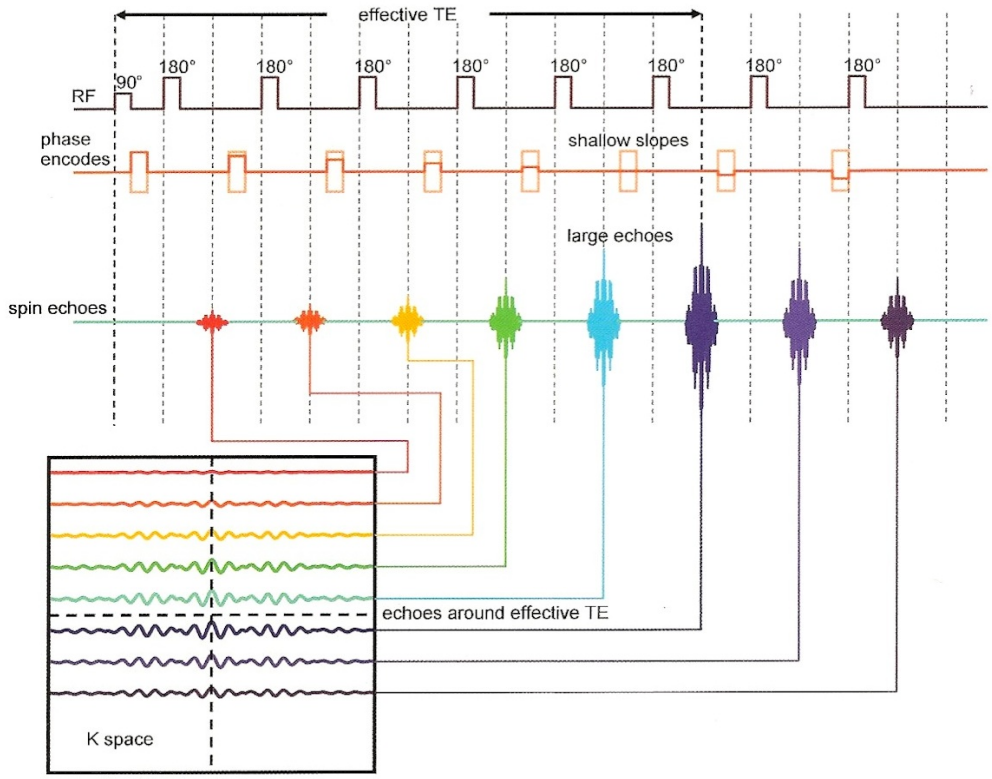

Figure 22 A FSE sequence. Multiple echoes are obtained during one TR. Each echo will fill a line in k-space. The echo with the lowest gradient will be placed in the middle of k-space, because this echo has the highest signal and the center of k-space contains all contrast. The largest echo that is received determines the contrast that is being used, T1-, T2, or PD-weighted images. [18]

Inversion recovery (IR) techniques

FSE was used to increase the speed of scanning, but IR is used to increase the signal of certain tissues by suppressing signals from other tissues. This is done by applying a 180° RF-pulse that flips all nuclei into the negative z-direction (Figure 23), before the excitation pulse of 90° is applied. In figure 23 two tissues (A & B) experience a 180° RF-pulse. Their magnetization flips into the negative z-direction and after they start to recover. Both tissue A and B will pass the transversal plane when the longitudinal magnetization is zero. If tissue A needs to be suppressed then the 90° RF-pulse must be applied when tissue A is in the transversal plane. The time between the 180°- and 90° RF-pulse is called the inversion time (TI). The 90° RF-pulse will flip tissue A back into the negative z-direction. This means the magnetization in the transversal plane is zero for tissue A, but tissue B does give a signal, which can be seen in the decay graph of Figure 23.

When the signal of fat is totally suppressed it is called short tau inversion recovery (STIR), for fluids it is called fluid attenuated inversion recovery (FLAIR). IR is not a very specific technique because all nuclei are flipped into the negative z-direction and thus all are affected. However, when a spectral saturation pulse is used only the frequency of one tissue is flipped. This frequency resembles the Larmor frequency of that tissue and thus saturates the magnetization of the nuclei in that tissue.

IR techniques can both be used in SE sequences and GE sequences. For imaging atherosclerotic plaques, fat suppression can be used to improve the image quality when going from fatty lipids to watery tissue.

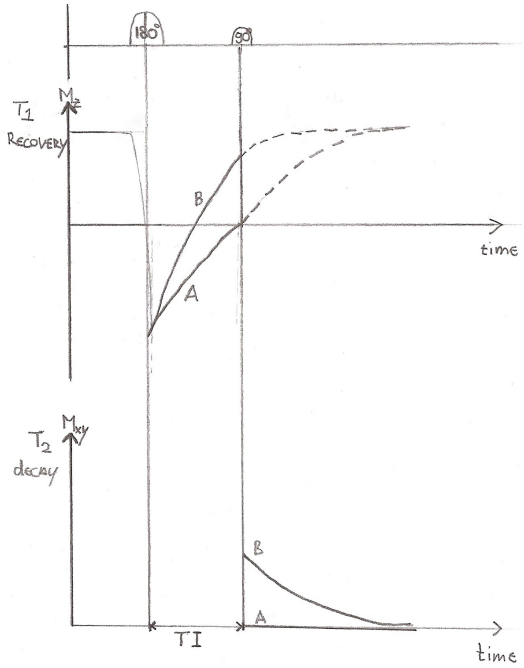

Figure 23 When a 180° RF-pulse is applied the magnetization of both tissue A and B flip into the negative longitudinal axis. If after the inversion time (TI) a 90° RF-pulse is applied, Then tissue A is suppressed.

2.4.3 Gradient echo sequences

The big differences between GE and SE are, that in GE there is no 180° refocusing pulse and the FA is not 90°. The consequences of these changes are fast de-phasing of the magnetization and thus a fast decay of signal and there is no time for full recovery if a 90° FA is used, so instead an α-pulse is used (α is between 1-90°). The GE sequences that can be used for this research are 2D and 3D GE, 2D and 3D fast spoiled GE sequences.
Right after the α-pulse the signal will start to decay (FID) (Figure 24, first signal). It is not possible to measure the FID, because this signal decays too fast to measure. By first de-phasing the FID signal and re-phasing it right after that, the signal is somewhat slowed and then it can be measured (Figure 24, Gx). The echo is the delayed version of the FID and this can be measured.

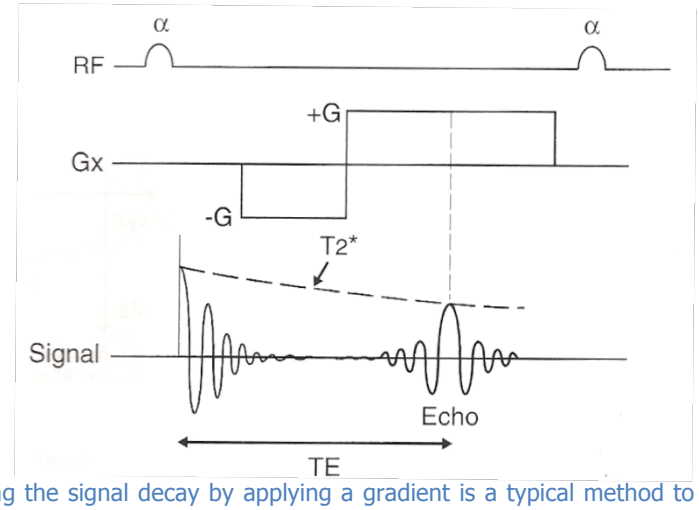

Figure 24 Slowing the signal decay by applying a gradient is a typical method to obtain signal for GE sequences. [2]

A typical gradient echo sequence can be seen in Figure 25. As can be seen only one slice is imaged each TR. However, the TR is very short (20-50ms) so the total acquisition time does not increase due to this fact.

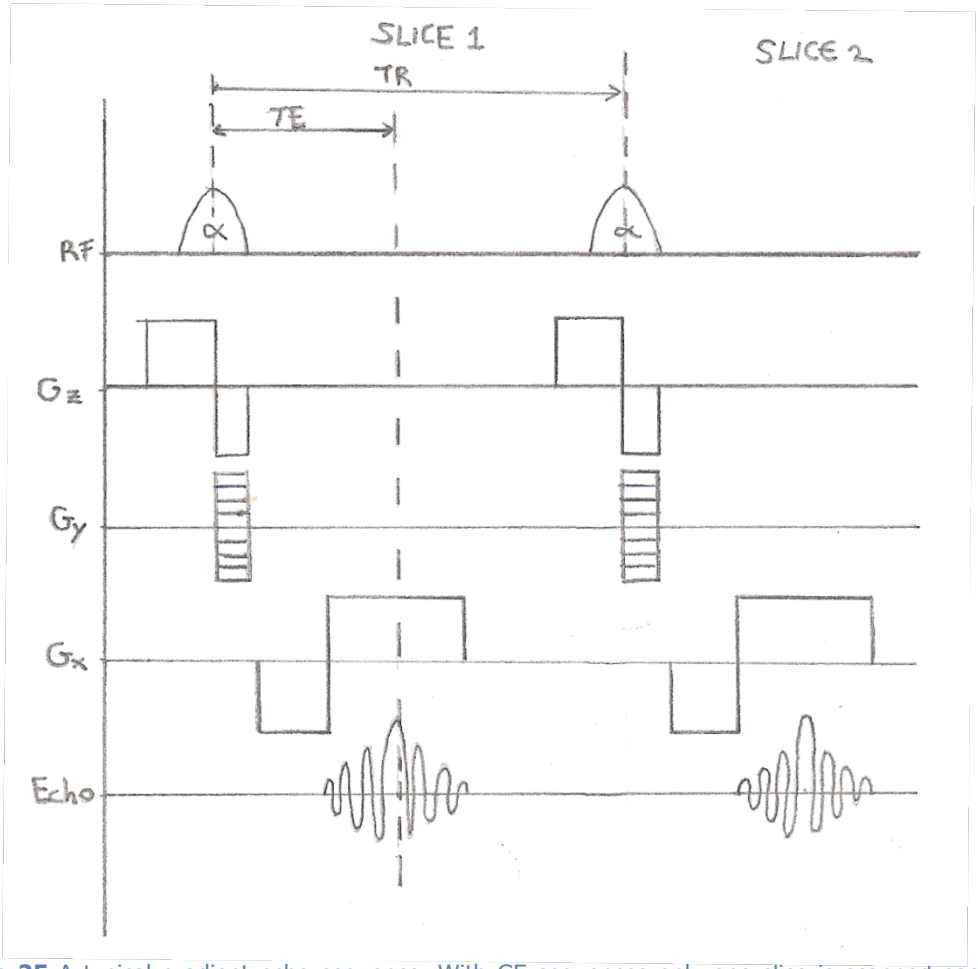

Figure 25 A typical gradient echo sequence. With GE sequences only one slice is scanned each TR. This would increase the scanning time a lot with respect to SE sequences, if the TR of GE sequences were not so short.

The z-gradient is turned on and shortly after the RF-pulse is transmitted. During this time the y-gradient is turned on as well to introduce a phase change for phase encoding. This is done simultaneously with the slice selection to decrease the time for one TR. When this is done the x-gradient is turned on to create and read the echo. After time TR the whole process is repeated for the next slice.

Spoiled GE

After the echo is read there is still transverse magnetization left. With spoiled GE imaging the gradient in the end of the PSD is placed in the same direction as the first to bring the leftover transverse magnetization more out of phase. Due to this de-phasing the signal that is left will not contribute to the contrast of the next slice. For this de-phasing both z- and y-gradients can be used. However, it is also possible to use an RF-pulse that only excites molecules in a certain phase. Because the magnetization is totally out of phase it will not contribute to the next echo measurement and thus the influence of the transverse magnetization on contrast is suppressed

Fast gradient echo

Fast GE is used to increase the speed of the whole process. The speed of GE imaging is increased by using only a portion of the RF-pulse and only reading a portion of the echo. This reduces the TE times needed and thus reduces the TR. Extra contrast is obtained by using pre-saturation pulses before the first excitation pulse, just as in inversion recovery.

2.4.4 Artefacts

Besides a good SNR, high resolution and short AT, it is also important to see the right anatomy. Many artifacts can occur during an MRI scan and many can be overcome by adjusting your sequence. Artefacts that can occur during an MRI scan of an atherosclerotic plaque are:

- Flow artefact
- Aliasing or wrap around
- Chemical shift artefact
- Chemical misregistration (Chemical shift artefact of the 2nd kind)
- Magnetic susceptibility artefact
- Cross excitation and cross talk
- Shading artefact
- Ghosting
- Partial volume artefact

Flow artefact

When imaging atherosclerotic plaques in vivo in the human body there will be a blood flow. However, this project will be done ex vivo, which means that there will not be any flow. In Apendix A the artefact due to flow will be explained, because eventually in further research the atherosclerotic plaques need to be imaged in vivo to test the model on humans.

Aliasing and wrap around

Aliasing is produced when anatomy outside the field of view (FOV) is imaged inside the FOV. The anatomy that is outside the FOV still produces a signal though it has a different frequency and phase. There can be wrap in both the frequency direction and the phase direction. Aliasing in the frequency direction occurs if frequencies are not sampled often enough (Figure 26).

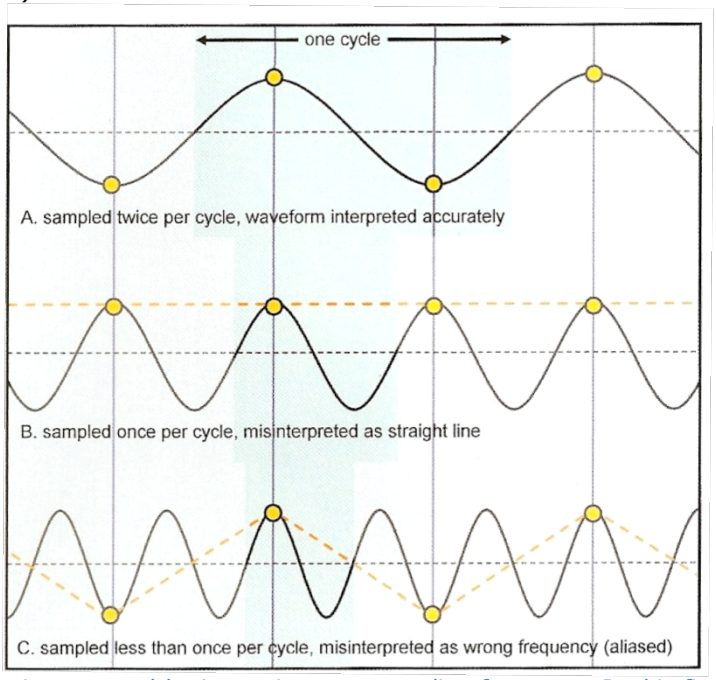

Figure 26 Aliasing is prevented by increasing your sampling frequency. In this figure it can be seen how under sampling changes frequency that is received. [18]

The sampling frequency should at least be twice as high as the received maximum frequency. When there is wrap around in the phase encoding direction, than phases outside the FOV have the same phase as certain phases inside the FOV and this folds anatomy outside the FOV inside the FOV (Figure 27).

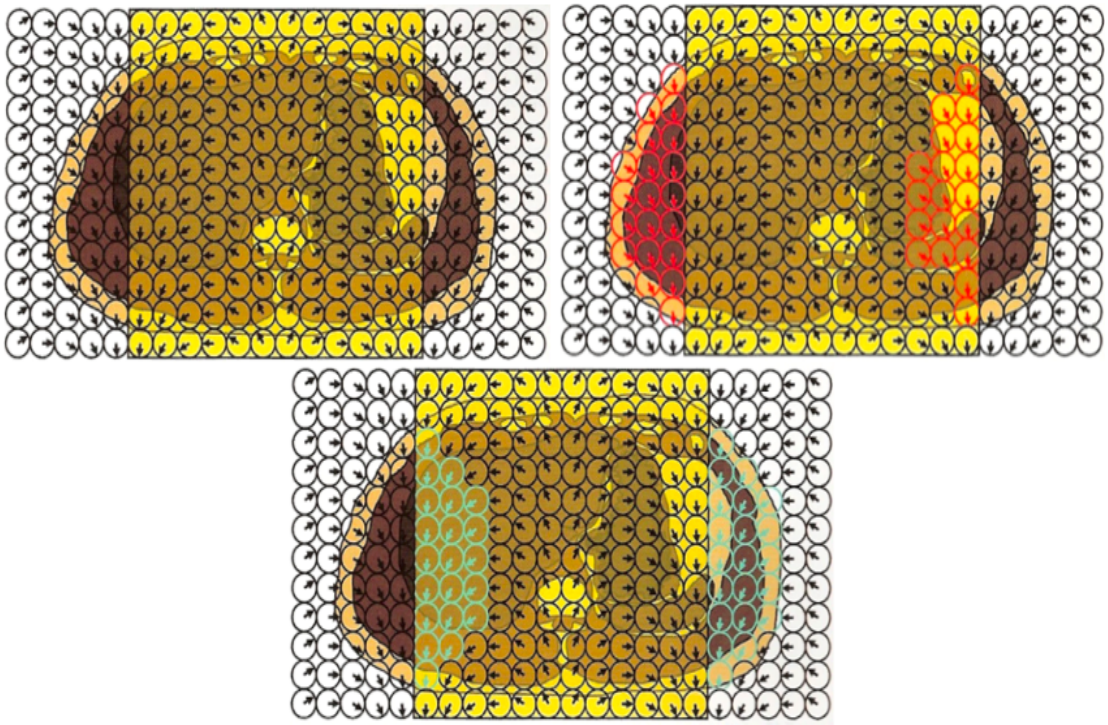

Figure 27 In the top left picture it can be seen that not the whole volume is included in the FOV. The phase gradient however, does continue outside this FOV. In the top right picture it can be seen that certain phases inside the FOV resemble those outside the FOV. This will cause a wrap around in the final image as is seen in the bottom picture. [18]

To compensate for frequency aliasing the sample frequency must be increased. This also means that more noise is sampled, but this can be reduced by applying a frequency filter.
Phase wrap can be compensated for by increasing the FOV in the phase direction. If al the anatomy is in the FOV there will not be any wrap around. However, by increasing the FOV in the phase direction, the spatial resolution also reduces.

Chemical shift artefact

This artifact occurs when there is a transition from fat to water. The lipid pool in an atherosclerotic plaque consists mostly of fat and the buffer has a lot of water in it so a chemical sift might occur. Though both water and fat have H_1-atoms, the Larmor frequency of the atoms is different. At 1,5T they differ 220Hz (Water precesses faster than fat). If the field strength becomes stronger this difference increases. If the receive bandwidth (BW) is ±16kHz and the matrix in the x-direction is 256, then each pixel has a BW of 125Hz. Since the difference in frequency, between water and fat, is 220Hz this means that the fat border will shift 2 pixels to the right. In between there is no signal reported so a black line will be seen on one side and a white on the other (Figure 28) in the frequency direction. This artefact can be solved in several ways. One way is to reduce the main magnetic field of the scanner. This will decrease the frequency difference, but also the signal that is obtained. Decreasing the FOV also decreases the size of the chemical shift. If the FOV is 20cm with a matrix of 256 then the resolution is 0.78mm. As was calculated before the chemical shift is two pixels so this results in a black line of 1.56mm. By decreasing the FOV

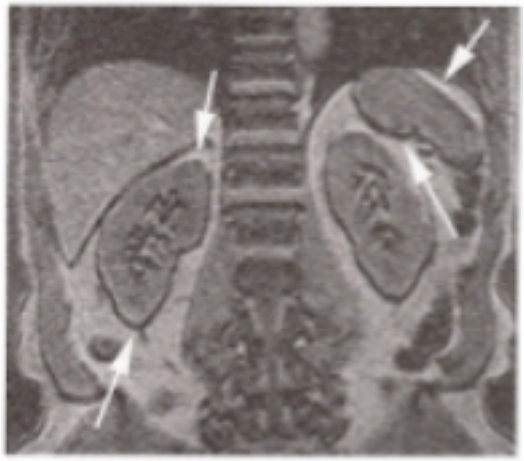

Figure 28 The arrows show where the chemical shift has occurred. On the top arrows a white line can be seen and at the bottom the black border is seen. [2]

the size of the chemical shift will reduce. Reducing the FOV also means less signal is obtained thus a lower SNR. Increasing the receiver BW will increase the BW of a pixel. If the receive BW is increased to 64kHz then the BW of a pixel is 250 and thus only 1 pixel shift will be seen, which reduces the width of the black line. However, by increasing the receive BW you also measure more noise which decreases the SNR.
Another possibility is using a suppression technique. If either water or fat is suppressed, chemical shift cannot occur because there is no signal coming from one of these substances.

Chemical misregistration (chemical shift of the 2nd kind)
This artefact happens due to the phase difference that occurs because of the precessional difference between water and fat. When the image is acquired at the moment that water and fat are out of phase, then the signal will be nulled at their interface. This creates a black line around the border. This artefact can be overcome by selecting the right TE (Figure 29a-b).

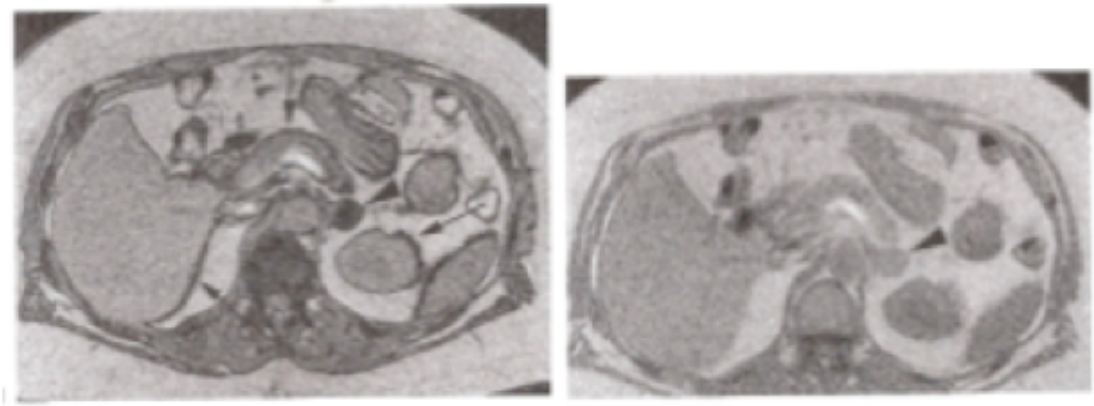

Figure 29 a, A chemical shift of the 2nd kind is seen as a black line around the organs. b, This is the same image only now the image was taken when both water and fat are in phase and thus there is no chemical shift of the 2nd kind. [2]

The frequency difference at 1.5T between water and fat is 220Hz, which means that they are in phase every 1/220=4.5msec. If the TE is 2.25msec the black line will appear around the water/fat interfaces, but when TE is 4.5msec this will not happen.

Magnetic susceptibility artefact
Magnetic susceptibility occurs when there is a substance (usually a metal) that can become magnetized. This causes de-phasing and thus a loss of signal. This artefact can be reduced with SE sequences, because they use a 180° pulse to re-phase the nuclei. This will reduce the susceptibility artefact, but GE does not use this refocus pulse and thus will be more affected.
Decreasing the TE also reduces the time the nuclei have to de-phase. So the best sequence that can be used is either a PD- or T1 SE sequence. When there is a hemorage this might cause some susceptibility artefact, because blood contains iron.

Cross excitation and cross talk
An RF-pulse is not perfectly square, but has a parabolic form and the basis is a bit bigger then the slice thickness (Figure 30). This means that neighboring slices get a bit excited as well and get saturated. This will influence the contrast of the next slice. This is called cross excitation. Preferably the distance between slices is zero so this artefact might occur during this research.

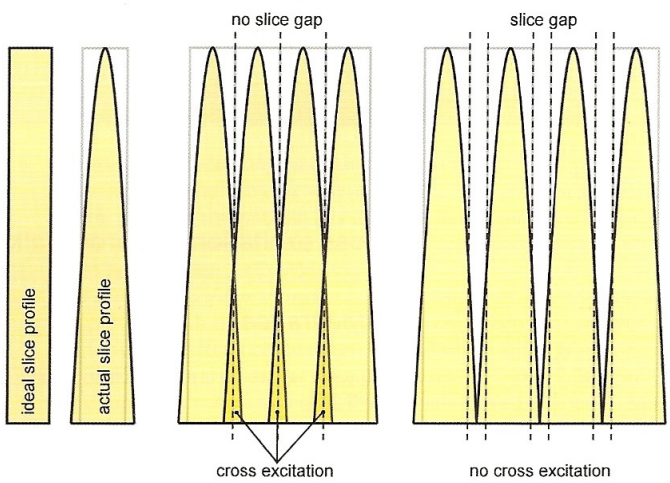

Figure 30 Cross excitation occurs because the RF-pulses are not perfectly square. By leaving a gab between slices this problem can be overcome. [18]

A second effect happens due to the relaxation of the nuclei. The nuclei will exchange energy to their neighboring nuclei (spin lattice relaxation). The nuclei in the neighboring slice thus receive energy, which is called cross talk. Cross talk cannot be eliminated, because it is natural dissipation. Cross excitation on the other hand can be reduced by leaving a gap between slices. A second solution is that first slices 1,3,5,7,9,… are acquired and after 2,4,6,8,… This way the even slices have time to recover from cross excitation before they are imaged.

Shading artefact

The shading artefact produces a difference in intensity along the imaging volume. This artefact occurs if a surface coil is used. The further the point in the object is from the surface coil the weaker the signal will be.

Ghosting

Ghosting occurs when the sample inside the MRI scanner moves. This movement can occur due to vibrations in the gradient coil. This artefact only occurs if there is movement in the phase encoding direction, because every TR only one phase encoding step is acquired so when the sample moves the data is no longer aligned. One way to overcome this problem is by switching the phase encoding direction with the frequency encoding direction. This only works if there is no movement in the frequency direction.

Partial volume artefact

When the resolution is low the size of the voxels increases. A big voxel might contain two different tissues, which means that the resulting contrast is an average of both tissues. In an atherosclerotic plaque there are small structures, so if a low resolution is used the different structures will merge resulting in fading boundaries between structures. This artefact can be reduced by increasing the resolution.

2.5 Concluding remarks

At this point the basic concepts of MRI, contrast mechanisms, spatial encoding, trade offs between imaging parameters, imaging sequences, and artefacts have been discussed in this chapter. How this knowledge is converted to an optimal sequence for plaque imaging depends on the scanner at hand. Both the hardware, including the field strength of the main magnetic field and the receiving coils, and the software play a big role in choosing the parameters to achieve good image quality. The image quality needed for this project is reflected by the imaging demands, which are:

- Good contrast between, the intima, media, adventitia, lipid pool and calcium (Figure 3).
- A good signal to noise ratio (SNR) to make delineation of the contours possible.
- An in-plane resolution lower then 65μm, which is the upper limit for cap thickness in a vulnerable plaque [21].
- A maximum slice thickness of 1mm to minimize partial volume artefact.
- Minimize the AT to prevent degradation of the artery.

The first image demand is achieving a good contrast between the different components in the plaque. We have learned that the contrast is determined by the TR, TE and FA. The value for these parameters depend what kind of contrast is needed: T1-, T2- or PD-weighted. The values however change when the strength of the main magnetic field changes. So if we want to find TR, TE and FA values in literature we need to find a paper that uses an MRI scanner with the same field strength as ours (7 Tesla). A study that uses the same magnetic field strength as us is from Jahnke et al. [22]. In this study a 3D SE sequence was used that gave good contrast between plaque components. The in-plane resolution is high (79x79μm) and the SNR is good as well. However, the AT was 13 hours, which is to long. This means that this sequence is not an option and needs to be adjusted to suffice the time demand. The contrast parameters TR and TE however, can be used as a guideline to achieve contrast in SE sequences. Also GE sequences, used to image atherosclerotic plaques, were found in literature, but the field strength of the scanners used for these images was lower then 7 Tesla [23-25]. This means that it is not possible to use contrast parameters from these papers.
The use of a coil in the MRI scanner increases the SNR, which on itself will give more flexibility in increasing resolution or decreasing the AT. When looking in literature different coils are used for different setups. The difference in use of coils is mainly apparent when comparing in vivo experiments with ex vivo experiments. When in vivo experiments are done the arteries close to the skin (carotids) are imaged by using a surface coil [26-29]. With ex vivo experiments most papers use a birdcage coil or whole body mouse coil [22, 24, 25, 30]. Both these coils envelope the whole volume and thus give a good SNR.
Since no paper is found that resembles the scanner we use, the coil we use, or that suffices the imaging demands that we state, it is important that we perform pilot experiments. The knowledge obtained from this chapter will be used to find a good imaging sequence during these pilot experiments. The methods and results from these pilot experiments will be discussed in the next chapter.

3. MRI sequences for atherosclerotic plaques: Pilot experiments

In the previous chapter the theoretical background of MRI is discussed. This knowledge together with the information found in literature will be used to find an imaging sequence that fulfills the imaging demands (Section 2.5). To be able to perform pilot experiments, arteries with atherosclerotic plaques are needed (Section 3.1). The arteries must be placed in a setup and the setup must be placed in the MRI to make imaging possible (Section 3.2). If the arteries and setup are ready the pilots can be started to find the best imaging protocol (Section 3.3). From the results of the pilots an imaging protocol is obtained (Section 3.4).

3.1 Atherosclerotic plaques

For this study we used atherosclerotic arteries from ten pigs. The pigs had a varying degree of diabetes and were placed on a western diet to induce plaque growth. The pigs were used to evaluate stents. Visual inspection showed that the iliac arteries contained plaque as well. Since these arteries were not used for other studies we were able to obtain them. From each of these pigs we were able to obtain the left external iliac and the internal iliac (Figure 31). After the arteries were removed we collected them in a bowl filled with phosphate buffered saline (PBS). The PBS was used to keep the artery fresh.

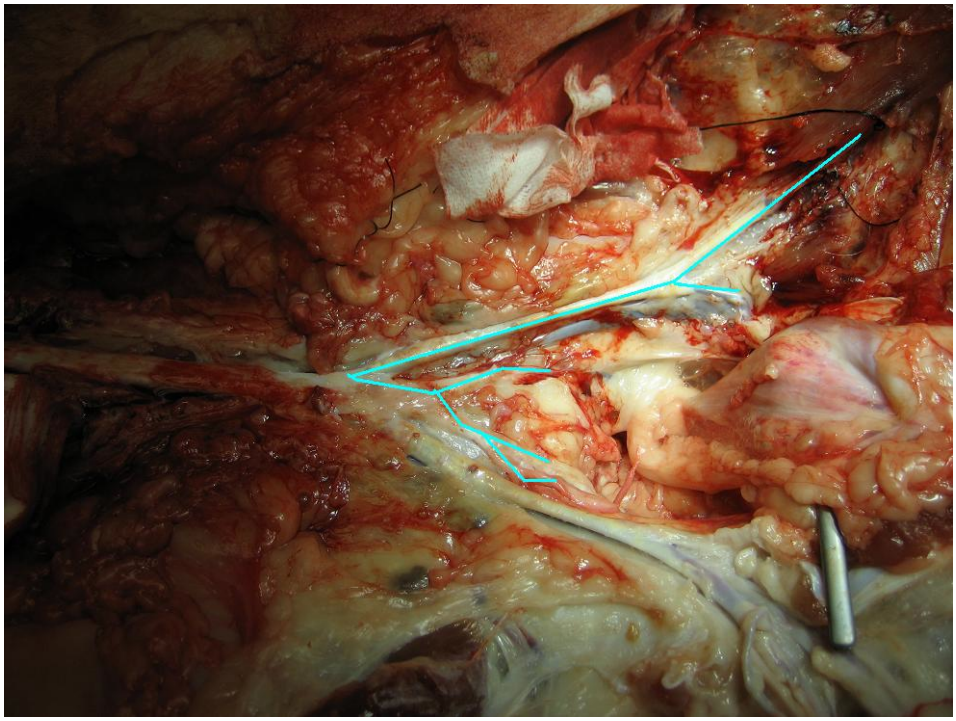

Figure 31 A picture of the external- and internal iliac artery. The external iliac artery is the long blue line at the top. The smaller blue lines, below the long line, that form a 'Y' are the left and right internal iliac.

The arteries were cut into segments (Figure 32). Each segment was imaged with an ultrasound scanner to see how diseased the arteries were. To preserve the arteries they were snap frozen and stored at -80°C. Snap freezing was performed by putting a segment in an empty tube and place the tube in liquid nitrogen. The temperature drop will be fast, which prevents ice crystals from forming. This technique has shown to preserve the mechanical properties of arteries [31]. More information about the preservation techniques can be found in Appendix B. From the ten pigs, 55 segments were obtained. For the pilot three arteries

were chosen that had a diameter smaller then 10mm, a length in between 20-30mm, contained plaque and contained calcium.

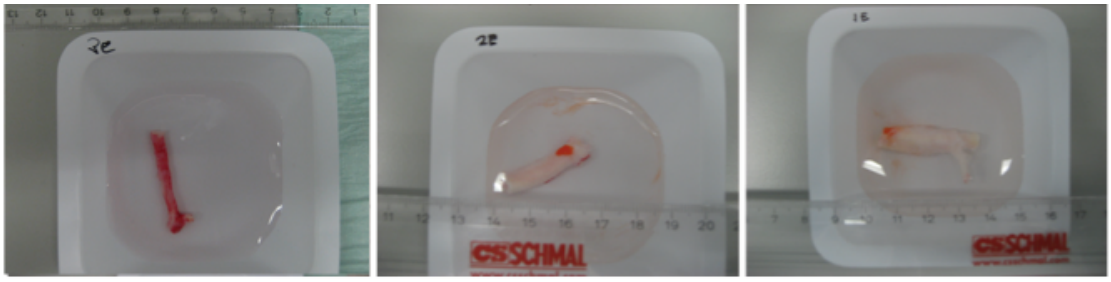

Figure 32 These three arteries were used in the pilots. a Pilot 1, b Pilot 2&3, c Pilot 4&5.

3.2 The setup

Figure 33 shows the setup that is used during the pilots. The artery is connected to cannules and placed in a closed tube. In both the tube and artery will be Krebs buffer to keep the artery fresh. On the left of the setup is an in-flow tube for the buffer and on the right is the outflow tube. There is also a pressurizing inlet (Pin) on the left of the setup. A syringe is connected to this inlet to control the pressure in the artery, to prevent collapsing of the artery. When the artery is removed from the body it will shrink about 30% in length [32, 33]. The artery can be pre-stretched by pulling on the tube to the left. This will move the left cannule backwards and thus the artery is stretched. The left tube can then be fixed with the left fixating screw.

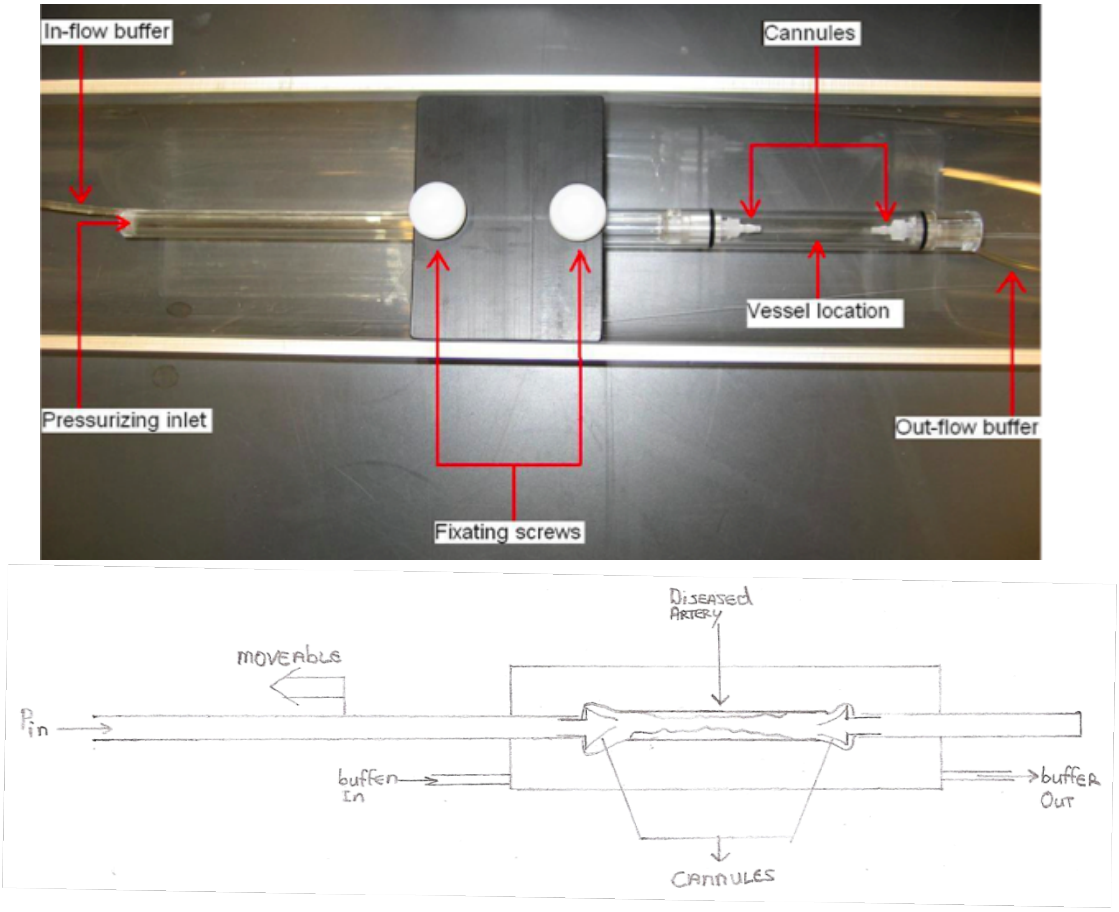

Figure 33 Photo and sketch of the setup that was used for the pilots.

The setup is placed in a half cylinder, which fits in the MRI scanner. Underneath the tube that contains the artery segment a cardiac surface mouse coil is placed to increase the SNR (Figure 34a). The setup is placed in a Discovery MR901 7T MRI-scanner (General electrics, Fairfield, Connecticut, USA) (Figure 34b).

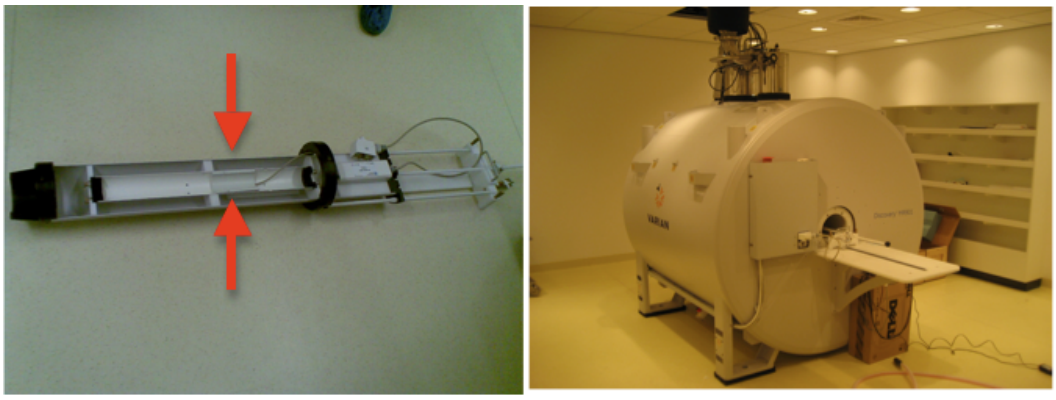

a b

Figure 34 a, Here the sliding table is shown where the setup will be placed on. Between the red arrows the cardiac mouse surface coil can be seen. b, The sliding table will be placed in this 7 Tesla MRI scanner.

3.3 The imaging protocols

In total five pilots were performed to find the optimal settings for imaging atherosclerotic plaques. From theory can be concluded that GE and SE techniques can be used to obtain images. In literature we found only one paper that used SE at 7 Tesla. The parameters from this paper can be used to obtain images similar to the once obtained by Jahnke et al. [22]. In the first pilot some random sequences were used to get acquainted with the MRI scanner. The pilots 2-4 were used to optimize the contrast. In pilot 5 the resolution, SNR and AT were optimized with respect to our imaging demands.

Pilot 1

Figure 35 shows two of the results that were obtained during the first pilot. Table 3 shows the parameters that were used for these two images.

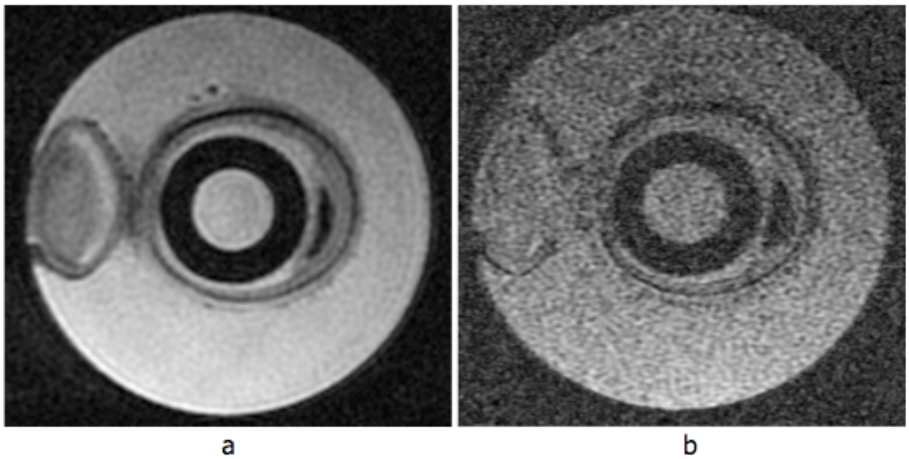

a b

Figure 35 a, A T2 2D FSE. b, A T1 2D spoiled GE.

In the middle a bright circle can be seen. This is the Krebs buffer that is in the artery. The black circle is the cannule to which the artery is tied and fixed to the setup. Then there is again some buffer that is also in the artery. Between two and five o'clock a small plaque can be seen, with a black spot inside of it. This black spot can be calcium. The artery wall can clearly be seen. Between seven and eleven o'clock a second artery wall can be seen. This is a side branch of the artery.

In Figure 35a we used a T2 2D FSE sequence and in Figure 36b we used a T1 2D fast spoiled GE sequences. In Table 3 the MRI parameters can be seen for these two images. As can be seen the SNR with the FSE is better then with the GE sequence. This is due to the fact that the resolution for the GE is higher and the compensation with the NEX is not high enough. The AT is very low so it would be possible to increase the NEX 4 times, which would increase the SNR. Contrast wise both the FSE and GE sequence seem to be able to identify the plaque and the calcium. However, the plaque is small and this makes it hard to give a qualitative conclusion on the contrast.

Table 3 Parameters used for the images from Figure 42a,b.

	Figure 36a	Figure 36b
TR (ms)	2200	40
TE (ms)	36.8	14.3
FA (°)	90	40
FOV	40	25
Aq. Matrix	384x384	384x256
Resolution (μm)	104x104	65x97
Slice thickness (mm)	0.5	0.3
Spacing (mm)	1	0.3
# Slices	12	10
NEX	8	12
ETL	6	1
BW (kHz)	22.7	32.1
AT (min)	12	2.5

Pilot 2

For the second pilot a more diseased segment was selected as can be seen in Figure 36a-d. Table 4 contains the parameters used for these images.

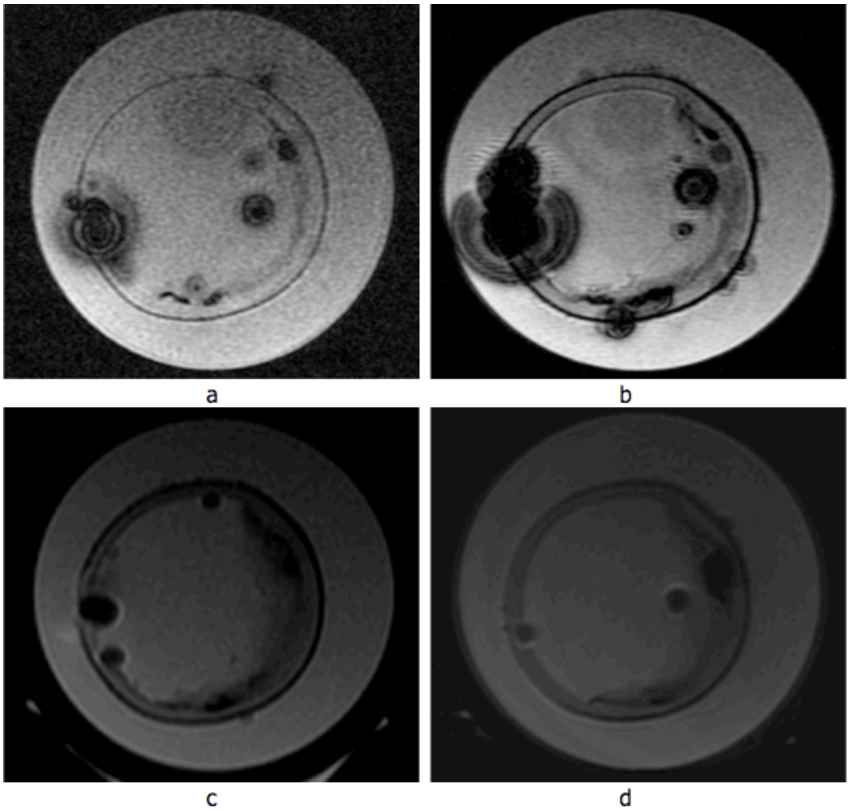

Figure 36 a, T1 3D fast spoiled GE. b, T2* 3D GE. c, T2 2D SE. d, T2 2D FSE.

The black circles that are seen in the images are artefacts created by air bubbles. The plaque is located between one and seven o'clock. Some calcium can be seen between one and three o'clock and five and seven o'clock. The contrast in Figure 36a belongs to a T1 3D fast spoiled GE, which shows almost no contrast in the plaque and the artefact due to the bubbles makes it impossible to delineate contours. In Figure 36b a T2* 3D GE sequence is used. The contrast in this sequence has improved in comparison with the T1 3D fast spoiled GE. Some contours can be seen in the plaque, but the artefact due to the bubbles is still too big. The reason why both GE sequences have so many artefacts due to the bubbles is, because with GE there is no refocusing pulse for the phase. This means that the artefacts become clearer when the spins go more out of phase (Section 2.4). Figure 36c is an image of a T2 2D SE, which does have a refocusing pulse. It can be seen that the artefact of the bubbles has decreased significantly. The contrast within the plaque has also increased, but the contrast between the plaque and the lumen is not good enough to delineate. The same counts for Figure 36d, which is a T2 2D FSE. The SNR seems to be higher then in the SE sequence and can be attributed to the NEX of this sequence, which is eight times higher then in the other sequences (Table 4). A difference that can also be seen between the SE and FSE is that with the FSE you can see some ghosting, which is not seen in the SE sequence. The reason why this ghosting appears is unknown. However, if we want a better SNR in the SE sequence the time will increase a lot in comparison with the FSE. Because the SNR in the SE is lower the shading artefact due to the cardiac surface coil can be seen more clearly. In all of the images a thick circular black line can be distinct. This line can be an artefact due to chemical misregistration (Section 2.4.4).
It seems that in case of bubbles the SE sequences are preferred over the GE sequences. For the contrast the T2/T2* sequences seem to give better contrast then the T1 sequence. With respect to artefacts both SE and FSE have their pros and cons.

Table 4 Parameters used for the images in Figure 43a-d.

	Figure 37a	Figure 37b	Figure 37c	Figure 37d
TR (ms)	40	30	4000	2200
TE (ms)	4	20	30	37
FA (°)	50	20	90	90
FOV	25	25	25	40
Aq. Matrix	384x256	384x256	256x192	384x384
Resolution (μm)	65x97	65x97	97x130	104x104
Slice thickness (mm)	0.6	0.6	1	0.5
Spacing (mm)	0.6	0.6	1	1
# Slices	8	28	12	12
NEX	1	1	1	8
ETL	1	1	1	6
BW (kHz)	31.2	14.7	11.9	22.7
AT (min)	2.05	4.15	7.8	11.8

Pilot 3
For the third pilot the same artery as in pilot 2 is used, which can be seen in Figure 37a-c. The parameters for these images can be found in Table 5. In this pilot we tried to reduce the amount of bubbles in the artery to improve the result of the GE sequence. The resolution of the SE and FSE were increased to see how much the SNR would decrease. We also tried to improve the contrast between the plaque and the lumen.

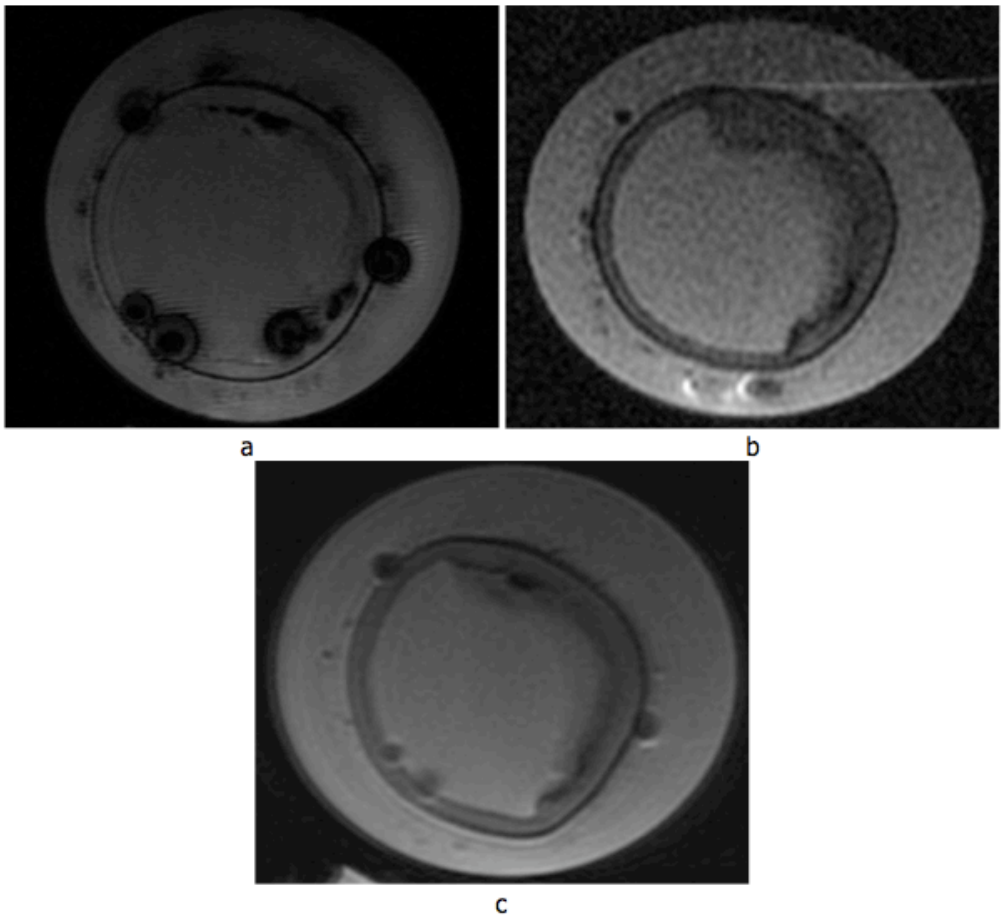

Figure 37 a, T2* 3D GE. b, T2 2D SE. c, T2 2D FSE.

There are still too many bubbles in the artery, which cause artefact for the T2* 3D GE sequence (Figure 37a). For the T2 2D SE sequence the resolution was increased from 97x130 µm to 59x78µm with respect to the last pilot. It can be seen that the SNR has decreased significantly (Figure 37b). The increase in AT will be to great to compensate for the loss in SNR and thus the SE sequence does not qualify to perform high resolution scans in a reasonable AT. For the T2 2D FSE echo the increase in resolution did not influence the SNR (Figure 37c). For this sequence several changes in TR and ET have been tried to improve the contrast between plaque and lumen, but the result seen in Figure 37c was the best contrast that was achieved. The contrast between the plaque and the lumen is still not sufficient.

Table 5 Parameters used for the images in Figure 44a-c.

	Figure 38a	Figure 38b	Figure 38c
TR (ms)	30	1500	2500
TE (ms)	10	30	31.8
FA (°)	20	90	90
FOV	25	15	12.5
Aq. Matrix	384x256	256x192	190x162
Resolution (µm)	65x97	59x78	65x77
Slice thickness (mm)	0.6	0.5	0.5
Spacing (mm)	0.6	0.6	0.6
# Slices	28	30	11
NEX	1	1	8
ETL	1	1	8
BW (kHz)	14.7	31.3	15.6
AT (min)	4.15	3.9	6.75

Pilot 4

A new segment was used for this pilot, which is heavily diseased as can be seen in Figure 38a-f. The parameters used to obtain these images can be seen in table 6. In this pilot we want to compare the sequences obtained from pilot 3, with the sequence from Jahnke et al. [22]. We also want to try a PD- and T1-weighted image to see if the contrast is better than the T2-weighted image. The arteries in this pilot are collapsed due to problems with the setup. This does not influence the results for the image protocol.

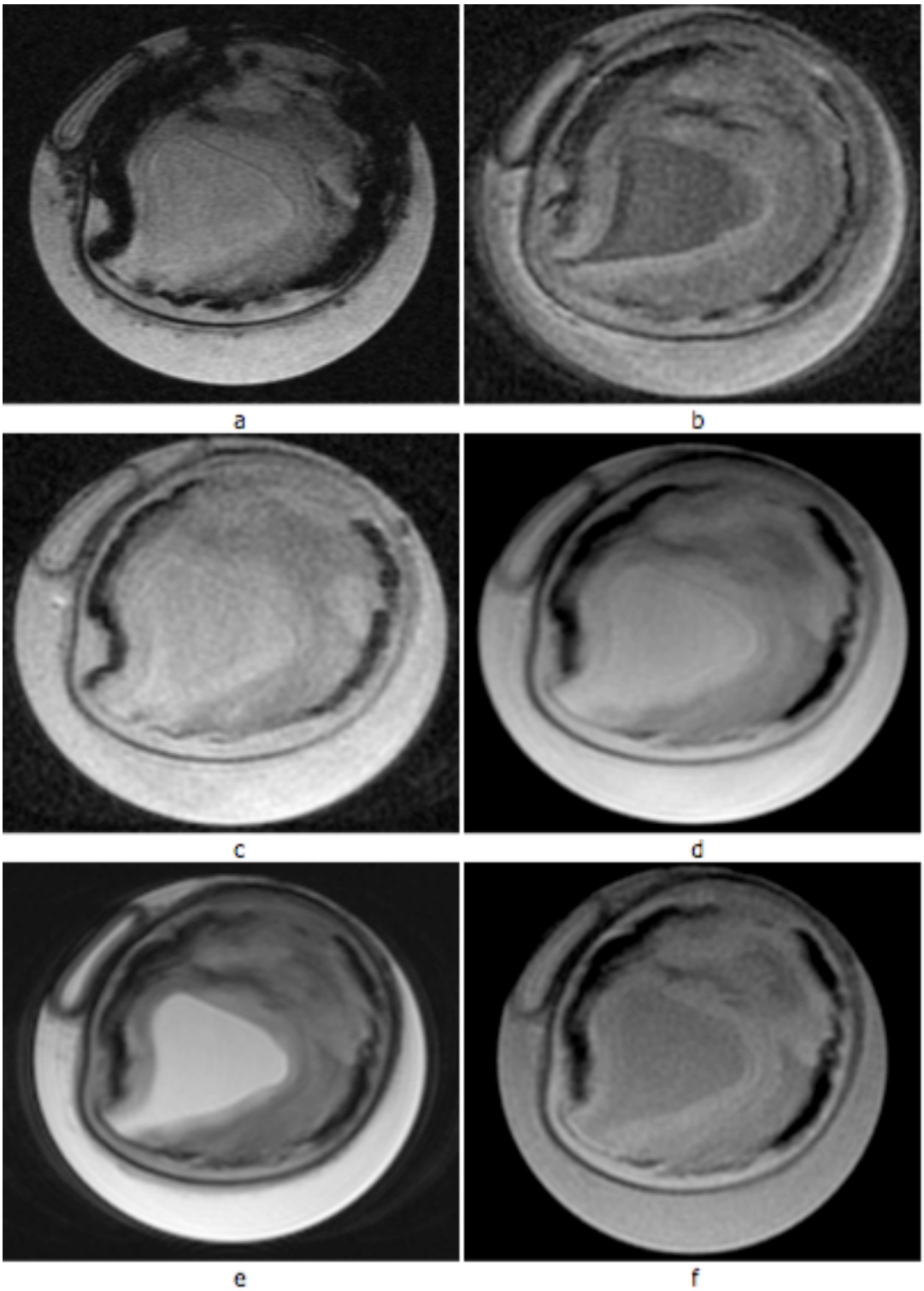

Figure 38 a, T2* 3D GE (Pilot 2). b, T2 2D FSE (Pilot 2). c, PD 2D FSE. d, PD 2D FSE (Jahnke et. al). e, T2 2D FSE (Jahnke et al.). f, T1 2D FSE (Jahnke et al.).

The 3D T2* GE sequence still gives too much artefact and will be discarded (Figure 38a). The 2D T2 FSE gives good contrast and plaque components can be seen, but the SNR is lower than in pilot three (Figure 38b). The reason for this is unknown since the sequence was copied from the last pilot. The 2D PD FSE also shows contrast inside the plaque, but the contrast between the lumen and the plaque is unclear (Figure 38c). The following three images were created with the TR, TE and FA from Jahnke et al. [22] as shown in Table 6. Instead of using a SE we used a FSE to decrease the AT. A 2D scan was taken instead of a 3D scan, because software to make 3D FSE is not available on this machine. The PD weighted image (Figure 38d) shows good contrast within the plaque, but the contrast between the lumen and the plaque is less pronounced. The difference with the PD weighted image from Figure 38c is that the TR has increased, which means that a stronger signal will be obtained because the magnetization has more time to relax. The contrast of the T2 weighted image is very good, also between the plaque and the lumen. Two important differences with the T2 weighted image from Figure 38b, is the increase in TR and TE. This means that a stronger signal will come from water, which will increase the contrast between the plaque and lumen as can be seen in Figure 38e. The T1 weighted image also shows good contrast within the plaque, but the contrast between the plaque and lumen is not sufficient (Figure 38f).
The contrast of the T2 weighted image from Figure 38e gave the best contrast, showing a lot of contrast within the plaque as well as a good contrast between lumen and plaque. The resolution of the image is still a bit low. The AT however is reasonable, but this will change when the resolution is increased. The best thing to do to increase the resolution is to keep the matrix the same and decrease the FOV, because this will not influence your AT. However, the SNR will decrease and this can be compensated for by using a small receiver bandwidth and a higher NEX. The increased NEX however, will also increase the AT.

Table 6 Parameters used for the images in Figure 45a-f.

	Fig. 39a	Fig. 39b	Fig. 39c	Fig. 39d	Fig. 39e	Fig. 39f
TR (ms)	35	2200	2200	2500	2500	500
TE (ms)	20	36.8	10	13.5	67.4	12.9
FA (°)	20	90	90	90	90	90
FOV	25	40	40	40	40	40
Aq. Matrix	384x256	384x384	384x384	384x384	384x384	384x384
Resolution (μm)	65x97	104x104	104x104	104x104	104x104	104x104
Slice thick. (mm)	0.6	0.5	0.5	2	2	2
Spacing (mm)	0.6	2.5	2.5	3	3	3
# Slices	50	12	12	10	10	10
NEX	1	8	8	8	8	8
ETL	1	6	6	8	8	8
BW (kHz)	13.9	22.7	31.2	62.5	14.7	20.8
AT (min)	8.1	11.8	11.8	10.1	10.1	6.1

Pilot 5

The T2 2D FSE sequence form the previous pilot provided the contrast that is needed. In this pilot a balance will be found between resolution, SNR and AT, within our imaging criteria. The result that was found can be seen in Figure 39. The parameters used to obtain this image can be seen in Table 7.

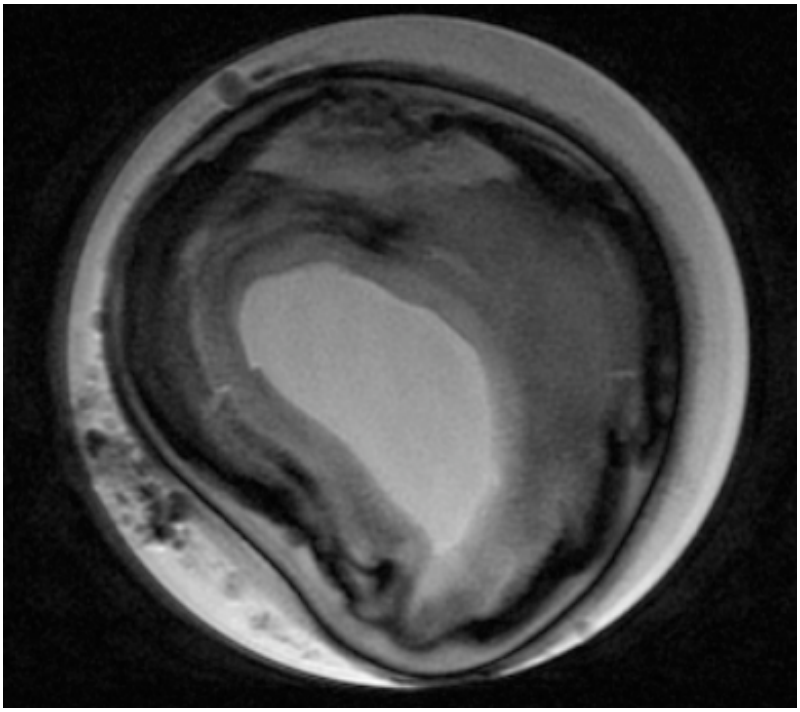

Figure 39 T2 2D FSE.

The resolution of the image was increased by decreasing the FOV, because this does not influence the AT directly. The loss of SNR was compensated by using a small receiver BW and a high NEX. The contrast of the image is again very good and the SNR is good enough to still draw contours. The resolution of this image is 52x52μm in plane and has a slice thickness of 1mm, with an AT of 64 minutes. The shading artefact is still present, but can hardly be seen. The black line around the artery is due to chemical misregistration artefact, but this does not obscure the image itself.

Table 7 Parameters used for the images in Figure 46.

	Figure 40
TR (ms)	2500
TE (ms)	70.9
FA (°)	90
FOV	20
Aq. Matrix	384x384
Resolution (μm)	52x52
Slice thick. (mm)	1
Spacing (mm)	0
# Slices	16
NEX	32
ETL	10
BW (kHz)	10
AT (min)	64

3.4 Discussion & conclusion

In total 85 sequences were used on three arteries to find an image sequence that fulfilled all the imaging requirements. Figure 39 shows an image that has contrast between several components in the plaque, the SNR is high enough to delineate contours and the in plane resolution is below the 65µm needed to identify the cap of a vulnerable plaque [21]. The high in-plane resolution was achieved at the cost of slice thickness and AT. The slice thickness is 1mm, but the biggest deformations are expected to be in-plane and not in the longitudinal direction so 1mm is not to big. The AT is 64 minutes, which is too long if several pressure induced deformations need to be done. For the experiments one high resolution scan will be obtained from which the contours will be extracted that are needed to make a 3D model. After this low resolution scans with an in-plane resolution of 100x100µm and AT of 19 minutes will be obtained to image pressure induced deformation. This will minimize the AT of the total experiment and thus reduce degradation of the tissue.
The setup that was used limits the size of the arteries that can be imaged. In figure 39 can be seen that few space is left for the artery to expand during pressure induced deformations. A new setup will be created that can contain bigger arteries. This means that the volume to be imaged will increase and thus the FOV should also be increased to prevent aliasing. A pilot will be done to see if small changes should be made to the imaging protocol. The results of this pilot will be discussed in the next chapter.
Although the image in Figure 39 looks nice there are 2 artefacts present, which are ghosting and chemical misregistration. The ghosting is minimal and does not obstruct the image of the artery. Ghosting is normally created due to movement of the sample. However, this is not possible in the setup since the artery is fixed to the setup and the setup is fixed to the sliding bench. The ghosting artefact is created either by the software, the hardware or the movement of the whole scanner due to external factors .The chemical misregistration leaves a black circle on the edge of the artery and gives the boundary between the buffer and the tissue in the artery. If there would be one kind of fat in the artery and the Larmor frequency was known of this fat then this artefact could be prevented, but this is not the case. The black line does not influence the contrast in the plaque and is therefore less important.
It can be concluded that two image sequences are obtained that fulfill all the imaging requirements that are needed to make a 3D model and image pressure induced deformations. The parameters of the final sequence can be seen in Table 8.

Table 8 Imaging sequences that will be used in the experiments

	High resolution	Low resolution
TR (ms)	2500	2500
TE (ms)	70.9	66,5
FA (°)	90	90
FOV	20	20
Aq. Matrix	384x384	192x192
Resolution (µm)	52x52	104x104
Slice thick. (mm)	1	1
Spacing (mm)	0	0
# Slices	16	16
NEX	32	32
ETL	10	10
BW (kHz)	10	10
AT (min)	64	19

4. MRI of atherosclerotic plaques

Through the knowledge that was obtained in chapter two and the pilots done in chapter 3 we found an MRI sequence that can be used to image atherosclerotic plaques with a high in-plane resolution and a sequence that can image pressure induced deformations. In Figure 39 a high resolution MRI scan of an atherosclerotic plaque can be seen with a lot of contrast. Some contours can be distinguished, but we cannot identify what component belongs to what contour. Histology will be performed on the artery after scanning to identify the contours found in the image. Histology will also be a good resource to identify artefacts that were not noticed in the pilots, such as magnetic susceptibility artefact and partial volume artefact.
Before the high and low resolution scans are obtained the methods need to be discussed (Section 4.1). The comparison between the high resolution MRI scans and histology will be discussed in Section 4.2. After the validation the pressure induced deformation experiments will be done. This data is important to validate biomechanical plaque models. These experiments are discussed in Section 4.3.

4.1 Methods and materials

To start with the experiments on pressure induced deformations, arterial segments need to be selected (section 4.1.1). As explained previous, the setup was too small to fit larger arteries, so a new setup is created that can fit larger arteries and a pilot test will be done to see if any changes have to be made to the original imaging sequence (Section 4.1.2). The protocol used for these experiments is discussed in Section 4.1.3.

4.1.1 Selection of the diseased arteries

In section 3.1 was explained that porcine iliac arteries were used for this project. Ultrasound images were obtained from the arteries before preservation. The following criteria are used for the selection of the arteries from the US images:

- Plaque length and area
- Plaque inhomogenety
- Eccentric VS concentric plaque
- Artery length and diameter
- Side branches
- Is the artery straight or bend

When the plaque length and area are of proportional size more signal will come from the plaque and this will improve the quality of the images. The length of the artery needs to be around 20mm when unstretched, since the cannules will occupy between 8-10 mm of the artery. If the artery becomes shorter then there will not be enough length to image. The diameter of the artery also is limited. When the diameter is to small the cannules will not fit and the signal from the artery will be too low to get a good MR-image.
When there is a side branch it means that a suture needs to be placed. This side branch might become a weak point when the pressure is increased and a leakage might occur. It also becomes problematic if a big side branch is exactly in the middle, since it might influence the deformations. Some of the samples are curved, but when pre-stretched they will be straight. However, the pre-stretching will apply more stresses to the more curved surface of the artery and this will distribute the stresses in the arteries unevenly.
Sixteen arterial segments were qualified to be used for the experiments. From these sixteen arteries, three external iliac arteries were selected and one internal iliac artery.

4.1.2 The setup

The new setup was created to fit larger arteries (Figure 40). The dimensions of the setup are chosen so that the artery is as close to the surface cardiac mouse coil as possible to have

maximum signal. The setup will be stabilized in the coil as well, which will prevent movement of the setup during scanning.

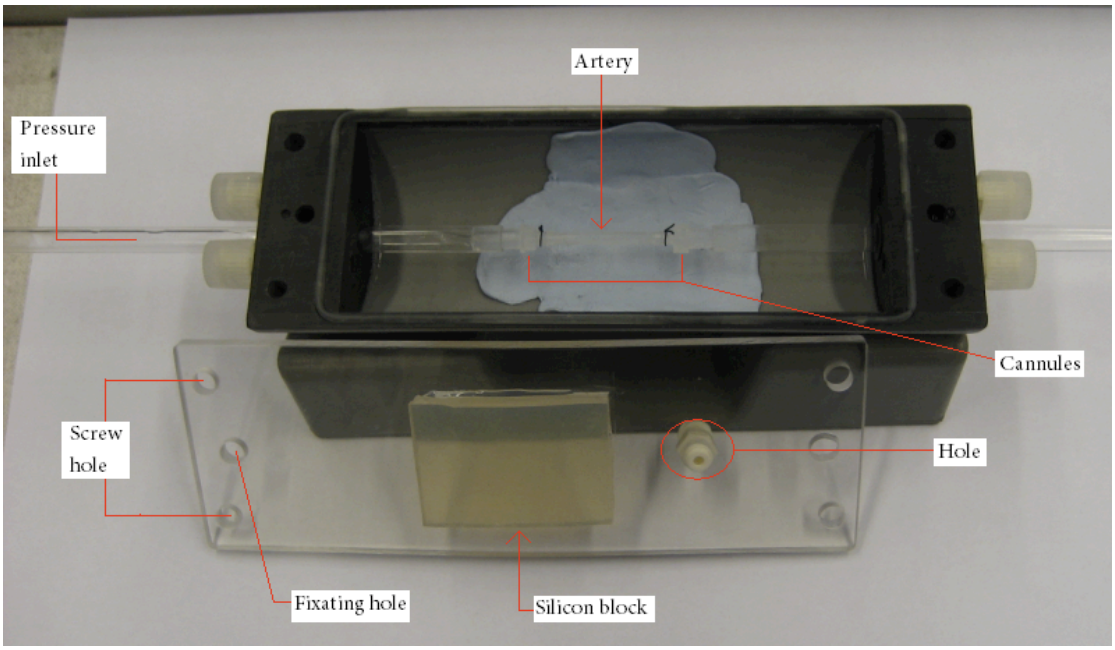

Figure 40 The new setup that can contain larger arteries.

The artery is placed in the middle of the setup by connecting the cannules in the two holding tubes. These holding tubes can be moved back and forth to stretch the artery. On either the left or right side of the holding tubes the pressure is measured with a DMT pressure myograph (DMT A/S, Aarhus, Denmark). The valve on the opposite side must be closed when this is done. The inside of the setup is filled with buffer and a lid can be placed over the whole setup. The lid is screwed with four screws on each corner. In the middle of these four screws are fixating screws, which fixate the holding tubes when the artery is pre-stretched. There is also a hole in the lid to keep the pressure of the buffer around the artery constant when the artery is expanding due to pressure induced deformations. As can be seen there is a silicon block in the middle of the lid. The silicon gives no signal when it is in the MRI. The FOV should be as small as possible to keep the resolution the same. When there is buffer outside the FOV it will alias and disturb the image of the artery. This silicon block decreases the FOV that is needed to prevent aliasing.
Because a new setup is being used another pilot was performed to see if any of the imaging parameters for the T2 sequence had to be changed. Due to the bigger compartment in which the artery is placed, aliasing was observed in the pilot experiment. To remove the aliasing the FOV was increased. This resulted in a decrease in resolution, which was solved by increasing the matrix. By increasing the matrix we also increase the AT, which was reduced by reducing the NEX. The difference in image sequences can be seen in Table 9.
The adjustments in the low resolution images caused a lower SNR, but the SNR was still high enough. The resolution has increased a bit and the AT decreased. The adjustments in the high resolution image have decreased the resolution, but the image quality has remained about the same.

Table 9 Comparison between the old image sequences and the new image sequences.

	High res. old	High res. new	Low res. old	Low res. new
TR (ms)	2500	2720	2500	2500
TE (ms)	70.9	53,7	66,5	66,2
FA (°)	90	90	90	90
FOV	20	25	20	25
Aq. Matrix	384x384	448x448	192x192	256x256
Resolution (μm)	52x52	56x56	104x104	98x98
Slice thick. (mm)	1	1	1	1
Spacing (mm)	0	0	0	0
# Slices	16	18	16	12
NEX	32	22	32	16
ETL	10	10	10	10
BW (kHz)	10	11	10	11
AT (min)	64	64	19	12

4.1.3 The experimental protocol

At the day of the experiment the artery was taken out of the -80° freezer, cannulated and placed in the setup. Before the scanning starts and a static pressure was applied, the artery was preconditioned. When handling biological tissue it is important to precondition to ensure that reproducible results will be obtained [34-40]. Normally a sample is preconditioned between the pressures at which measurements are going to be taken. In our project the pressure was increased to the upper boundary of the blood pressure in the pigs, which was 120mmHg. Ten cycles were used to precondition from 0- to 120mmHg.

At the MRI scanner 4 scans were obtained. First three low resolution scans were made at 100-, 120- and 80mmHg respectively. After, one high resolution scan was made at 100mmHg. The parameters that were used for these scans can be seen in Table 9. The total scan time needed at the MRI was 110 minutes. However, there was also some time needed for preconditioning, pre-scanning and setup preparation, which approximately took 90 minutes.

When the MRI scans were obtained the artery needed to be prepared for histology. The artery will be fixated under approximately 100mmHg with 3.5-4% formaldehyde (Figure 41).

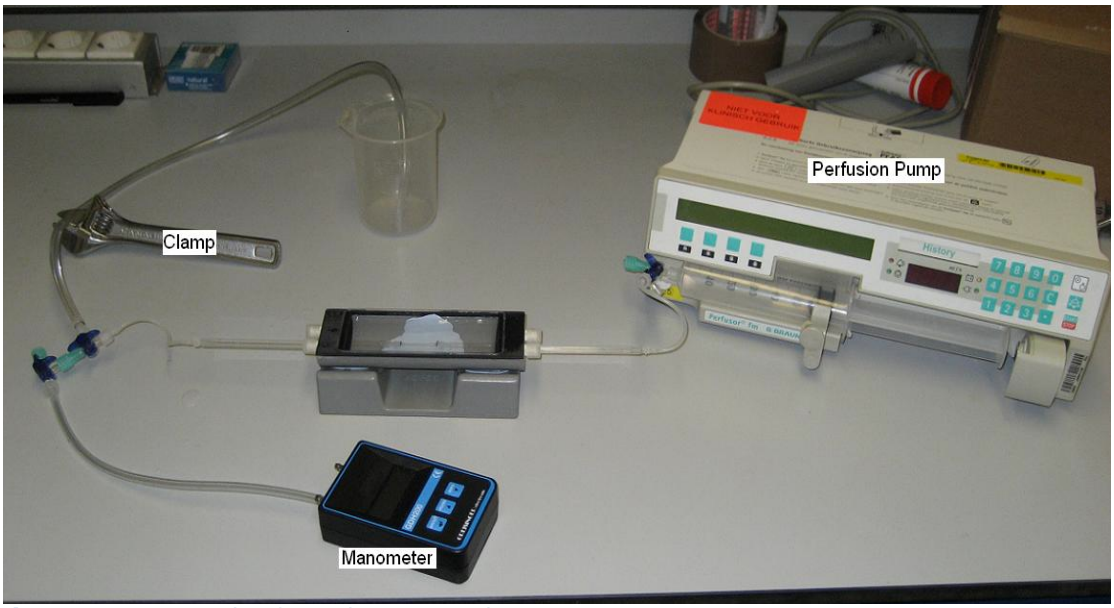

Figure 41 Setup used to fixate the artery under pressure.

A syringe with 50ml formaldehyde was placed in a B-Braun perfusion pump (B-Braun medical Inc., USA). The perfusion pump has a flow of 300ml/h, which means it took 10 minutes to pump the formaldehyde through the artery. A clamp was placed around the outflow tube to increase the resistance of the flow of formaldehyde, which increased the pressure in the artery. On the manometer the pressure inside the artery was monitored.

4.2 High resolution MRI versus histology

Histology is needed to identify the different components seen on the high resolution MR image at 100mmHg. Before the comparison can be done the artery needs to be cut in blocks and each block must be appointed to a slice from the MRI scan. Then slices need to be cut from the block and stained with a dye to identify materials in the artery (Section 4.2.1). When these slices are obtained and linked to the MRI slices it is possible to compare them (Section 4.2.2). A discussion and conclusion of the obtained results will be given in Section 4.2.3.

4.2.1 Registration and histology staining

To match the histology slices to the MRI a good aligning procedure is needed. After the artery is fixated, it will be flushed with Tissue-Tek (Sakura Finetek USA Inc., Torrance, CA, USA) and placed in the freezer. Tissue-Tek is a substance similar to wax and is used for embedding tissue after fixation and before cryo-sectioning. After one hour the artery is taken out (Figure 42a). The cannules will be cut from the artery (Figure 42b) and the length of the residue tissue is measured with a caliper (Figure 42c). The artery will be cut into 1mm blocks (Figure 42d,e). The distance from the first block to the cannules is measured with a caliper.

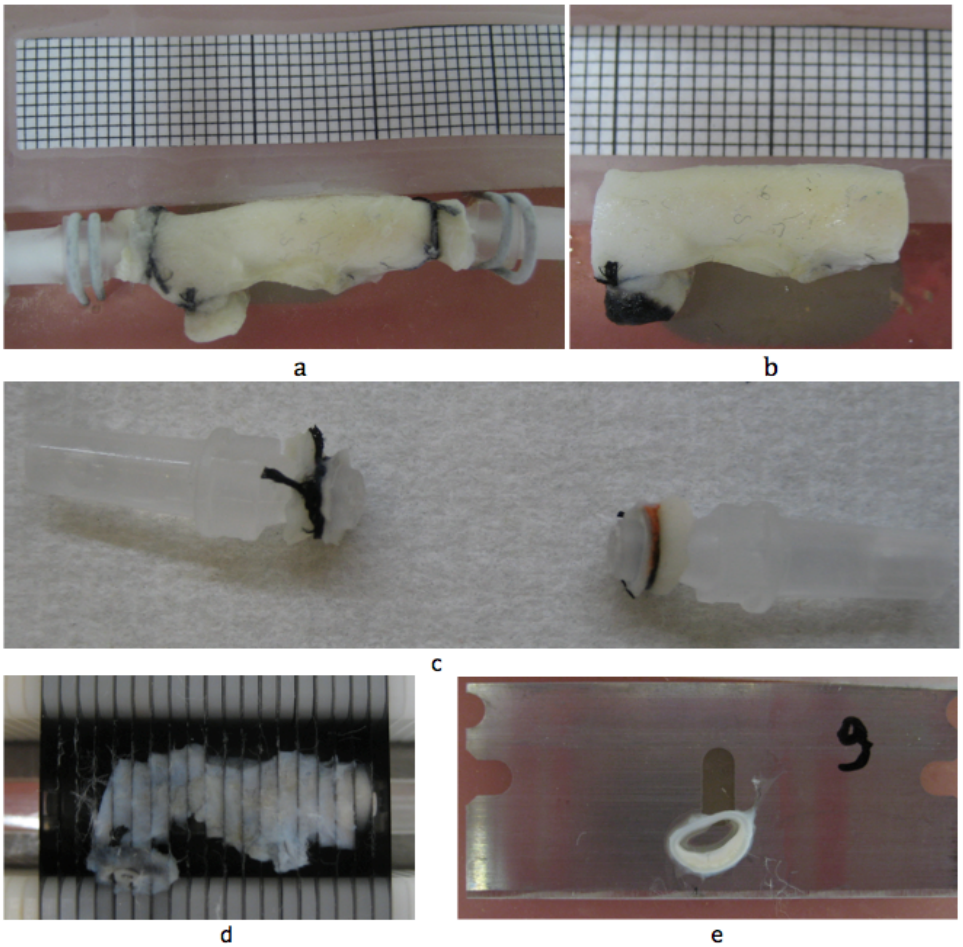

Figure 42 a, The artery after it is frozen in the freezer. b, The artery with the cannules cut off. c, The cut loose cannules with the residue tissue on it. The distance from the residue tissue to a reference point on the cannule will be measured with a caliper. d, The slice cutter used for making the 1mm blocks. e, One of the blocks shown on the knife that was used to cut it.

In the pre-scan made on the MRI the slice locations are shown (Figure 43). With the Osirix imaging software the distance between the cannule and the first MR slice can be calculated. Because the distance from the first histology and MRI slice to the cannule is measured it is possible to link the histology slices with the MRI slices. The histology slices will be 5µm thick, which is much smaller then the 1mm thick MRI slices. The maximum error for aligning the MRI slices with the histology slices will thus be ~0.5mm.

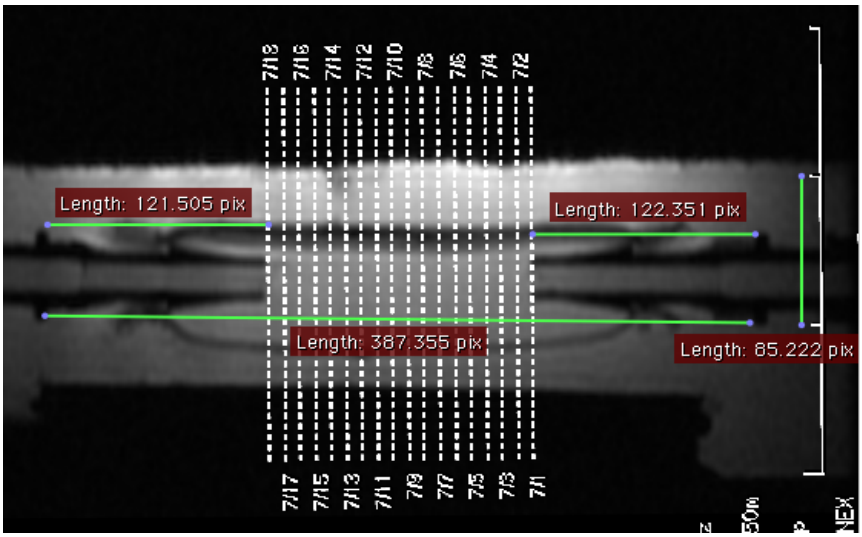

Figure 43 Pre-scan of the artery and the slices obtained from this artery. The distance from the cannule to the first slice is 122 pixels, which can be translated to millimeters.

The blocks will be cut in 5µm slices and stained with two different stains; the oil red O (ORO) stain and the elastic Van-Giesson (EVG) stain. ORO is used to identify lipids and fatty acids, which will stain red. It also colors calcium dark, which makes it possible to verify where calcium is located in the plaque. EVG stains connective tissue such as elastine and collagen. The media is separated from the intima and adventitia with elastine fibers, which makes the EVG stain very useful to identify the media. The media will be dark pink to purple. The EVG is also very useful to identify collagen pore and rich areas, which color pink in the EVG stain. Combined the ORO and EVG stain can tell us the composition of the plaque and identify the adventitia, media and several components in the intima.

4.2.2 Results for MRI versus histology

In total four experiments were done and of each experiment one slice will be compared with histology. The contours in these four MRI slices have been drawn before the staining from histology was obtained. Each experiment will be discussed separately and first a detailed explanation of the histology is given and after the contours found in MRI will be compared with the findings in histology.

Experiment 1

Figure 44 shows us the EVG staining of a large eccentric plaque. A small part of the adventitia can be seen at the bottom and in the plaque different intensities of pink are observed. Four interesting parts in the EVG staining are zoomed in and will be discussed. In the first zoom-in box of Figure 44, the EVG staining reveals a compact multilayered media in the plaque-free area of the artery. The borders of the media are identified by the internal and external elastic lamina (IEL and EEL), which are the dark purple lines. In the second zoom-in box the media is shown again, but here the IEL has disappeared and only a thin compact elastin-rich layer remains. Normally the IEL should be clearly seen in an EVG staining, but in this EVG staining it seems that as soon the media goes into the plaque the IEL disappears and is replaced by collagen fibers. In the third zoom-in box a structured collagen rich area can be seen at the luminal side, which can be classified as a thick fibrous cap. The rest of the collagen in the EVG staining is less organized and less densely packed, except for the middle

part of the plaque as showed in zoom-in box 4. Here a high density of collagen with fibers pointing in all directions is seen.

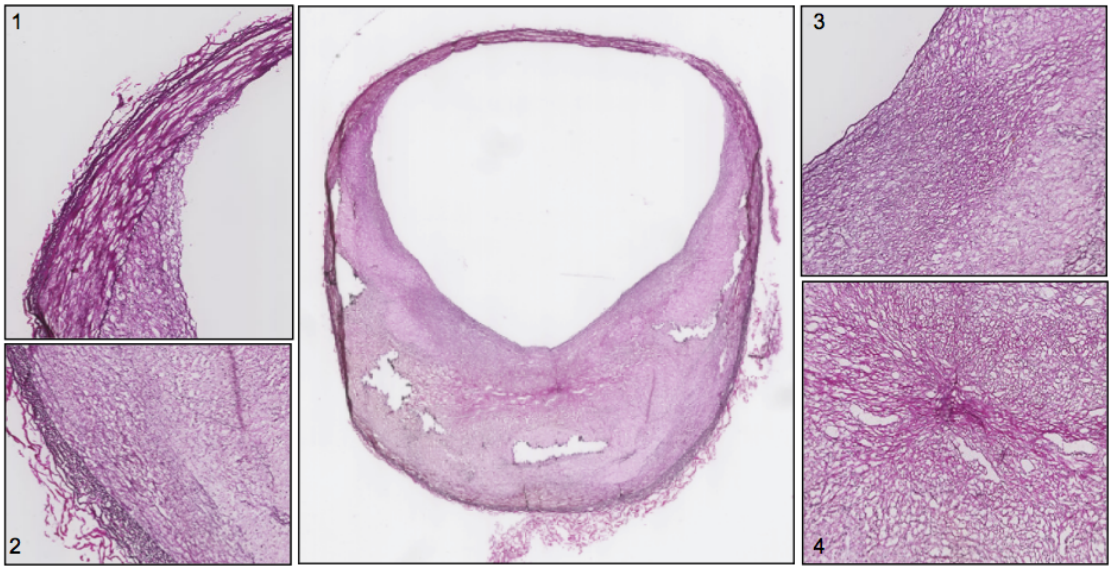

Figure 44 Image of the EVG staining with four zoom-in boxes. 1. Shows the external- and internal elastic laminas that are the border of the media. 2. Shows the degraded media where only a compact media is seen that consists out of the external elastic lamina. 3. Compact aligned collagen fibers at the luminal side, which can be classified as a thick fibrous cap. 4. Shows a small area, in the middle of the plaque, with a high density of collagen fibers in random directions.

The second staining that was used was the ORO staining (Figure 45) and this staining confirms the main findings from the EVG stain regarding the media. Zoom-in box 1 in Figure 45 shows that the media is infiltrated with lipid droplets as soon as it enters the plaque area. From this point the media starts to degenerate. Two areas with high lipid concentration are located at the plaque shoulders and extend from 8 to 10 o'clock and from 1 to 4 o'clock. Between 4 and 8 o'clock the concentration of lipids is lower.

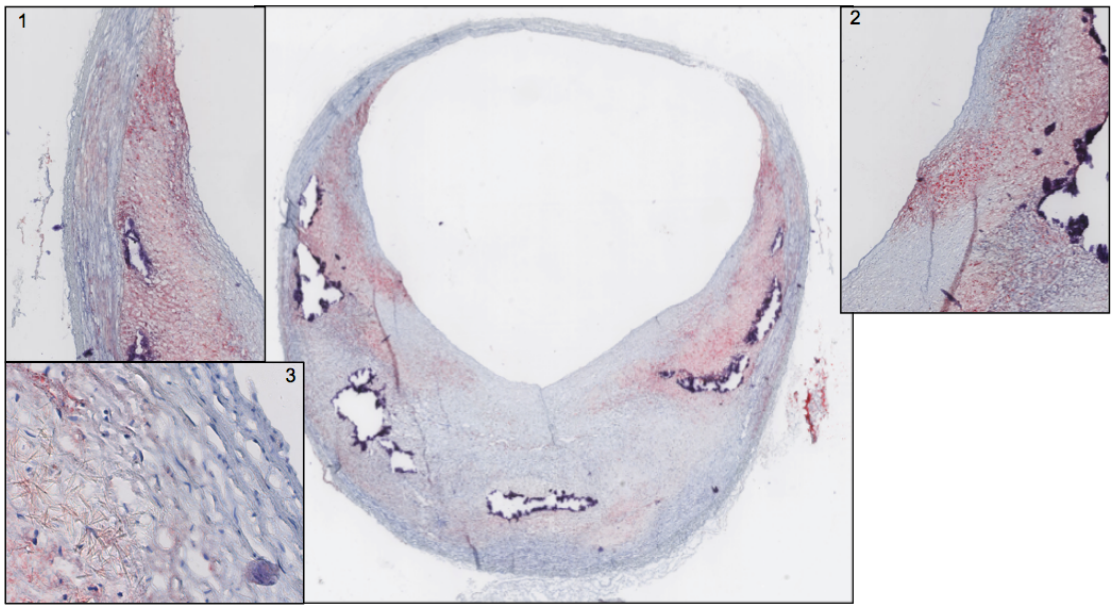

Figure 45 Image of the ORO staining with three zoom-in boxes. The left and right side of the plaque show higher concentrations of lipids. The calcium spots are the white areas with a dark purple surrounding. 1. In the media lipid droplets can be seen when it enters the plaque area. 2. At 4 o'clock an increased concentration of lipids can be seen in the cap. 3. Some cholesterol crystals are located right underneath the cap of the left shoulder. They look like little needles.

The cap in zoom-in box 2 is infiltrated with lipids. Cholesterol crystals are found right underneath the cap in the left shoulder, which are seen in zoom-in box 3 (the needle like structures). The free cholesterol crystals and the infiltration of the lipids in the cap might indicate that the plaque is turning into a vulnerable plaque.
Both the EVG and ORO stain show the calcifications clearly. In the ORO stain the white regions with a dark blue ridge indicate where calcium was present. The calcifications are localized near the intima-media interface. The calcifications in the shoulders are surrounded by lipid rich regions, but those in the middle are surrounded by lipid pore regions.
In Figure 46 the high resolution MRI slice is presented that was registered to the previous analyzed histology slices. There is a good qualitative resemblance of the MRI slice with the histology slices. The lumen and adventitia can easily be delineated for this slice.

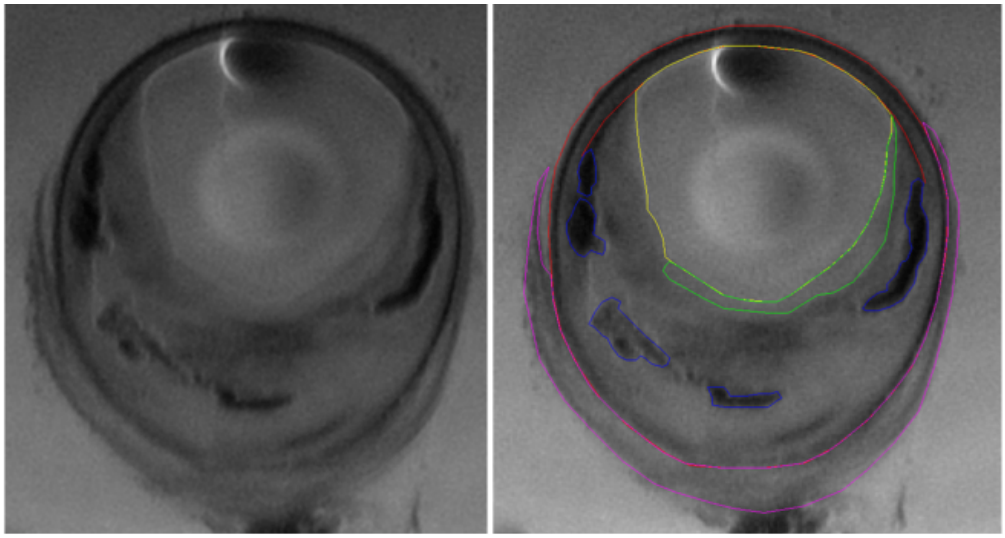

Figure 46 a, The 10th slice from the high resolution MRI scan of the first experiment. b, The sharp contours that were identified are drawn.

In Figure 46a a multi layered media is identified at the top of the MRI slice, but as soon as the shoulders of the plaque are reached it seems that the inner layer has disappeared on the MRI scan (Figure 46b, red line), which was also seen on the EVG stain. Only the EEL seems to remain visible inside the plaque, but it becomes unclear at the bottom of the plaque as well. The EVG stain also showed that the IEL of the media was degrading as soon as it went into the plaque region. The adventitia, media and intima are well defined, but the contours inside the intima still need to be observed. The identified calcium spots on the ORO stain resemble those on the MRI slice very well (Figure 46b, blue lines). The calcified spot between 7 and 8 o'clock has a lower contrast than the others, but it still has a sharp border. The shapes of the calcifications differ a bit from the calcifications seen on the ORO stain. When two calcifications are closely packed, as those between 9 and 10 o'clock, it becomes a bit harder the separate borders. In Figure 46a a slightly lighter contrast can be seen on the right lumen plaque interface. This lighter area is identified with the green line in Figure 46b. The green area that is drawn in Figure 46b resembles the structured collagen fibers that were classified as a thick fibrous cap. In the EVG stain this cap continued into the left shoulder of the plaque, but on the ORO can be seen that this part of the cap is infiltrated with lipids. In the MRI can be seen that the part after the green contour becomes darker which can be the result of the lipids that have infiltrated the cap. In the middle of the plaque in the MRI slice a darker area is seen with un-sharp edges. At the same location a high concentration of unorganized collagen was observed in the EVG stain. The area on the left and right shoulder of the plaque seem to be a bit darker in comparison to the lower middle of the plaque. At these shoulders a high concentration of lipids is seen in the ORO stain and in the lower middle area, underneath the calcium spot, this lipid concentration was lower, which resembles the lighter contrast of the MRI in this part.

Experiment 2

The EVG staining of the 11th slice of the high resolution MRI scan, obtained in the second experiment, shows a large eccentric plaque (Figure 47). The healthy part of the artery contains a multilayered media (Figure 47 zoom-in box 1) and above the media some less dense collagen fibers can be seen which is the adventitia. In zoom-in box 2 the media has degraded to a single line of elastine, which is the dark purple line between the plaque and the adventitia. The border between the diseased intima and IEL is diffuse and cannot be identified. These characteristics for the media were also seen in the sample of the previous experiment. At the lumen side the plaque is covered with a high concentration of organized collagen fibers that form a fibrous cap (Figure 47 zoom-in box 3).

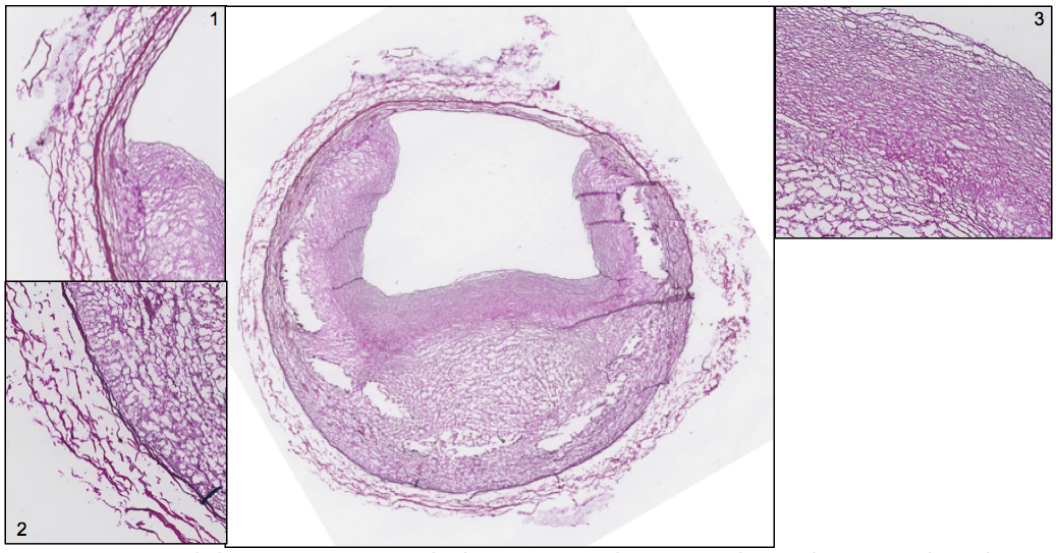

Figure 47 Image of the EVG staining with three zoom-in boxes. 1. Shows the external- and internal elastic laminas that are the borders of the media. 2. Shows the degraded media where only a single elastic lamina is seen. 3. Compact aligned collagen fibers at the luminal side, which can be classified as a thick fibrous cap.

The ORO staining of the 11th slice of the high resolution MRI scan can be seen in Figure 48.

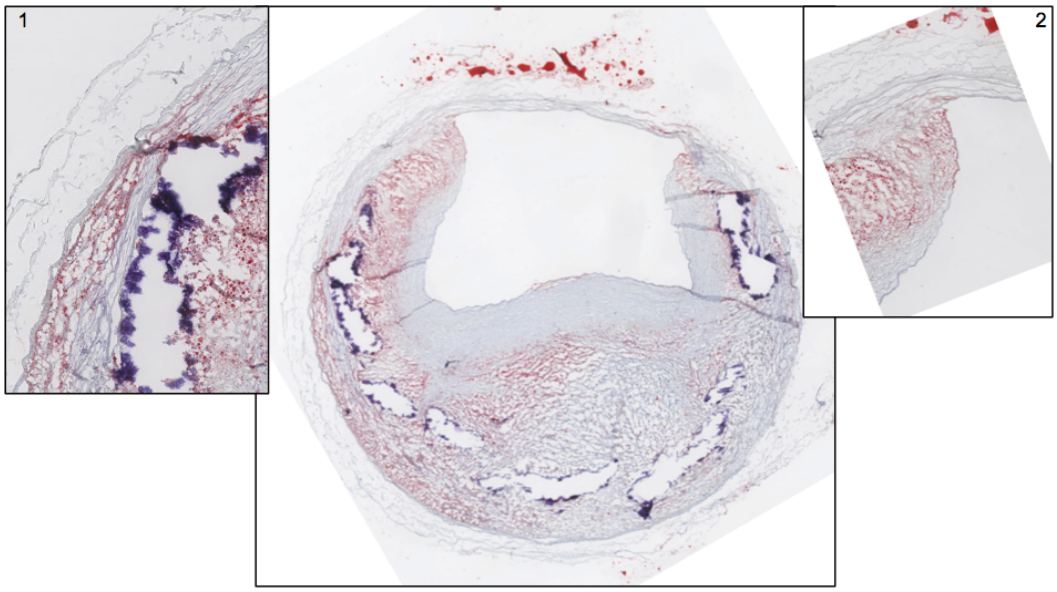

Figure 48 Image of the ORO staining with two zoom-in boxes. The left side of the plaque shows a high concentration of lipids. The calcium spots are the white areas with a dark purple surrounding. 1. Lipids have infiltrated the media when it entered the plaque area. 2. Lipids also have infiltrated the fibrous cap at the shoulders of the plaque.

In zoom-in box 1 can be seen that lipids are penetrating the media. This occurs when the media is entering the plaque area, which confirms the findings in the EVG stain that the media is degrading. The lipids also seem to penetrate the fibrous caps at both shoulder ends (Figure 48, zoom-in box 2). These two characteristics also occurred in the plaque found in experiment one. No free cholesterol crystals are found in this plaque. The left side of the plaque contains high concentrations of lipids and the concentration decreases towards the center of the plaque. In the center low density collagen areas are seen with only few lipids. In the right shoulder the lipid concentration increases a bit. A lot of calcifications are present in the plaque, but all are located close to the media-intima interface. The calcifications in the middle of the plaque are not surrounded by lipids in contrary to the calcifications in the shoulders.
In Figure 49 the MRI slice of the second experiment is shown that resembles the histology slices. The sharp contours seen in this image are drawn.

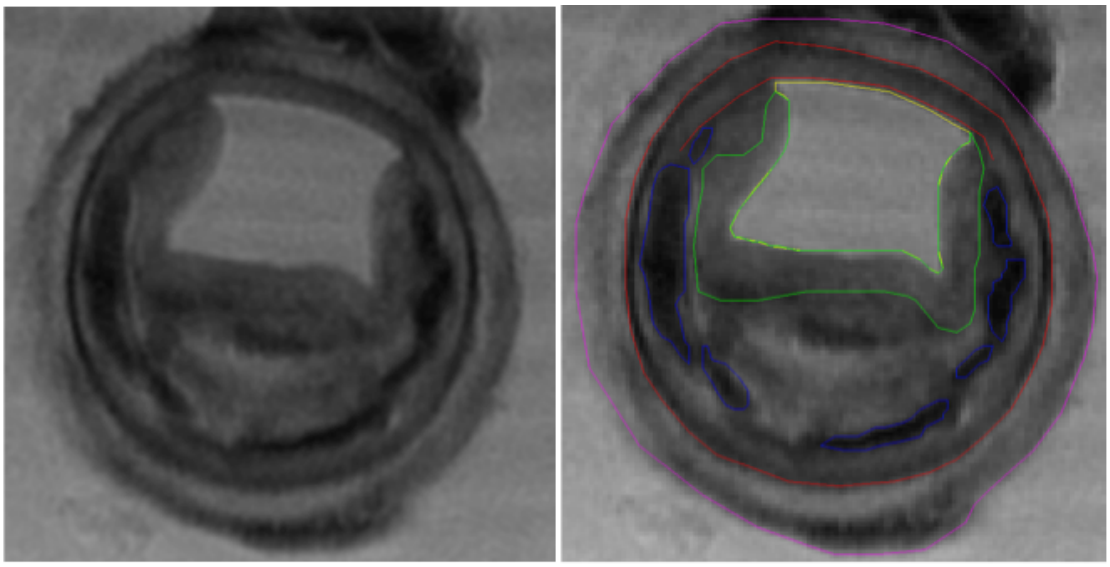

Figure 49 a, The 11th slice from the high resolution MRI scan of the second experiment. b, The sharp contours that were identified are drawn.

The adventitia (magenta line) and the lumen (yellow line) could easily be delineated. The outer red line can be linked to the EEL seen in the EVG stain. The contour that the inner red line was following disappeared when it entered the plaque area, which is confirmed by the EVG stain. This characteristic was also seen in the previous sample. The adventitia, media and intima are identified, but the contours in the intima still need to be classified. The blue contours at the media-intima interface of the plaque clearly resemble the calcifications shown in the ORO stain. The green line surrounds the whole plaque-lumen interface. In the EVG stain can be seen that this can be identified as the fibrous cap. However, in the ORO staining this fibrous cap is penetrated by lipids at the top of the shoulders, but this is not seen in the MRI scan. In the EVG stain can be seen that the lower part of the fibrous cap is a bit darker pink, which indicates a slightly higher concentration of collagen. This slight increase in density is also seen in the MRI at this location, where the contrast becomes a bit darker at the bottom of the fibrous cap. It is hard to allocate the lipid concentrations in the MRI scan, but it seems that the contrast in the shoulders is a bit darker then in the middle. However, there is one dark spot in the middle of the plaque that cannot be linked to either of the histology slices.

Experiment 3
The plaque that is seen in the EVG stain in Figure 50 is eccentric, but smaller then in the previous samples. No adventitia is seen in this segment. In this sample the media can be seen clearly throughout the whole artery. Zoom-box 1 shows the media in the healthy part, but it can be seen that underneath the media some intima thickening is present. This means

that the plaque might have been growing from an eccentric plaque into a concentric plaque. Around the whole lumen an increased collagen concentration is seen, which is identified as a fibrous cap (Figure 50, zoom-in box 2).

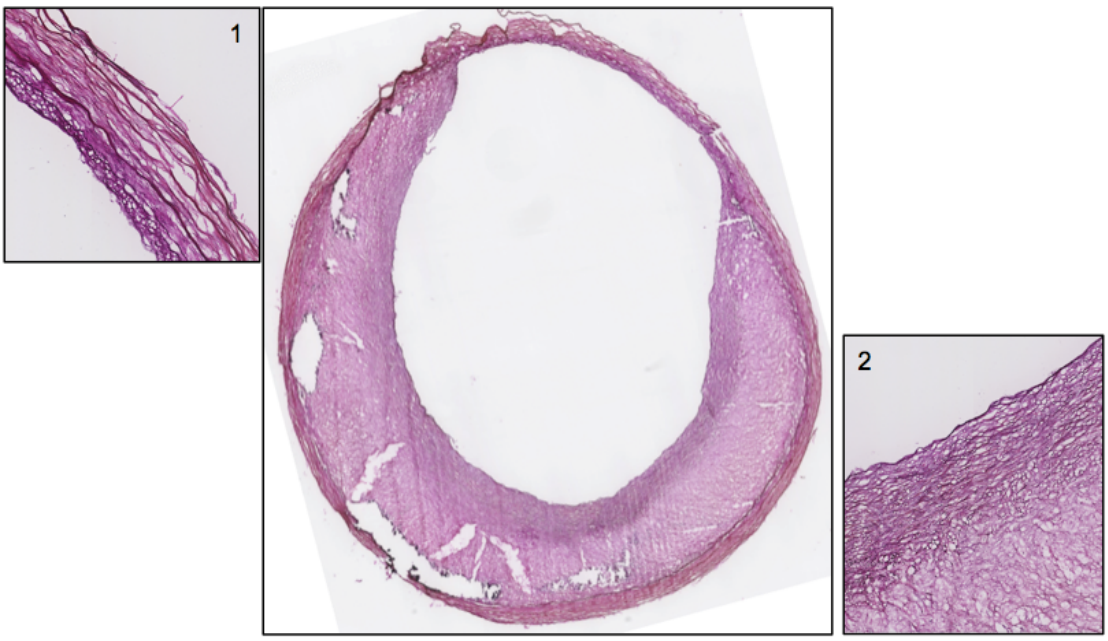

Figure 50 Image of the EVG staining with two zoom-in boxes. 1. Shows the media and it can be seen that there is some intima thickening in this part. 2. Compact aligned collagen fibers at the luminal side, which can be classified as a thick fibrous cap.

The tears in the radial direction are cutting artefacts from the histology procedure. The moon shaped area underneath the fibrous cap seems to be fairly homogeneous, with some calcifications at the media-intima interface. In the ORO staining the moon shaped area underneath the fibrous cap can be identified as lipid rich area (Figure 51).

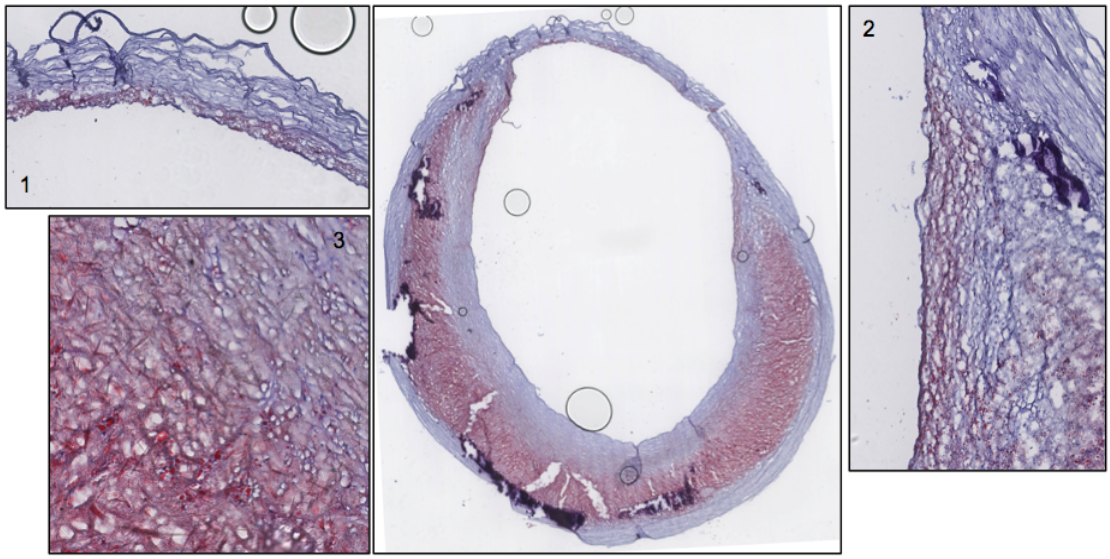

Figure 51 Image of the ORO staining with three zoom-in boxes. The moon shaped area underneath the cap contains high concentrations of lipids. The calcium spots are the white areas with a dark purple surrounding. 1. Underneath the media lipid droplets can be seen in the intima, which show intimal thickening. 2. The caps in the shoulders are infiltrated with lipids and there are also small calcifications. 3. Low concentrations of cholesterol crystals are located throughout the whole lipid rich area. The cholesterol crystals look like small needles.

Zoom-in box 1 shows that there are lipids present in the intima at the top of the artery. At the shoulder of the plaque, lipids seem to have infiltrated the cap (Figure 51, zoom-in box 2). Zoom-in box 2 also shows a small calcification in the shoulder, which is also seen in the other shoulder. The ORO stain confirms the calcifications at the media-intima interface, which were also seen in the EVG staining. When zoomed in on the lipid rich area, as in zoom-in box 3, cholosterol crystals can be observed. These cholesterol crystals are present in low concentration throughout the whole lipid rich area, after close inspection.
Figure 52 shows the MRI slice that corresponds to the histology slices that were discussed above. The MRI slice seems to have a lot of ghosting in the lumen, on the outside of the artery and in the plaque region.

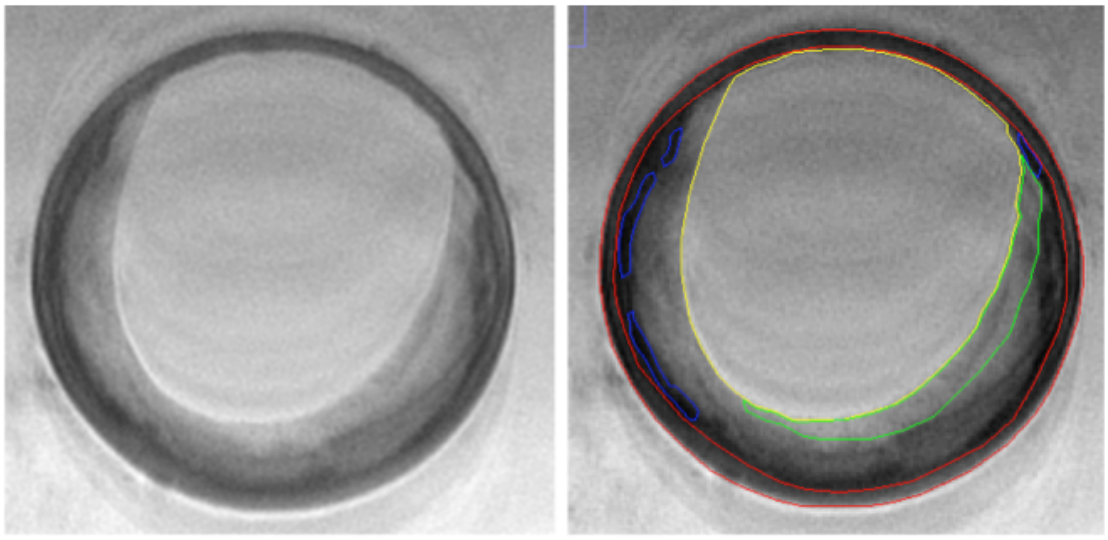

Figure 52 a, The 3rd slice from the high resolution MRI scan of the third experiment. b, The sharp contours that were identified are drawn.

The yellow line in Figure 52b is the contour of the lumen and it can be seen in Figure 52a that this contour was easily drawn. Unlike from the previous samples in this MRI scan the whole media is visible, which was also seen on the EVG staining. The calcification seen in the MRI scan are also seen in the ORO stain, but the location seems to differ a bit from each other. The two small calcifications in the shoulder are also identified in the MRI slice.
The green contour seems to resemble a part of the fibrous cap that was seen on the EVG staining. However, it stops halfway in the MRI slice, but continues on the EVG stain slice. The ORO stain showed that there was a homogeneous high lipid concentration throughout the whole plaque, but in the MRI slice can be seen that the contrast in the plaque differs a lot.

Experiment 4
The 9th slice of the high resolution MRI scan was registered to the slice with EVG staining shown in Figure 53. This arterial segment has a small plaque in the bottom and a very small plaque more to the top. The small plaque at the top has a fold, which is an artefact from the histology process. The media seems to be uncompromised by the plaque area and can clearly be seen in this EVG stain. However, at the top of the arterial segment the media seems to be cut loose, which is due to cutting in the histological process (Figure 53, zoom-in box 1). In this sample the structured collagen rich area changes into a higher density collagen area that is less structured (Figure 53, zoom-in box 2). Only one calcification is seen in the plaque, close to the media-intima interface.

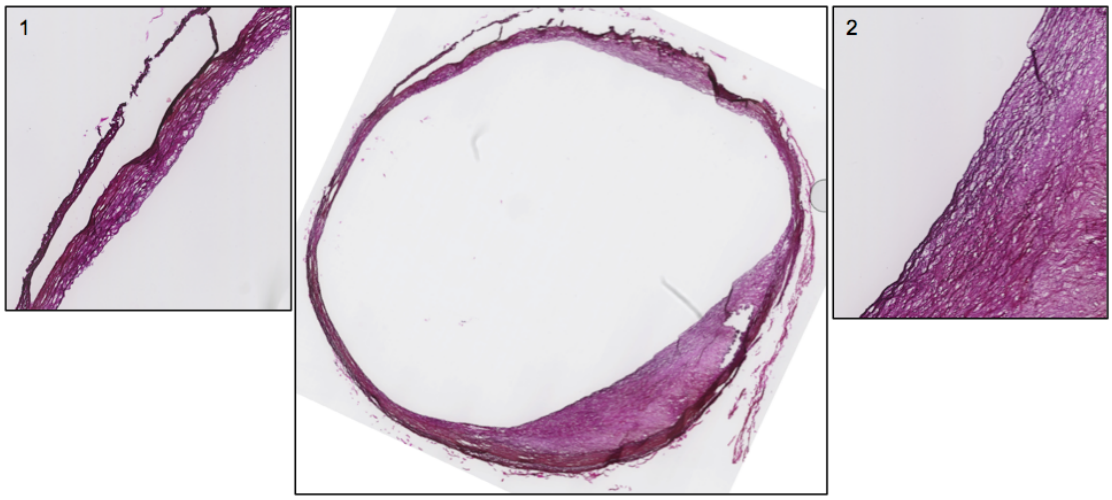

Figure 53 Image of the EVG staining with two zoom-in boxes. 1. Shows a cutting artefact in the media, which has occurred during the histology process. 2. Compact aligned collagen fibers at the luminal side change into a higher density of collagen fibers that are less organized.

The ORO stain shows that the small plaque at the top of the artery is infiltrated by small lipid particles (Figure 54). The larger plaque seems to have the highest concentration of lipids on the right side. A small concentration is observed at the left shoulder of the plaque (Figure 54, zoom-in box 1).

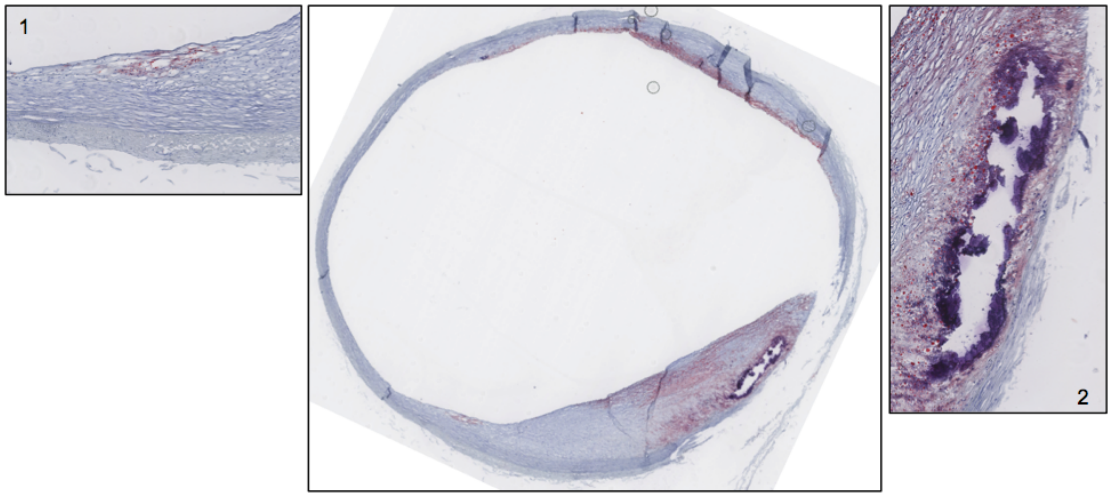

Figure 54 Image of the ORO staining with two zoom-in boxes. The right side of the plaque shows a high concentration of lipids. Lipids infiltrated the very small plaque at the top. 1. Lipids have also infiltrated the shoulder of the plaque. 2. Around the calcification a higher concentration of lipids are observed.

Only one small calcification is present in the larger plaque. In zoom-in box 2 can be seen that lipids surround this calcification. No cholesterol crystals are seen in this plaque, which is logical for such a small plaque.
The MRI slice that is registered to the previous discussed histology slices can be seen in Figure 55. When the MRI slice is observed it can be stated that ghosting is also present in this slice. The yellow contour shows the lumen again and in this slice it was somewhat difficult to follow the contour at the plaque area due to the ghosting. The contours of the media could be traced throughout the whole artery (Figure 55a), which was also possible in the EVG stain. The media was identified with the red contour (Figure 55b).

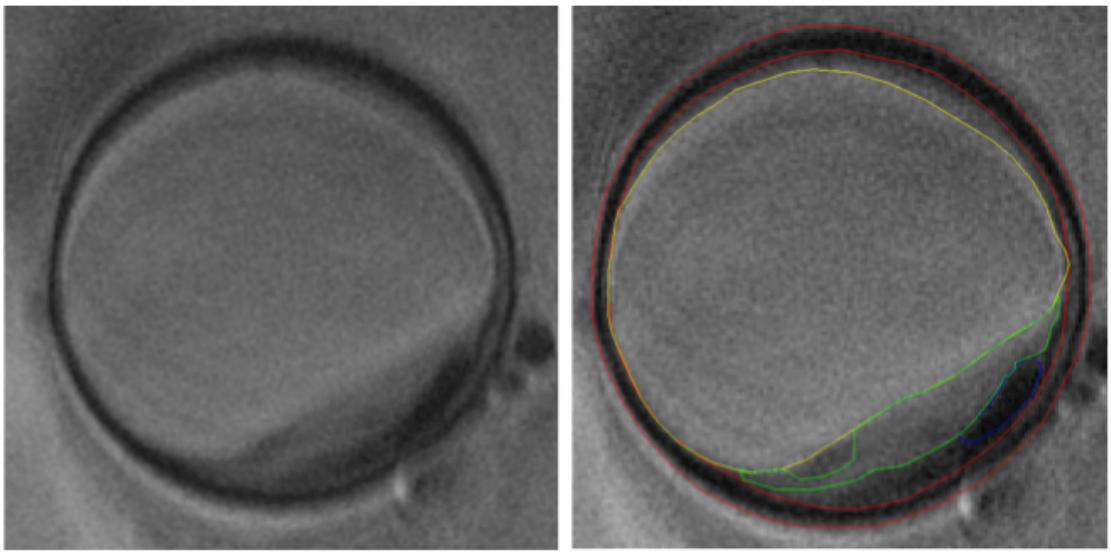

Figure 55 a, The 9th slice from the high resolution MRI scan of the fourth experiment. b, The sharp contours that were identified are drawn.

The calcification in the MRI is located at the same place as in the ORO staining and could be delineated easily. The contrast left to the calcification is a bit dark and when this is compared to the ORO stain a high concentration of lipids is seen at that location. The slightly darker area in the left shoulder of the MRI, might resemble the infiltration of the lipids in the cap in that location in the ORO stain (Figure 54, zoom-in box 1). The green contour could not be identified from the histology stains that were used. The fibrous cap that is present in the EVG changes halfway but this is not seen in the MRI slice.

4.2.3 Discussion and conclusion of MRI versus histology

We have compared the findings from histological analysis to high-resolution MRI for four diseased porcine iliac arteries. In the histology slices it was seen that all of the arterial segments contained eccentric plaques, but they all differed a lot from each other. When the adventitia was present it was clearly seen in the EVG staining. In the large plaques (experiment 1 and 2) was observed that the media was compromised and got diffuse as soon as it entered the plaque. In the smaller plaques (experiment 3 and 4) the media was clearly seen and not diffuse at all. The calcifications found within the intima were always located close to the media-intima interface. The fibrous cap could be well identified in the EVG staining and it was seen in the ORO stain that the fibrous cap got infiltrated with lipids at the shoulder regions. In the ORO stain the lipid rich and poor regions were identified and cholesterol crystals were not abundant and in the EVG the collagen rich and pore regions were identified within the intima.

The contours found in the high resolution MRI scans were compared to histology slices. The adventitia and lumen area could easily be matched with histology. When the media was not present in the histology images it was also not seen in the MRI scans, but when it was present this was also seen in the MRI slices, from which we can conclude that the media can be identified in the MRI and matched with histology. The calcifications were identified in every arterial segment, but the shape and location did not always exactly match those found in histology. The lipid rich/poor and collagen rich/poor regions within the intima were identified quite well when there were no artefacts (experiment 1 and 2), but when artefacts were present these areas were very hard to identify.

With T2 MRI sequences fat shows up dark and water shows up bright [2, 18]. Lipids are fatty tissue that do not contain a lot of water and are thus expected to be darker. Collagen is located in the extra cellular matrix (ECM), which contains more water and should thus turn out to be lighter. In experiment one, it could be seen that organized collagen rich areas (fibrous cap) gave a lighter contrast. The high density collagen with unorganized fibers gave darker contrast, which might be explained due to the decrease of ECM in this area. The lipid

rich areas did show up dark in the MRI scans and lipid poor with collagen poor regions gave a lighter contrast. However, in experiment three and four the lipid rich/poor and collagen rich/poor regions could not be identified. There are four factors that can explain this; partial volume artefact, ghosting artefact, a small contrast difference between regions and mis-registration. The slice thickness of the MRI scans is 1mm and the slice thickness of a histology slice is 5μm. All the components that are found in one voxel of 1mm thick are averaged in the MRI signal. This means that if in the first half of the voxel a lipid rich region was present and in the other half a lipid pore region was present, that the average contrast of the voxel will be lower than a voxel that only contains a lipid rich volume. This artefact is called partial volume artefact (Section 2.4.4) and could explain why it is sometimes hard to identify the lipid rich/poor and collagen rich/poor regions. This also explains why it might sometimes be difficult to estimate the shape of the calcifications. In experiment 3 and 4 there was ghosting present in the plaque. The contrast difference between lipid rich/poor and collagen rich/poor regions is not very high so ghosting will influence the contrast difference between these regions greatly. This makes it hard to separate the different regions. The fact that the contrast is low between the lipid rich/poor and collagen rich/poor regions is on itself a reason why it is hard to identify the different regions. The registration process used to match the histology slices with the MRI slices gave a maximum error of 0.5mm, which might mean that not the exact same location in the histology slices is compared with the MRI slices. Due to this a darker contrast might be present in a lipid poor region.

A possibility why the location of the calcium in the MRI slice does not always match the location on the ORO stain, is because of the deformation of the lumen. During the cutting of a 5μm histology slice, the slice starts to wrap. When the wrapped slice is on the glass plate it needs to be stretched again. When this is not done properly folds are seen in the structure. This means that the shape of the lumen on the MRI scan does not always match the histology slice and thus the calcium might seem to be in a slightly different location. Another artefact that was caused by the histology process is cutting artefacts. The cutting artefacts occur due to the presence of calcium. Calcium is a hard material in comparison to the arterial tissue. When the blade goes from the soft tissue to the calcium it will push the calcium down into the tissue beneath it or rip the calcium out. In both cases the tissue gets damaged and cutting artefacts occur. To prevent this the luminal area of the arteries was frozen in Tissue-Tek to reduce the difference between the calcium and the arterial tissue. Even though this method was used some slices still showed cutting artefacts.

It can be concluded that the imaging sequence used for this experiment enables us to identify the adventitia, media and intima accurately, which confirm the results by Jahnke et al. [22]. Within the intima the calcifications are also identified, but the shape and location sometimes slightly differ. The lipid rich/poor and collagen rich/poor regions are sometimes identified quite well, but when artefacts are present the identification of these regions is very hard.

4.3 Pressure induced deformation

Three low-resolution MRI scans of atherosclerotic plaques at 80-, 100-, and 120mmHg were acquired, which will be used to calculate the pressure induced deformations. First, the methods used to quantify and verify deformations will be discussed (Section 4.3.1). Results obtained from the analysis will be shown in Section 4.3.2. The results will be discussed in Section 4.3.3.

4.3.1 Methods for analyzing pressure induced deformations

The pressure induced deformations can be divided into global deformations and local deformations. In this project the focus will be on the global deformations, but a pilot to obtain local deformations by the use of the program Elastix [41] will be performed.
The global deformations are represented by the increase of surface area after the pressure is increased. The contours of the lumen and EEL are drawn for each pressure in the low resolution MRI scans. This is done for each of the four experiments at the same slices that were used in the previous section. The contours will be drawn in Matlab (MathWorks, Natick, Massachusetts, U.S.A). The spatial displacement will be visually evaluated by placing the coordinates of these contours in one graph. The surface area of the lumen and EEL are calculated for each pressure, which will be used to calculate the surface increase between the pressure steps.
A pilot will be done with the program Elastix to explore what the possibilities are to calculate local deformations with this program from the low-resolution MRI scans. Only one example will be shown in Section 4.3.2. More local deformation calculations are shown in Appendix C. Elastix is a medical imaging program that registers the displacement of biological structures. An initial image is used as a fixed image and a deformed image (also called moving image) of the same object is transformed until it fits the original shape. In this project the fixed image is the 120mmHg scan and the moving image the 80mmHg scan. Several transformations can be used to register the moving image on the fixed image like a rigid transformation, a similarity transformation, an affine transformation, a B-spline transformation and a thin-plate spline transformation. More information of these transformations can be found in the Elastix manual [33]. The transformation that is most suited for this project is the B-spline transformation, which was chosen for us by one of the writers of this program. For the registration a mask will be used to filter out the ghosting and bubbles that are present on the MRI scans. When the registration is done successfully the displacement field can be calculated from the registration with Transformix, which is a plugin of Elastix.

4.3.2 Results of the deformation analysis

The local deformations will be discussed for each experiment separately. First the contours that are drawn in Matlab are shown, after which these contours are placed in one graph to view the spatial displacement of the contours. The surface areas will be calculated for the EEL and lumen for all four experiments. When all four experiments are discussed the difference in surface area between pressures will be shown in a graph for all four experiments.
At the end of this section one example of local deformation calculations in Elastix will be shown and compared with the spatial displacement of the surfaces from the global deformations.

Experiment 1

In experiment 1 slice ten was used to compare MRI with histology and it will also be used for deformation measurements. The contours that were drawn for each of the pressure steps can be seen in Figure 56 together with a graph that shows all contours simultaneously.

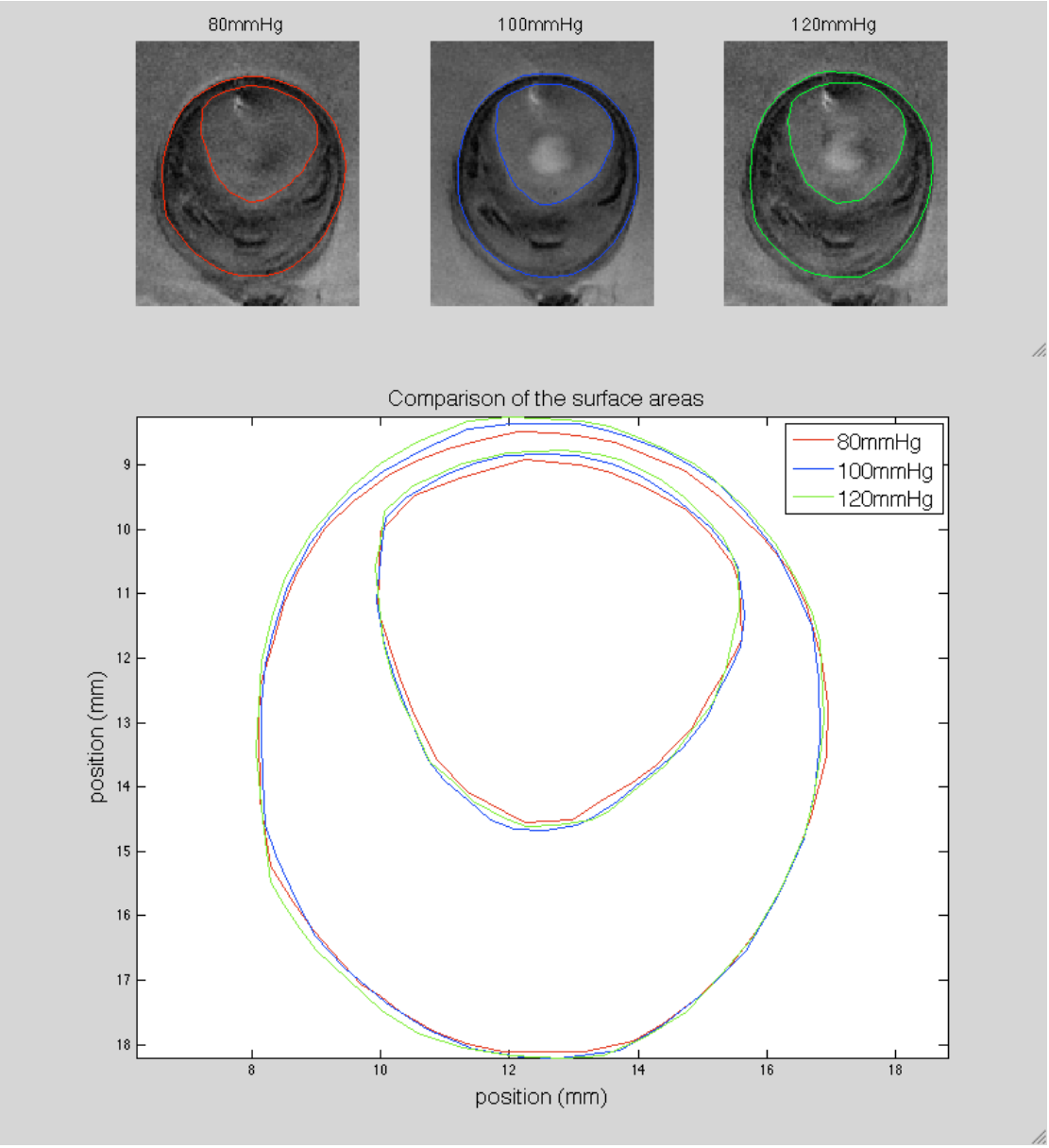

Figure 56 At the top the contours of the lumen and EEL are drawn in the MRI scans for the pressures 80-, 100- and 120mmHg. In the graph the counters of the EEL and lumen can be seen simultaneously.

From visual inspection can be seen that the artery describes an elliptical shape, the height of the long axis is ±10mm and the width of the short axis is ±9mm. The wall thickness of the eccentric plaque is ±3.5mm. The surfaces of 120 and 100mmHg overlap mostly, but the surface of 80mmHg is clearly a little bit smaller then those of 120 and 100mmHg. The surface area of the lumen and the outer media wall can be seen in Table 10.

Table 10 Surface areas of the six contours at 80-, 100- and 120mmHg.

	80 mmHg	100mmHg	120mmHg
Surface area EEL (mm^2)	67.3	68.3	70.0
Surface area lumen (mm^2)	23.7	25.4	25.6

Experiment 2

The contours that were drawn for slice 11 in experiment 2 are shown in Figure 57 together with a graph that shows all contours simultaneously.

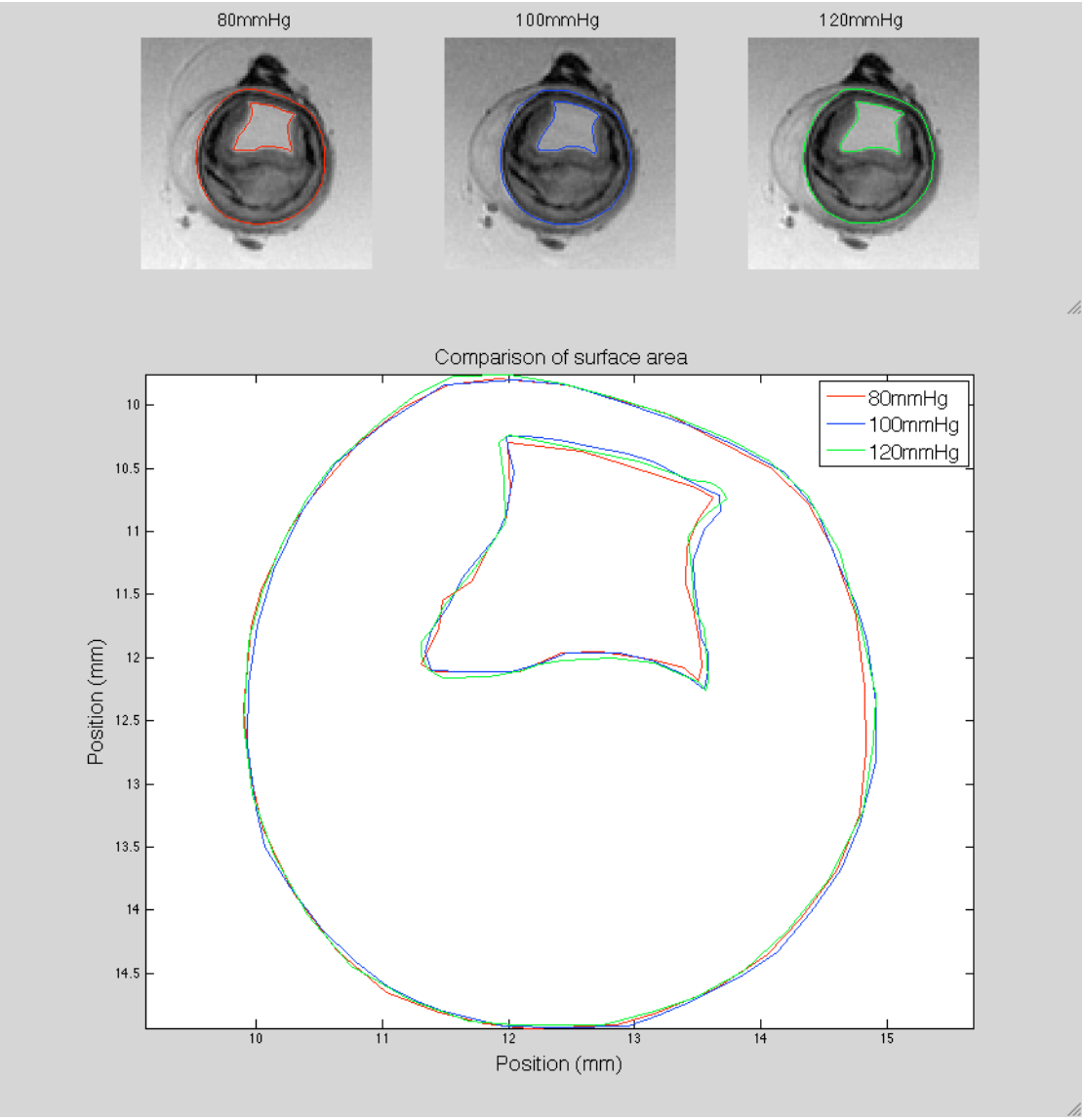

Figure 57 At the top the contours of the lumen and EEL are drawn in the MRI scans for the pressures 80-, 100- and 120mmHg. In the graph the counters of the EEL and lumen can be seen simultaneously.

The shape of the EEL is approximately circular with a diameter of ±5.5mm. This arterial segment is almost half the size of the previous segment. The wall thickness of the eccentric plaque is ±3mm. The shape of the lumen shown in Figure 57 races the suspicion that the arterial segment is not pressurized correctly, since it is expected to be circular. However, when looking at Table 11 it can be seen that the surface area does increase for each pressure step, which means that there is a pressure increase.

Table 11 Surface areas of the six contours at 80-, 100- and 120mmHg.

	80 mmHg	100mmHg	120mmHg
Surface area EEL (mm^2)	20.2	20.3	20.4
Surface area lumen (mm^2)	2.9	3.1	3.1

Experiment 3

The contours that were drawn for slice 3 in experiment 3 are shown in Figure 58 together with a graph that shows all contours simultaneously.

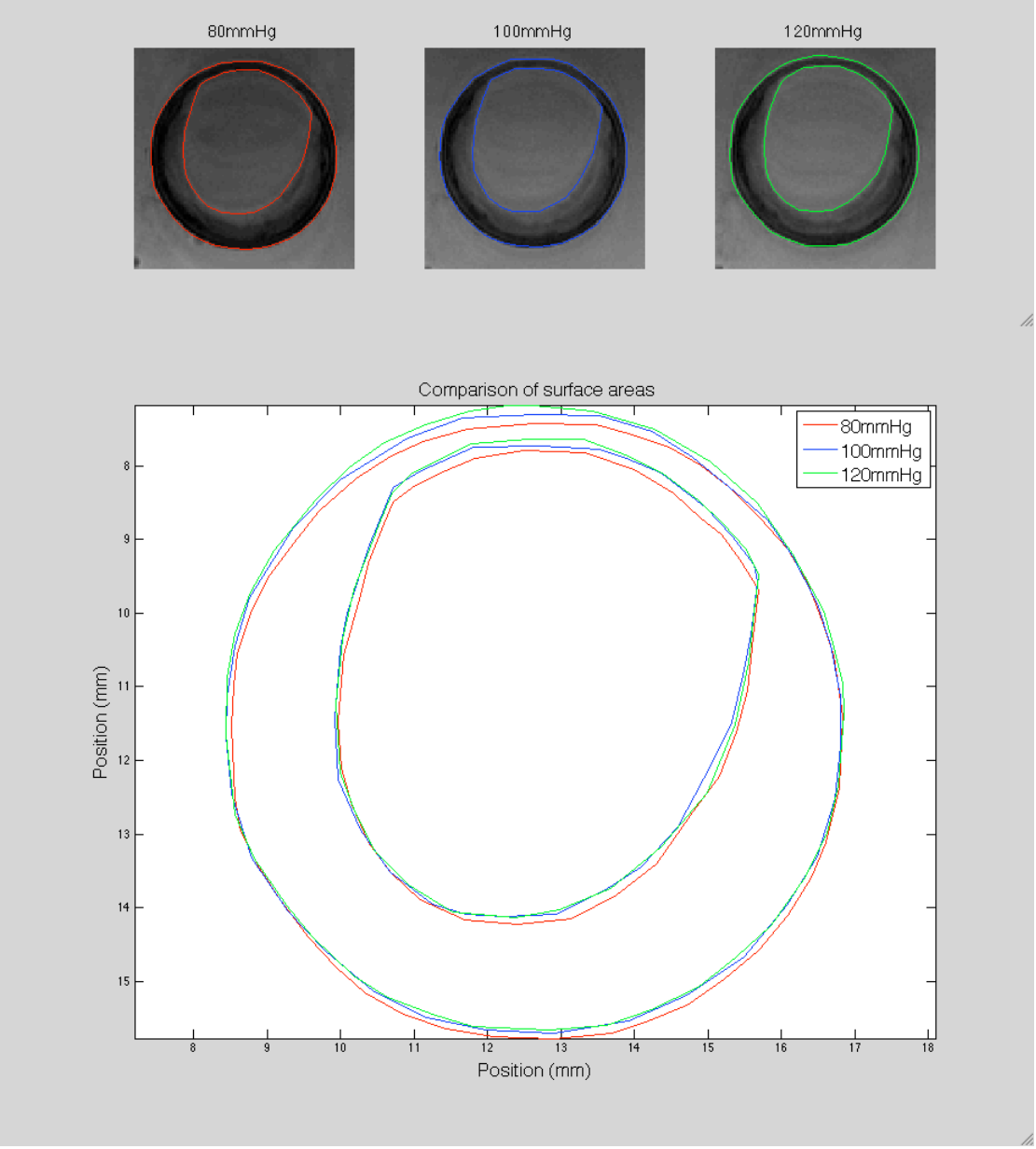

Figure 58 At the top the contours of the lumen and EEL are drawn in the MRI scans for the pressures 80-, 100- and 120mmHg. In the graph the counters of the EEL and lumen can be seen simultaneously.

In Figure 58 can be seen that this arterial segment has a smaller plaque then the previous two segments. The EEL describes a circular shape with a diameter of ±8.5mm. The wall thickness of the eccentric plaque is ±2mm. The contours of 120mmHg and 100mmHg seem to align, but the contour of 80mmHg seems to be shifted down as a whole. The values for the surface areas can be seen in Table 12.

Table 12 Surface areas of the six contours at 80-, 100- and 120mmHg.

	80 mmHg	100mmHg	120mmHg
Surface area EEL (mm^2)	55.5	55.8	56.3
Surface area lumen (mm^2)	28.8	29.1	29.3

Experiment 4

The contours that were drawn for slice 9 in experiment 4 are shown in Figure 59 together with a graph that shows all contours simultaneously.

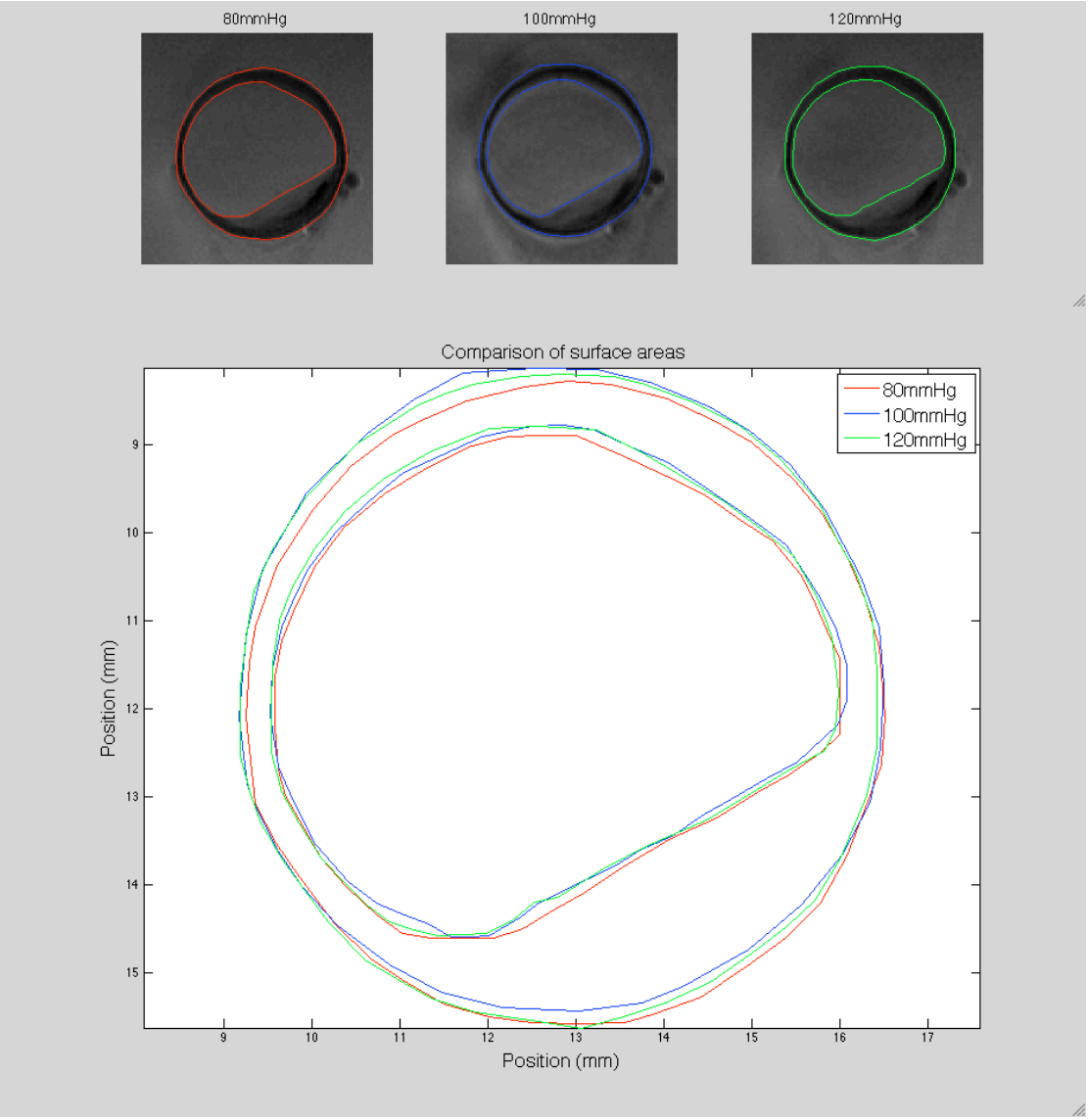

Figure 59 At the top the contours of the lumen and EEL are drawn in the MRI scans for the pressures 80, 100 and 120mmHg. In the graph the counters of the EEL and lumen can be seen simultaneously.

In Figure 59 can be seen that the plaque in this arterial segment is the smallest of the four segments. The EEL has a circular shape with a diameter of ±6mm. The contours from the 80mmHg scan seem to have moved a bit down with respect to the other contours. The 120mmHg seems to have moved a bit down with respect to the 100mmHg. In Table 13 the surface areas for the contours can be found.

Table 13 Surface areas of the six contours at 80, 100 and 120mmHg.

	80 mmHg	100mmHg	120mmHg
Surface area EEL (mm^2)	41.5	42.0	42.2
Surface area lumen (mm^2)	26.6	26.7	27.1

Surface area increase of the EEL and lumen

In Table 10 to 13 the surface areas of the EEL and lumen are shown. In Figure 60 the increase in surface area, with respect to 80mmHg, is shown for the EEL and lumen for all four experiments.

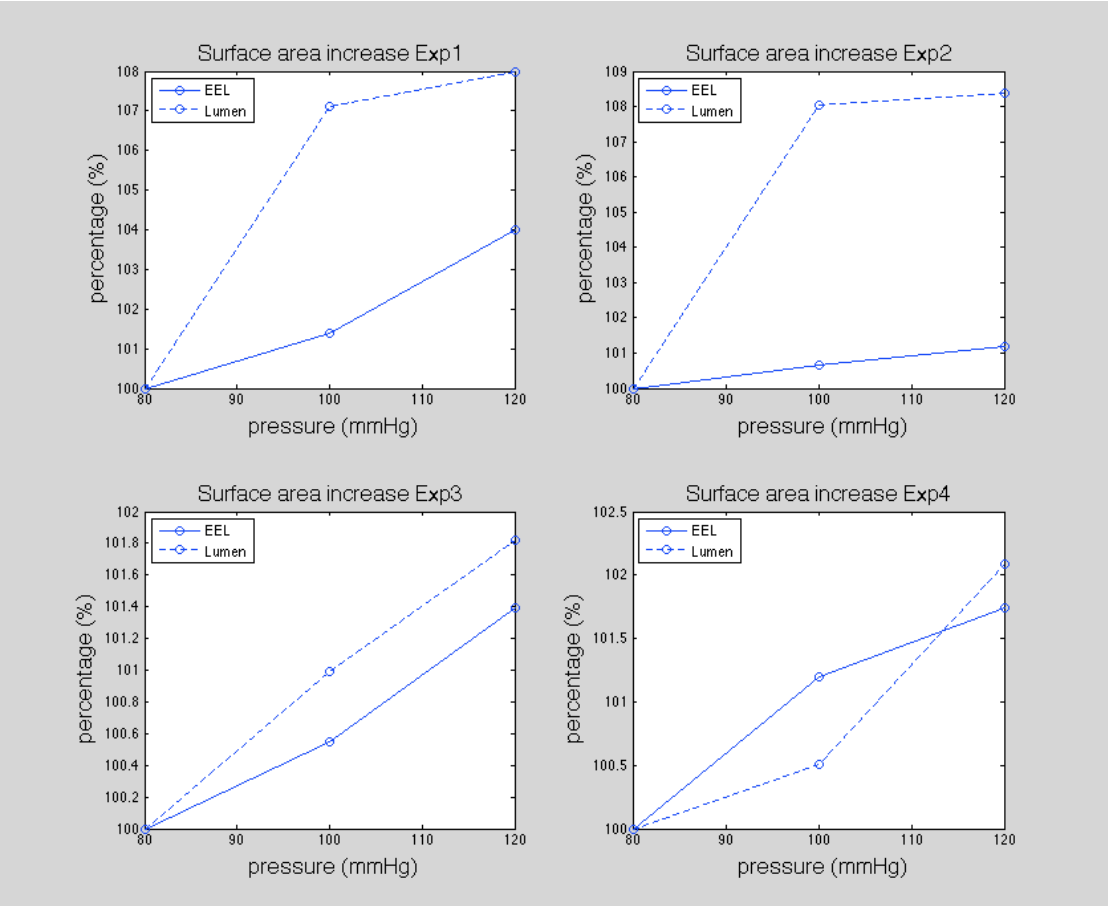

Figure 60 The increase in surface area with respect to 80mmHg for all four experiments. The increase is given in percentages.

The first thing that can be seen in Figure 60 is that the surface of both the EEL and lumen increases when the pressure increases. It also seems that the surface of the lumen increase more than the EEL for experiment 1-3. In experiment 4 it is the other way around for the first pressure step from 80 to 100mmHg. This artery has the smallest plaque of the arterial segments used for the experiments. The increase in lumen is largest for experiment 1 and 2, which are also the arterial segments with a large plaque.

Displacement calculations with the Elastix program

To explore the use of Elastix to determine local deformations patterns, we selected the slice with the largest displacement. Before the displacement field is calculated the registration is observed to see if it is done properly (Figure 61). The left image shows the result after subtracting the moving from the fixed image. Lines with elevated contrast can be seen, indicating that there is a clear difference between the fixed and moving image. After the registration, these differences for the artery disappeared, indicating that the registration procedure was able to minimize the difference between the two images. For this registration a mask was used to keep the artefacts away. The contours outside the mask are still in the difference image. These artefacts originate form the fixed image that is subtracted from the registration.

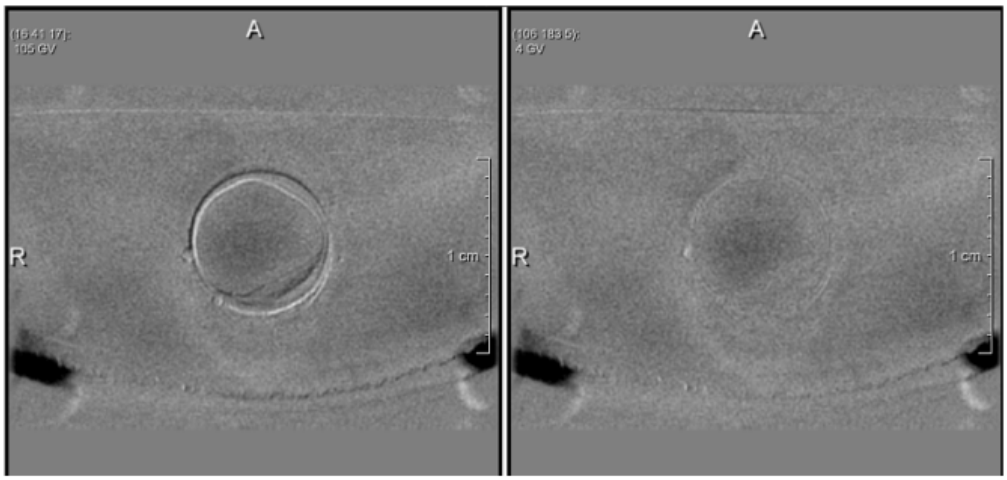

a b

Figure 61 a, Subtraction of fixed minus moving image. b, Subtraction of registration minus fixed image.

Since the registration was successful, the displacement field could be calculated and is shown in Figure 62.

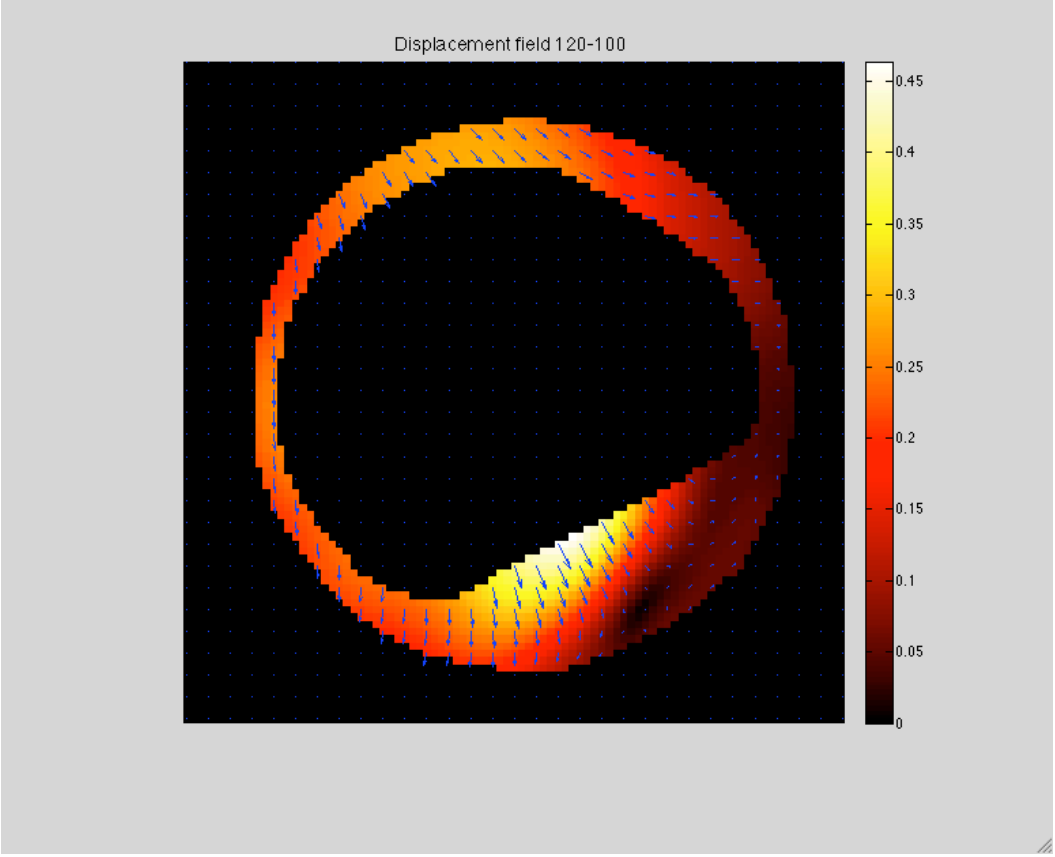

Figure 62 The displacement field from 120 to 80mmHg.

The vectors in Figure 62 represent the direction and magnitude of the displacement of the voxels. The color map also shows the magnitude of the displacements. The displacement field in Figure 62 shows that the artery is displaced downward when going from 80 to 120mmHg. This result is also seen in Figure 59 for the surface areas. It can be seen that the displacements vary locally in the plaque, indicating a non-uniform strain in the plaque. The smallest displacement is found near the location where the calcification was found in the comparison between MRI and histology.

The displacement fields for the other slices can be found in Appendix C. The results from these deformation fields are contradictory to these. The directions of the displacements do not seem to confirm the displacements of the surfaces found in the global deformations. The displacements of the other arterial segments are smaller than the displacements from the arterial segment used in experiment 4.

4.3.3 Discussion and conclusion for pressure induced deformations

The low-resolution MRI scans were used to calculate the global deformations of the lumen and EEL surface area. In the results was seen that for every experiment the surface area for both the EEL and lumen increased if the pressure increased. This is expected, because with a pressure increase the outward force on the lumen increases, which increases the deformation. Generally, deformations were rather small, also for the small plaques. For three of the four experiments the increase in surface area for the lumen was bigger than for the EEL. This might indicate that there is compressibility of the plaque. However, we only have used 4 arteries and we neglected the influence of the z-direction, which can also be the cause of this result.

The increase in surface area for all four experiments was small. Two explanations can be given for the small displacements, the setup did not pressurize the arterial segments correctly or the arterial segments were stiffer than expected. The pressure pump that was used was calibrated two times by use of a water column and even when simulating a leakage in the artery, which means that the pump should have worked correctly during the MRI even if a leakage in the arterial segment would have occurred. The arteries that were imaged all had quite a lot of calcium, which might explain the stiff behavior of the segments.

For experiment four a displacement field was calculated with Elastix. The registration went very well and the result of the deformation field seems to correspond to the results that were found for the displacement of the surfaces. For larger displacements, Elastix seems to be a promising tool. For the other slices the results were less convincing, because they did not correspond to the displacements of the surface areas. The reason for this is probably the small displacements. Due to these small displacements the influence of artefacts and noise influence the displacement calculations.

From the obtained results it can be concluded that it is possible to measure the global deformation for low-resolution MRI images obtained with the sequence from Table 9. Furthermore, Elastix seems to be a promising program to use for calculating local deformations when displacements are sufficiently large. However, more research needs to be done into Elastix to improve the deformation field calculations.

5. Discussion and conclusion

The aim of this project was to find an MRI protocol to image atherosclerotic arteries and to investigate if pressure induced deformation measurements can be done on these MRI scans. To achieve this aim several steps had to be taken. In chapter 2 the theory behind MRI was discussed and was used afterwards to obtain an imaging sequence that could be used for high- and low-resolution MRI scans of atherosclerotic plaques (chapter 3). In Chapter 4 the high resolution MRI scans of the atherosclerotic plaques were used to compare with histology. The low resolution MRI scans of the atherosclerotic plaques was used to calculate pressure induced deformations. In this chapter the results will be discussed that were obtained in chapter 4.

Pilot experiments

The aim of the pilot experiments was to obtain an image sequence for high- and low-resolution image acquisition. These images had to fulfill criteria such as a good contrast between different components, high enough SNR to delineate different components, an in-plane resolution higher then 65μm, a maximum slice thickness of 1mm and with a reasonable AT. Two 2D T2 FSE sequences were found for both the high and low resolution scans that met all the requirements. Both scans had enough contrast and a good SNR. The in-plane resolution for the high-resolution image was 56μm and for the low-resolution image 98μm. Their acquisition time was 64 and 12 minutes respectively. Both sequences had a slice thickness of 1mm, which is the maximum thickness.

Although the pilot experiments gave good results, some improvements can be made. One of the main problems we encountered was ghosting artefact. This artefact was highly unpredictable, because it was not always present during scanning even not when two exactly the same sequences were used. One of the sequences could have ghosting while the other did not have any. The experts from GE have been at the MRI scanner as well and could not explain the ghosting artefact that occurred in the images. In the time that we used the MRI scanner the gradient coil has been replaced, the body coil has been replaced and the cooling has been repaired. These reparations plus the fact that other studies also had to be performed at this scanner, limited the availability of the scanner. This gave us less time to do more experiments to resolve this problem. However, when more experiments are to be done, this problem should be fixed.

After the pilot experiments were done it was concluded that a new setup was necessary to fit larger arteries. In the new setup, some leakage was observed during scanning. Sometimes buffer leaked from the setup and went under the surface cardiac mouse coil. This caused aliasing. Which increased the ghosting artefacts. This resulted in images that were severely ghosted with aliased buffer. This problem needs to be solved to obtain better images.

MRI versus histology

The high-resolution MRI scans were compared to histology slices. The MRI slices and histology slices were matched by measuring for each method the distance from the first slice to the cannule. From the results could be seen that this registration method worked and was able to match the histology slices to the appropriate MRI slices. With the sequence obtained from the pilot experiments and the registration method used to match the histology slices with the MRI slices, we were able to delineate the adventitia, media and intima. Within the intima the calcifications could be identified, but the different concentrations of collagen and lipids was less apparent.

The identification of lipid rich/poor regions and collagen rich/poor regions was difficult, because the ghosting artefacts influenced the contrast inside the plaque. A second artefact that influenced the contrast in the plaque is the partial volume artefact. All the contrast in 1mm in the longitudinal direction is averaged, which means that the transition from lipid rich to lipid low regions in the longitudinal direction affects the contrast in the in-plane direction.

Another possibility is that the contrast difference between lipid and collagen is not high enough to be detected by the MRI.
To reduce the ghosting a SE sequence should be used, but this will be at the cost of AT, SNR or resolution. The partial volume artefact can be reduced by reducing the longitudinal resolution. If in the future the software for 3D FSE is available then this would make it possible to obtain thinner slices without compensating the resolution, SNR or AT to much. With these adjustments it might be possible to better delineate the fibrous cap, different lipid concentrations and varying collagen concentrations.
The results for the comparison of the MRI slices with the histology slices, was done qualitative and not quantitative, because there was not enough data. The arteries were cut into blocks of 1mm, which were matched with the slices obtained in the high resolution MRI image. Not every block could be processed for histology, because of the limited time available. The histology slices that were obtained contained cutting artefacts, which happened due to the large amount of calcium in the diseased arterial segments. This might be reduced by decalcifying the arterial segments. All these factors limited the amount of data that could be used to compare MRI with histology in a more quantitative manner.

Pressure induced deformation measurements

To evaluate the global pressure induced deformations, the contours of the lumen and the EEL were drawn in the low resolution MRI scans. The increase in surface area for the lumen and the EEL were calculated and it was seen that with every increasing pressure step the surface area increased. The surface area of the lumen seems to increase more then the surface area of the EEL. This might imply that the plaque is slightly compressed when the pressure increases. To find local displacements the program Elastix was used, to see what the possibilities were with the low-resolution MRI scans in Elastix. The registration of the low resolution MRI scans seems to go very well for all segments. For the bigger displacements it seems that the deformation fields calculated by Elatsix resemble the results found in the displacements of the surface area. However, for the other arterial segments where the displacements were smaller, the calculated displacement fields gave contradictory results. Because the displacements are very small, artefacts and noise will probably play an important role in miscalculating displacements. The program Elastix seems to be promising, but more research needs to be done.
Additional information that might be of interest to verify biomechanical models is rupture location and rupture pressure. To find this information within a reasonable range of pressure steps, many scans must be done. If steps of 20mmHg are made and we need to go up till 300mmHg or higher we need more then 12 scans when starting from 80mmHg, which will take to long when using MRI. When the rupture is smaller than 98μm the MRI will not detect it, so a higher resolution is needed to collect this data. Ultrasound (US) is a modality that scans fast enough and can obtain a very high resolution (25μm). For future experiments it might be a possibility to perform a quick US experiment, after the MRI experiments are done, to obtain rupture location and pressure. The setup used in this project can also be used for US acquisition, without changing the orientation of the artery.

Conclusion

With the results obtained in this project it can be concluded that it is possible to draw the contours of the adventitia, media, intima and calcium from the high-resolution MRI scans. This information can be used for a 3D model that is needed for a biomechanical model of an atherosclerotic plaque. It is also possible to calculate the global pressure induced deformations from the low-resolution MRI scans, but more studies need to be done to determine local deformation patterns with the program Elastix. This information can be used to validate biomechanical plaque models.

References

1. http://www.wikidoc.org/index.php/Basic_MRI_Physics.
2. R.H. Hashemi, W.G.B., C. J. Lasanti, *MRI the basics*. Vol. Third edition. 2010: Wolters Kluwer.
3. *World Health Organization*. Visited: 04-01-2011]; Available from: http://www.euro.who.int/en/what-we-do/health-topics/diseases-and-conditions/cardiovascular-diseases.
4. Libby, P., *Atherosclerosis: The new view.* Scientific American, 2002. **286**(5): p. 47-55.
5. Malek, A.M., S.L. Alper, and S. Izumo, *Hemodynamic shear stress and its role in atherosclerosis.* Jama-Journal of the American Medical Association, 1999. **282**(21): p. 2035-2042.
6. Slager, C.J., et al., *The role of shear stress in the destabilization of vulnerable plaques and related therapeutic implications.* Nature Clinical Practice Cardiovascular Medicine, 2005. **2**(9): p. 456-464.
7. Slager, C.J., et al., *The role of shear stress in the generation of rupture-prone vulnerable plaques.* Nature Clinical Practice Cardiovascular Medicine, 2005. **2**(8): p. 401-407.
8. http://blog.nialbarker.com/252/slow_is_faster.html.
9. Mayet, J. and A. Hughes, *Cardiac and vascular pathophysiology in hypertension.* Heart, 2003. **89**(9): p. 1104-1109.
10. Baldewsing, R.A., et al., *Finite element modeling and intravascular ultrasound elastography of vulnerable plaques: parameter variation.* Ultrasonics, 2004. **42**(1-9): p. 723-729.
11. Born, G.V.R.a.P.D.R., *Mechanical properties of human atherosclerotic lesions, in pathobiology of the human atherosclerotic plaque.* Springer, 1990.
12. Holzapfel, G.A., et al., *Determination of layer-specific mechanical properties of human coronary arteries with nonatherosclerotic intimal thickening and related constitutive modeling.* American Journal of Physiology-Heart and Circulatory Physiology, 2005. **289**(5): p. H2048-H2058.
13. Holzapfel, G.A., G. Sommer, and P. Regitnig, *Anisotropic mechanical properties of tissue components in human atherosclerotic plaques.* Journal of Biomechanical Engineering-Transactions of the Asme, 2004. **126**(5): p. 657-665.
14. Lee, R.T., et al., *STRUCTURE-DEPENDENT DYNAMIC MECHANICAL-BEHAVIOR OF FIBROUS CAPS FROM HUMAN ATHEROSCLEROTIC PLAQUES.* Circulation, 1991. **83**(5): p. 1764-1770.
15. Lendon, C.L., et al., *TESTING OF SMALL CONNECTIVE-TISSUE SPECIMENS FOR THE DETERMINATION OF THE MECHANICAL-BEHAVIOR OF ATHEROSCLEROTIC PLAQUES.* Journal of Biomedical Engineering, 1993. **15**(1): p. 27-33.
16. Loree, H.M., et al., *STATIC CIRCUMFERENTIAL TANGENTIAL MODULUS OF HUMAN ATHEROSCLEROTIC TISSUE.* Journal of Biomechanics, 1994. **27**(2): p. 195-204.

17. Barrett, S.R.H., et al., *Experimental measurement of the mechanical properties of carotid atherothrombotic plaque fibrous cap.* Journal of Biomechanics, 2009. **42**(11): p. 1650-1655.
18. C. Westbrook, C.K.R., J. Talbot, *MRI in practice*. Vol. Third edition. 2005: Blackwell Publishing.
19. Schepkin, V.D., et al., *Initial in vivo rodent sodium and proton MR imaging at 21.1 T.* Magnetic Resonance Imaging. **28**(3): p. 400-407.
20. http://mrsrl.stanford.edu/~brian/bloch/.
21. Burke, A.P., et al., *Coronary risk factors and plaque morphology in men with coronary disease who died suddenly.* New England Journal of Medicine, 1997. **336**(18): p. 1276-1282.
22. Jahnke, C., et al., *Experimental evaluation of the detectability of submillimeter atherosclerotic lesions in ex vivo human iliac arteries with ultrahigh-field (7.0 T) magnetic resonance imaging.* International Journal of Cardiovascular Imaging, 2007. **23**(4): p. 519-527.
23. Coombs, B.D., et al., *Structure of plaque at carotid bifurcation - High-resolution MRI with histological correlation.* Stroke, 2001. **32**(11): p. 2516-2521.
24. McAteer, M.A., et al., *Quantification and 3D reconstruction of atherosclerotic plaque components in apolipoprotein E knockout mice using ex vivo high-resolution MRI.* Arteriosclerosis Thrombosis and Vascular Biology, 2004. **24**(12): p. 2384-2390.
25. Plantenga, T., *Effect of time and loading protocol on mechanical behavior of healthy porcine coronary arteries.* 2009.
26. Cai, J.M., et al., *In vivo quantitative measurement of intact fibrous cap and lipid-rich necrotic core size in atherosclerotic carotid plaque - Comparison of high-resolution, contrast-enhanced magnetic resonance imaging and histology.* Circulation, 2005. **112**(22): p. 3437-3444.
27. Hofman, J.M.A., et al., *Quantification of atherosclerotic plaque components using in vivo MRI and supervised classifiers.* Magnetic Resonance in Medicine, 2006. **55**(4): p. 790-799.
28. Saam, T., et al., *Quantitative evaluation of carotid plaque composition by in vivo MRI.* Arteriosclerosis Thrombosis and Vascular Biology, 2005. **25**(1): p. 234-239.
29. Zhu, C.C., et al., *Normalized Wall Index Specific and MRI-Based Stress Analysis of Atherosclerotic Carotid Plaques - A Study Comparing Acutely Symptomatic and Asymptomatic Patients.* Circulation Journal. **74**(11): p. 2360-2364.
30. Sun, B.J., et al., *Characterization of coronary atherosclerotic plaque using multicontrast MRI acquired under simulated in vivo conditions.* Journal of Magnetic Resonance Imaging, 2006. **24**(4): p. 833-841.
31. Pegg, D.E., *The history and principles of cryopreservation.* Seminars in Reproductive Medicine, 2002. **20**(1): p. 5-13.
32. van Andel, C.J., P.V. Pistecky, and C. Borst, *Mechanical properties of porcine and human arteries: Implications for coronary anastomotic connectors.* Annals of Thoracic Surgery, 2003. **76**(1): p. 58-64.
33. van den Broek, C.N., et al., *A generic constitutive model for the passive porcine coronary artery.* Biomechanics and Modeling in Mechanobiology. **10**(2): p. 249-258.

34. Carboni, M., G.W. Desch, and H.W. Weizsacker, *Passive mechanical properties of porcine left circumflex artery and its mathematical description.* Medical Engineering & Physics, 2007. **29**(1): p. 8-16.
35. Carmines, D.V., J.H. McElhaney, and R. Stack, *A PIECE-WISE NONLINEAR ELASTIC STRESS EXPRESSION OF HUMAN AND PIG CORONARY-ARTERIES TESTED INVITRO.* Journal of Biomechanics, 1991. **24**(10): p. 899-906.
36. Fung, Y.-c., *Biomechanics: Mechanical properties of living tissues*, in *Biomechanics: Mechanical properties of living tissues*. 1993, Springer US. p. Page 270.
37. Kassab, G.S. and S. Molloi, *Cross-sectional area and volume compliance of porcine left coronary arteries.* American Journal of Physiology-Heart and Circulatory Physiology, 2001. **281**(2): p. H623-H628.
38. Roy, S., P. Silacci, and N. Stergiopulos, *Biomechanical proprieties of decellularized porcine common carotid arteries.* American Journal of Physiology-Heart and Circulatory Physiology, 2005. **289**(4): p. H1567-H1576.
39. Weizsacker, H.W., H. Lambert, and K. Pascale, *Analysis of the passive mechanical properties of rat carotid arteries.* J Biomech, 1983. **16**(9): p. 703-15.
40. Zulliger, M.A., et al., *Effects of longitudinal stretch on VSM tone and distensibility of muscular conduit arteries.* American Journal of Physiology-Heart and Circulatory Physiology, 2002. **283**(6): p. H2599-H2605.
41. S. Klein, M.S., K. Murphy, M.A. Viergever, J.P.W. Pluim, *elastix: a toolbox for intensity based medical image registration.* Transactions on Medical Imaging, 2010. **29**(1): p. 196-205.
42. Stemper, B.D., et al., *Mechanics of fresh, refrigerated, and frozen arterial tissue.* Journal of Surgical Research, 2007. **139**(2): p. 236-242.
43. Schaar, J.A., et al., *Effect of temperature increase and freezing on intravascular elastography.* Ultrasonics, 2002. **40**(1-8): p. 879-881.
44. Chow, M.-J., *Changes in the mechanical and Biochemical properties of aortic tissue due to cold storage.* Journal of Surgical Research, 2009.
45. Masson, I., et al., *Mechanical properties of arteries cryopreserved at-80 degrees C and-150 degrees C.* Medical Engineering & Physics, 2009. **31**(7): p. 825-832.
46. Pukacki, F., et al., *The mechanical properties of fresh and cryopreserved arterial homografts.* European Journal of Vascular and Endovascular Surgery, 2000. **20**(1): p. 21-24.
47. Thakrar, R.R., et al., *Vitreous cryopreservation maintains the viscoelastic property of human vascular grafts.* Faseb Journal, 2006. **20**(7): p. 874-881.
48. Venkatasubramanian, R.T., et al., *Effects of freezing and cryopreservation on the mechanical properties of arteries.* Annals of Biomedical Engineering, 2006. **34**(5): p. 823-832.
49. Rosset, E., et al., *Effects of cryopreservation on the viscoelastic properties of human arteries.* Annals of Vascular Surgery, 1996. **10**(3): p. 262-272.

Appendix A

Flow artefact

A slice in the body is selected by applying a gradient along the longitudinal direction. This gives a linear increase in angular frequency of the nuclei. By applying a RF-pulse with a certain bandwidth the slice you want is selected. After the slice selection an echo is created either by a 180° RF-pulse or another gradient. The 180° RF-pulse is also slice selective, but if the nuclei of the blood have traveled the thickness of the slice then they will not be affected by this 180° pulse. This causes a signal loss (Figure 63).

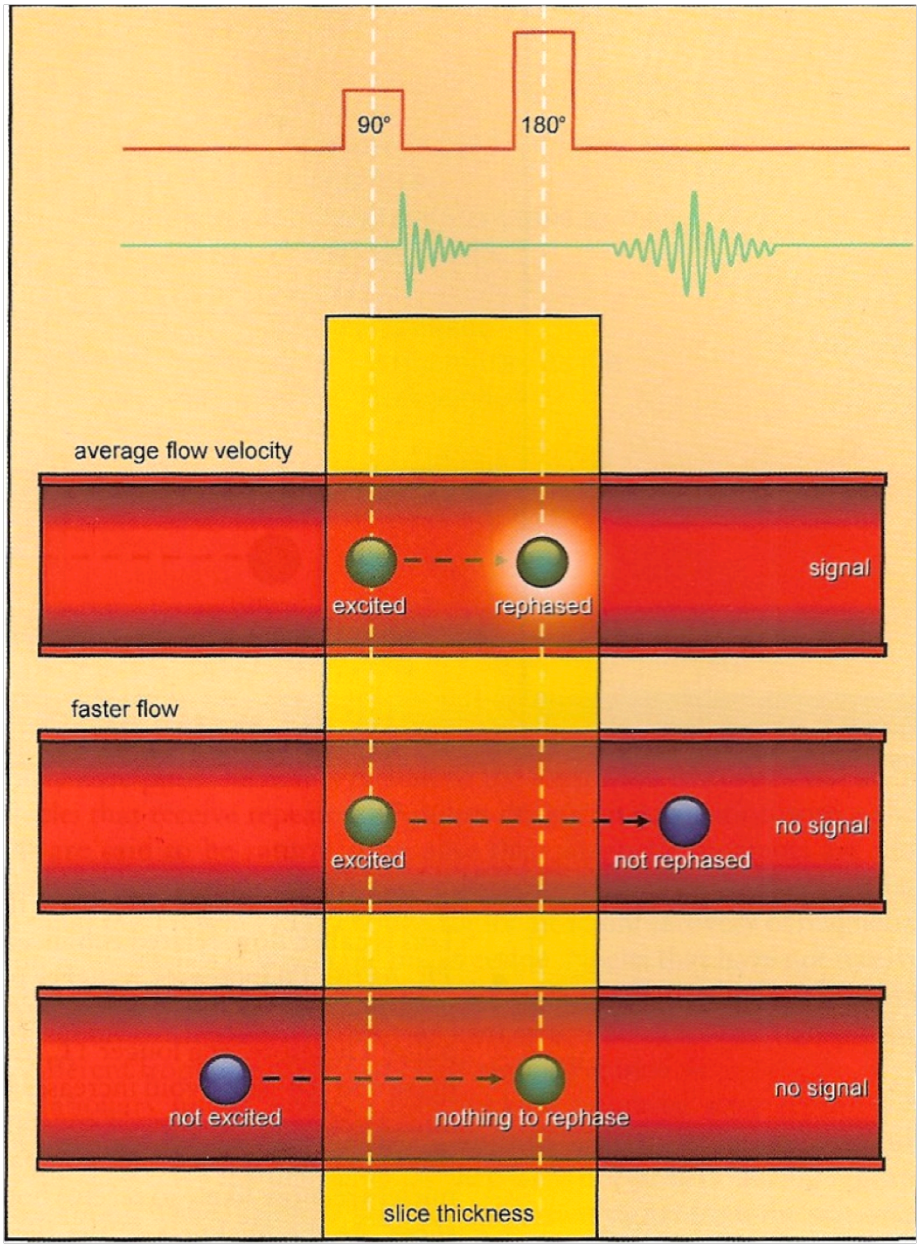

Figure 63 The effects of flow on the signal received. Signal is lost or misinterpreted due to a fast flow. If the nuclei stay within the slice during the excitation and readout, there is no signal loss, but if they miss one of both the signal will get lost. [18]

However, if a gradient is applied to re-phase the nuclei and obtain an echo, this changes. The gradient is not slice selective so even if the nuclei have passed the slice, they will still be affected and create a signal. The time it takes for a nucleus to travel from the start of the slice to the end is called the time of flight (TOF). If at time one a stationary and flowing nucleus experience a certain gradient, they will be in the same phase. However, the flowing nucleus will move in this gradient field and thus will get a different phase compared with the stationary nucleus. There are several techniques that can compensate for flow artefacts, even echo re-phasing, gradient moment nulling, and partial pre-saturation.
When the first echo is received the flowing nuclei will be misread, because they are out of phase. However, after a second RF-pulse these nuclei will re-phase again and thus at the second echo these nuclei are in phase. With even echo re-phasing every even numbered echo is read. With gradient moment re-phasing the phase difference is compensated by applying several extra gradients. With spatial pre-saturation a volume, before the actual slice that is to be imaged, receives a 90° RF-pulse to saturate all nuclei. When the saturated flowing nuclei enter the slice it gets another 90° RF-pulse and thus the nuclei in the blood will flip into the negative z-axis, but the stationary tissue goes into the transverse plane. Thus flowing nuclei will not give a signal due to this pre-saturation (black blood).

Apendix B

One of the points that is up for discussion, is the preservation technique for the arteries. Due to availability issues for the MRI and development of the setup, the arteries could not be tested right after the dissection. This means that the arteries need to be stored in a way that will preserve the mechanical properties. Several options are available:

- Freezing
- Cryopreservation
- Vitrification

These three methods all store the samples at subzero temperature. Two phenomena occur when going to subzero temperatures. Water is one of the few liquids that increase in volume when going into solid state. This solid state is formed out of ice crystals. The crystals can puncture the cells and the volume expansion causes rupture of cell structures. The second phenomenon is a response to the forming of these ice crystals. A cell has a lot of water and proteins, which are dissolved in each other. Because ice crystals consist mainly out of water, it means that the concentration of proteins in the remaining liquid water rises. The result is osmosis of liquid water from one cell to the other, which is the second cause of cell destruction[31].
Several papers investigate how the above named preservation techniques influence the mechanical properties of the arteries. Freezing brings the sample to -20 or -80°C in a tube filled with air. According to Stemper et al. [42] and Schaar et al. [43] this method does not significantly change the mechanical properties of an artery in comparison with a fresh sample. However, the results of Chow et al. [44] show that frozen samples do show a change in mechanical properties. With cryopreservation the artery is placed in a tube filled with a cryo-protective agent (CPA). This CPA reduces crystal forming during the freezing process. Literature showed controversial results. Out of the 5 papers found, two showed that cryopreservation did not significantly influence the mechanical properties [45, 46], two showed that it did influence mechanical properties [47, 48] and one showed different results for different arteries [49]. The difference between cryopreservation and vitrification is that the concentration of CPA in vitrification is higher and the arteries are snap frozen. Snap freezing is a method that brings the temperature of an artery to its final temperature in a matter of seconds by placing it in liquid nitrogen. Because of this rapid decrease in temperature, the proteins do not have the time to diffuse away from the water. A glass state is achieved without ice crystals [31]. Because the ice crystals do not form, osmosis is also prevented. Thakrar et al. compared vitrification with fresh and cryopreserved arteries and found that vitrification did not significantly change the mechanical properties of the artery, but cryopreservation did.
The difference between freezing and cryopreservation is the use of CPA. The difference between vitrification and cryopreservation is snap freezing and the concentration of CPA used. The use of CPA and the concentration needed to preserve biomechanical properties is controversial and the results do not point in the same direction. However, snap freezing does seem to give good results. This is why we choose to snap freeze our samples and store them at -80°C, without a CPA.

Appendix C

The global deformations were evaluated for this project, but we also did a test with the program Elastix to obtain local deformations. With Elastix we calculated the displacement field of the low-resolution MRI scans. One of the results was shown in Section 4.3.2, but the rest of the results are shown and discussed here.
Before a deformation field can be calculated one image must be registered with another image. With registering one image is fixed and the other is adjusting its shape till it fits the fixed image. To determine if the registration went well, the difference between the initial scans is compared to the difference of the fixed image and the registration image. If the registration was done correctly the difference between the fixed image and the registration should be close to zero.

Experiment 1
In Figure 64 the registration of the first experiment is seen.

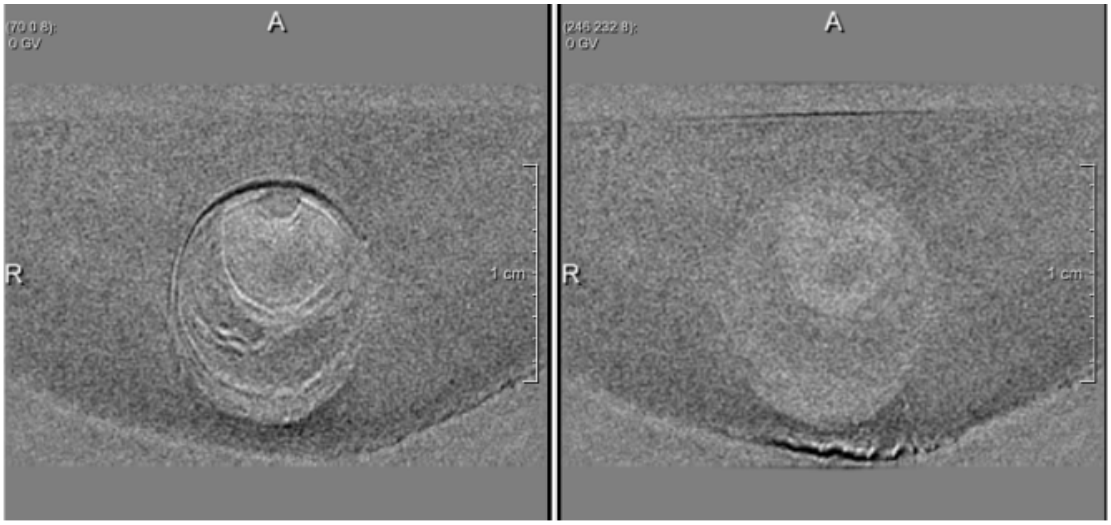

a b

Figure 64 a, Subtraction of fixed minus moving image. b, Subtraction of registration minus fixed image.

In Figure 64a can be seen that there are some black and white lines, which indicate that the fixed image differs from the moving image. In Figure 64b can be seen that all the lines in the artery are gone, which indicates that the registration was successful.
With Transformix the displacement field is calculated for 120-80mmHg, 120-100 mmHg and 100-80mmHg. The displacement field from 120-80mmHg is shown in Figure 65. The scale in Figure 65 shows that the maximum displacement is ±0.2mm, which is very small when a pressure step is taken from 80mmHg to 120mmHg. This small displacement also verifies that the change in surface area should be very small. The direction of the displacements is changing a lot. On the left side of the artery the displacements are going down and on the right side they are going up again. This displacement field does not resemble the displacement of the surface areas seen in Figure 56. In the surface area plots the 80mmHg contours seem to move downwards, however in the displacement field the left side moves downward and the right side of the plaque moves upward.

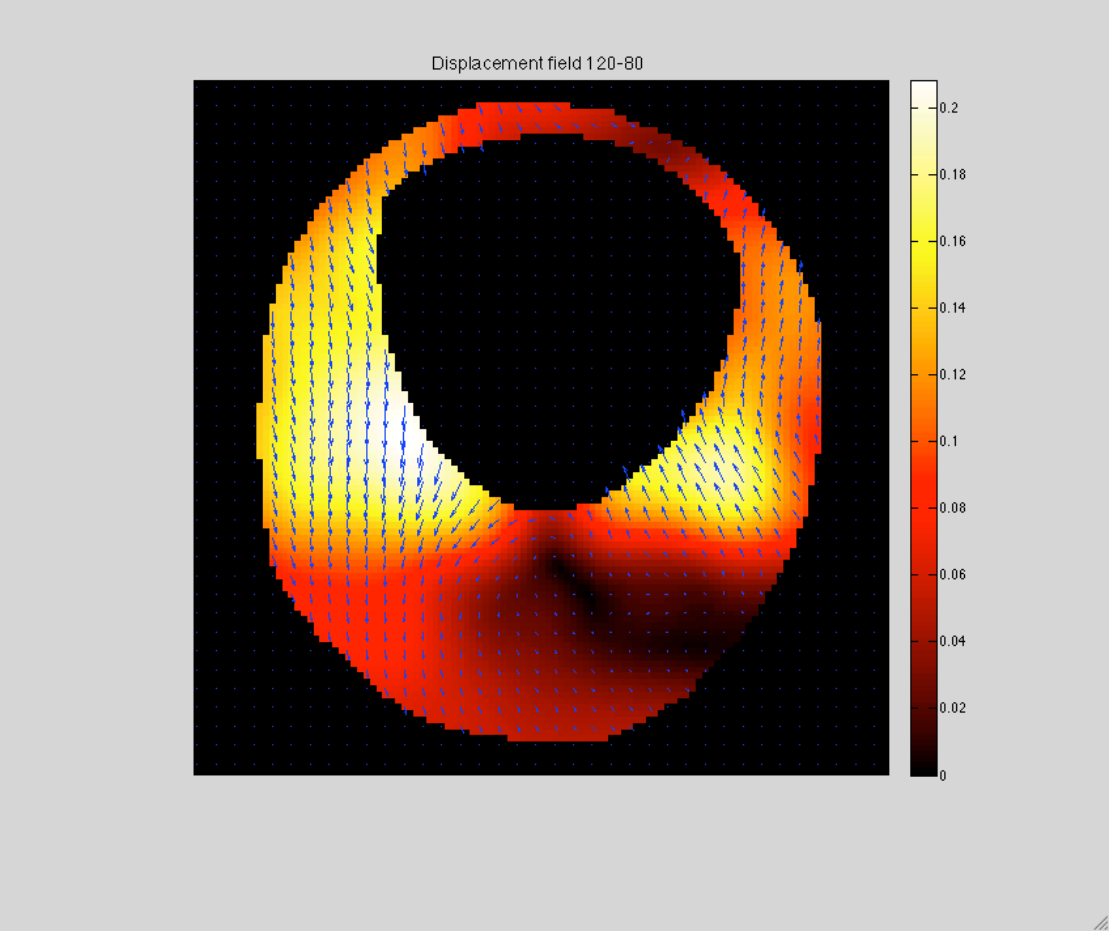

Figure 65 The displacement field from 120 to 80mmHg.

Experiment 2

Before the displacement field of experiment two is calculated the registration is observed to see if it is done properly (Figure 66).

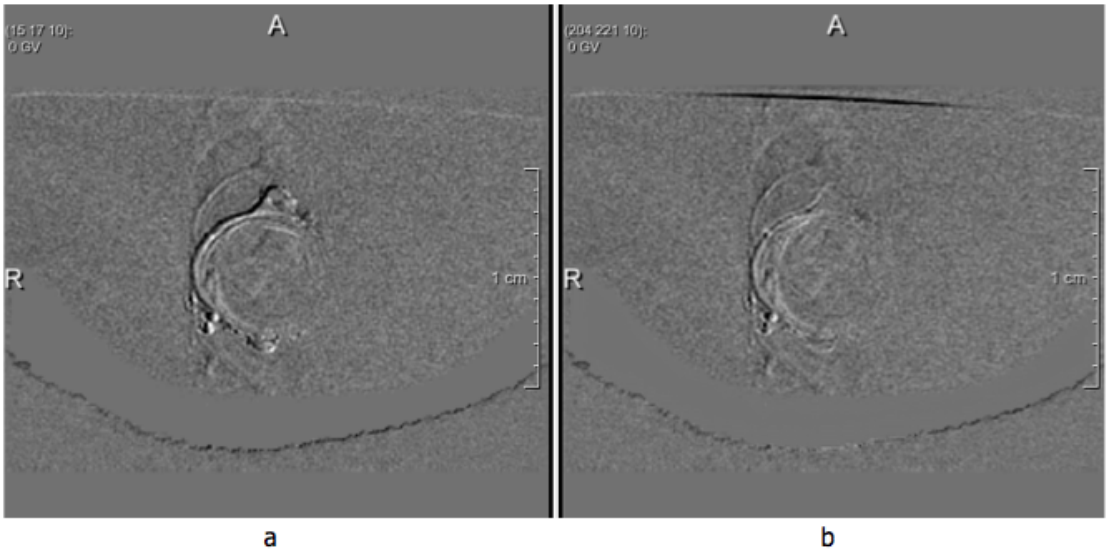

a b

Figure 66 a, Subtraction of fixed minus moving image. b, Subtraction of registration minus fixed image.

In Figure 66a can be seen that there is ghosting. This ghosting is also present in Figure 66b, which means that the ghosting originates from the fixed image (120mmHg), because the masks that are used for the registration remove the ghosting artefact from the registration.

The inside of the artery seems to have been registered reasonably. There are some small lines found in the adventitia, but also these are reduced.
Since the registration seems to be good, the displacement field can be calculated (Figure 67).

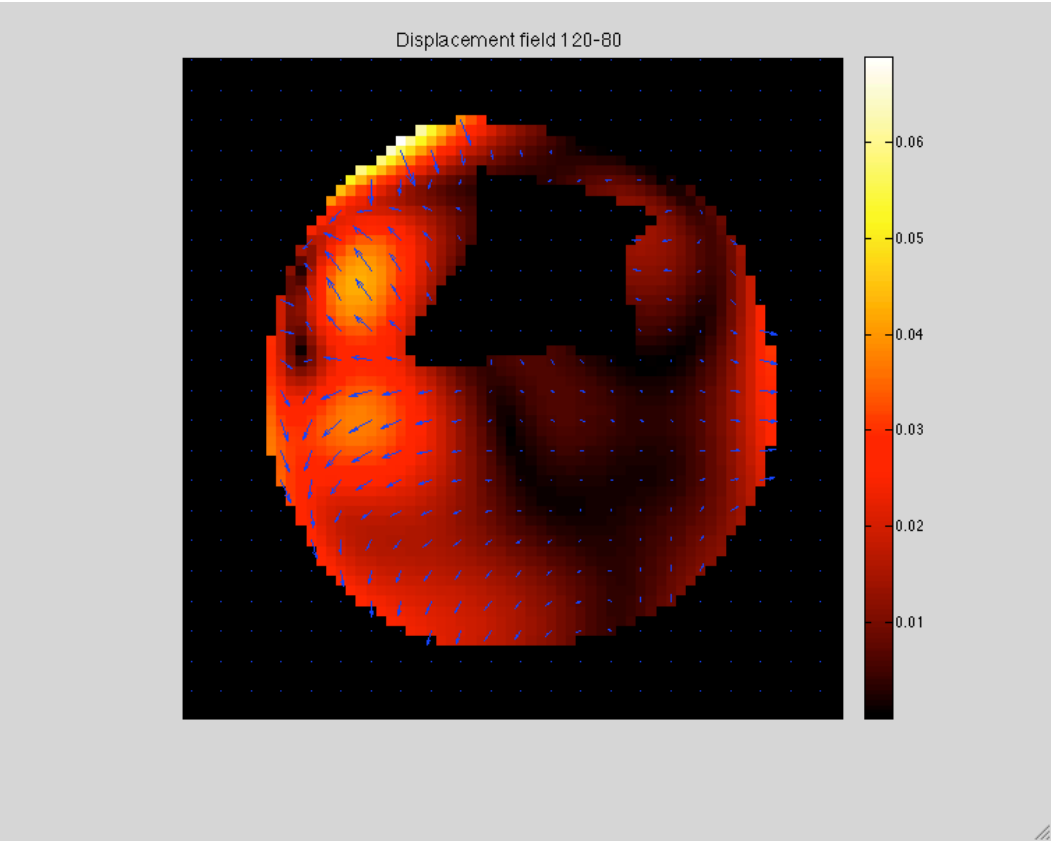

Figure 67 The displacement field from 120 to 80mmHg.

The biggest displacement in Figure 67 seems to be ±0.07mm, which is even smaller than the resolution of the MRI image that is acquired. The arrows point in random directions and do not resemble displacement of the surface areas seen in Figure 57.

Experiment 3
Before the displacement field is calculated the registration is observed to see if it is done properly (Figure 68).

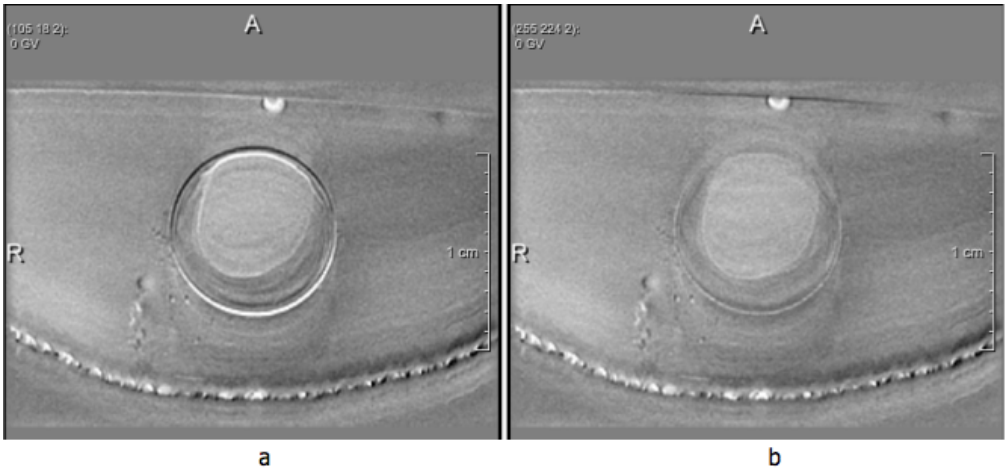

a b

Figure 68 a, Subtraction of fixed minus moving image. b, Subtraction of registration minus fixed image.

The black and white lines in Figure 68a have been reduced a lot after registration and are almost gone. This means that the registration has been successful and the displacement field can be calculated. The displacement field for this pressure step is shown in Figure 69.

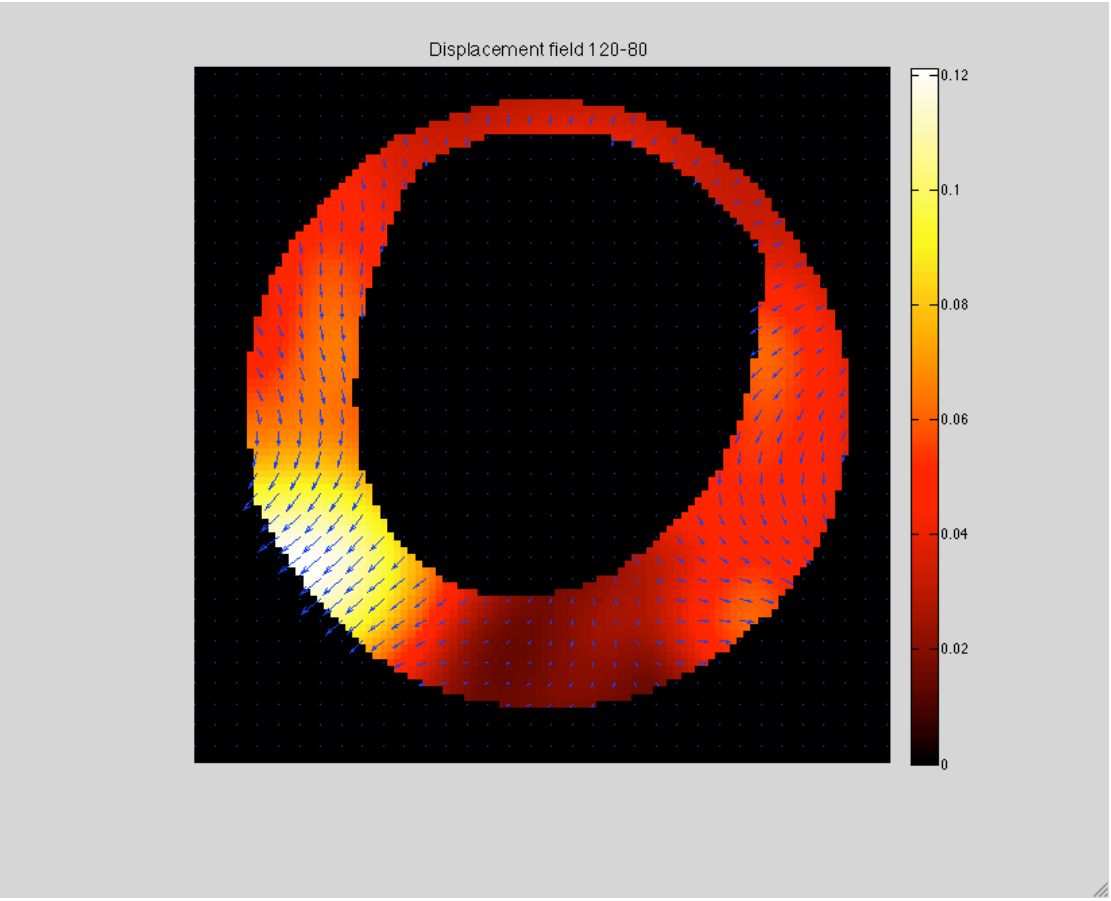

Figure 69 The displacement field from 120 to 80mmHg.

In the scale can be seen that the maximum displacement is ±0.12mm. The displacement in the middle of the plaque seems to be close to zero but at the side it is pointing outward. In Figure 58 can be seen that the contours of 80mmHg have moved down a little bit, but this is not seen back in the displacement field calculated by Elastix.